# Carbohydrate-Based Switch-On Molecular Sensor for Cu(II) in Buffer: Absorption and Fluorescence Study of the Selective Recognition of Cu(II) Ions by Galactosyl Derivatives in HEPES Buffer

**Nitin Kumar Singhal,[†] Balaji Ramanujam,[†] Vairamani Mariappanadar,[‡] and Chebrolu Pulla Rao*,[†]**

*Bioinorganic Laboratory, Department of Chemistry, Indian Institute of Technology Bombay, Mumbai 400 076, India, and Analytical Chemistry Division, Indian Institute of Chemical Technology, Hyderabad 500 007, India*

*cprao@iitb.ac.in*

**Received May 25, 2006**

**ABSTRACT**
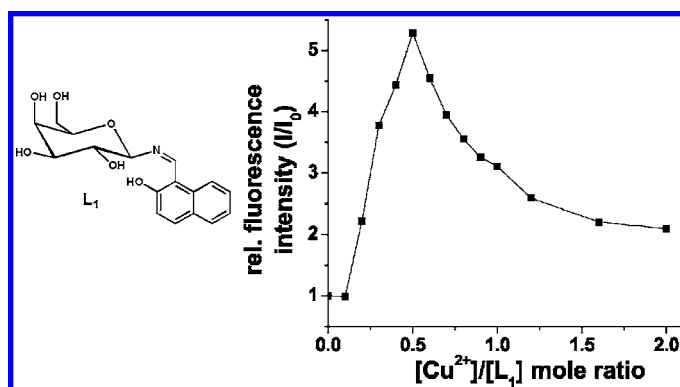


**1-($\beta$-D-Galactopyranosyl-1′-deoxy-1′-iminomethyl)-2-hydroxynaphthalene ($L_1$), possessing an ONO binding core, was found to be selective for $Cu^{2+}$ ions in $N$-[2-hydroxyethyl]piperazine-$N'$-[2-ethanesulfonic acid] buffer, at concentrations $\leq$580 ppb, at physiological pH by eliciting switch-on behavior, whereas the other ions, viz., $Mg^{2+}$, $Ca^{2+}$, $Mn^{2+}$, $Fe^{2+}$, $Co^{2+}$, $Ni^{2+}$, $Zn^{2+}$, and $Cd^{2+}$, caused no significant change in the fluorescence. Whereas the binding characteristics were ascertained by absorption spectroscopy, the species formed were shown by Q-TOF ES MS.**

Copper is an essential element of life by being involved in the functional part of a number of enzymes and also being involved in transcriptional events.[1] This necessitates sensing as well as quantifying copper in biological systems, and hence, there is a need to develop biologically compatible sensors. Because carbohydrates are biologically compatible as well as water soluble, it is desirable to have sensors based on such molecular systems. Synthetic carbohydrate-based sensors capable of reporting metal ions, including $Cu^{2+}$, are scarce in the literature. However, non-carbohydrate-based sensors suitable for biological applications are known in the literature for both copper[2] and zinc.[3] Therefore, the present communication deals with the absorption and fluorescence studies of a simple galactosyl-based naphthyl derivative, 1-($\beta$-D-galactopyranosyl-1′-deoxy-1′-iminomethyl)-2-hydroxy-naphthalene ($L_1$, Scheme 1) (Supporting Information, S1), in the recognition of $Cu^{2+}$ ions in HEPES buffer at pH 7.2−7.4.

---

[†] Indian Institute of Technology Bombay.
[‡] Indian Institute of Chemical Technology.
(1) (a) Messerschmidt, A.; Huber, R.; Poulos, T.; Weighardt, K.; Eds. *Hand. Metalloproteins* **2001**, *2*, 1149. (b) Hu, S.; Furst, P.; Hamer, D. *New Biol.* **1990**, *2*, 544.
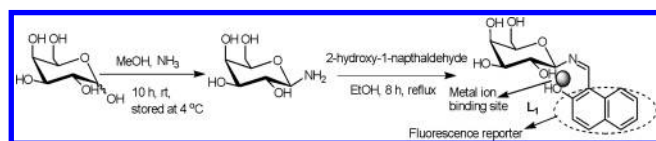
Titration of $L_1$ with $Cu^{2+}$ in MeOH resulted in a substantial increase in the fluorescence intensity of a 354 nm band until the $[Cu^{2+}]/[L_1]$ mole ratio is 0.5 ($I/I_0$ ratio is $18 \pm 1$) and then a decrease thereafter. Similar titration with $Zn^{2+}$ in MeOH shows a gradual increase in the fluorescence intensity of a 450 nm band until the $[Zn^{2+}]/[L_1]$ mole ratio of 1.0 ($I/I_0$ ratio of $18 \pm 2$) and saturation thereafter. The titration of $L_1$ in MeOH with other biologically relevant divalent ions of Mg, Ca, Mn, Fe, Co, Ni, and Cd exhibited no significant change in the fluorescence intensity of either the 350 or the 450 nm bands. On the basis of the Benesi−Hildebrand equation, $K_a$'s of $50\,000 \pm 1000$ and $50\,500 \pm 1000$ $M^{-1}$ were derived, respectively, for $Zn^{2+}$ and $Cu^{2+}$ (Supporting Information, S2).

The binding of $Cu^{2+}$ and $Zn^{2+}$ to $L_1$ in MeOH was further ascertained from the absorption spectral changes noticed in the titrations. A plot of absorbance vs the $[M^{2+}]/[L_1]$ mole ratio for various bands clearly indicated the formation of a 1:1 complex in the case of $Zn^{2+}$ and a 1:2 complex in the case of $Cu^{2+}$, the same as that obtained from the fluorescence studies, and the corresponding logarithmic plots yielded $K_a$'s of $44\,500 \pm 1500$ and $50\,500 \pm 3500$ $M^{-1}$ in the cases of $Cu^{2+}$ and $Zn^{2+}$, respectively. Similar titrations performed in MeOH with other metal ions did not show any interpretable changes in the spectra (Supporting Information, S3).

However, the fluorescence titrations performed between $M^{2+}$ and $L_1$ in HEPES buffer, at pH 7.2−7.4, yielded altogether different results. In buffer, only the titration of $Cu^{2+}$ with $L_1$ showed a gradual enhancement in the fluorescence intensity of the 350 nm band until the $[Cu^{2+}]/[L_1]$ mole ratio was 0.5 and a decrease thereafter with $I/I_0$ being

(2) (a) Zeng, Li; Miller, E. W.; Pralle, A.; Isacoff, E. Y.; Chang, C. J. *J. Am. Chem. Soc.* **2006**, *128*, 10. (b) Banthia, S.; Samanta, A. *New J. Chem.* **2005**, *29*, 1007. (c) Singh, A.; Yao, Q.; Tong, L.; Clark Still, W.; Sames, D. *Tetrahedron Lett.* **2000**, *41*, 9601. (d) Cano-Raya, C.; Fern'andez-Ramos, M. D.; Capit'an-Vallvey L. F. *Anal. Chim. Acta* **2006**, *555*, 299. (e) Brunner, J.; Kraemer, R. *J. Am. Chem. Soc.* **2004**, *126*, 13626. (f) Royzen, M.; Dai, Z.; Canary, J. W. *J. Am. Chem. Soc.* **2005**, *127*, 1612. (g) Torrado, A.; Walkup, G. K.; Imperiali, B. *J. Am. Chem. Soc.* **1998**, *120*, 609. (h) Xu, Z.; Qian, X.; Cui, J. *Org. Lett.* **2005**, *7*, 3029. (i) Xu, Z.; Xiao, Y.; Qian, X.; Cui, J.; Cui, D. *Org. Lett.* **2005**, *7*, 889. (j) Gunnlaugsson, T.; Leonard, J. P.; Murray, N. S. *Org. Lett.* **2004**, *6*, 1557.

(3) (a) Woodroofe, C. C.; Lippard, S. J. *J. Am. Chem. Soc.* **2003**, *125*, 11458. (b) Shults, M. D.; Pearce, D. A.; Imperiali, B. *J. Am. Chem. Soc.* **2003**, *125*, 10591. (c) Taki, M.; Wolford, J. L.; O'Halloran, T. V. *J. Am. Chem. Soc.* **2004**, *126*, 712. (d) Walkup, G. K.; Imperiali, B. *J. Am. Chem. Soc.* **1996**, *118*, 3053. (e) Nolan, E. M.; Burdette, S. C.; Harvey, J. H.; Hilderbrand, S. A.; Lippard, S. J. *Inorg. Chem.* **2004**, *43*, 2624. (f) Chang, C. J.; Nolan, E. M.; Jaworski, J.; Burdette, S. C.; Sheng, M.; Lippard, S. J. *Chem. Biol.* **2004**, *11*, 203. (g) Chang, C. J.; Jaworski, J.; Nolan, E. M.; Sheng, M.; Lippard, S. J. *Proc. Natl. Acad. Sci. U.S.A.* **2004**, *101*, 1129. (h) Chang, C. J.; Nolan, E. M.; Jaworski, J.; Okamoto, K.; Hayashi, Y.; Sheng, M.; Lippard, S. J. *Inorg. Chem.* **2004**, *43*, 6774. (i) Royzen, M.; Durandin, A.; Young, V. G., Jr.; Geacintov, N. E.; Canary, J. W. *J. Am. Chem. Soc.* **2006**, *128*, 3854. (j) Ajayaghosh, A.; Carol, P.; Sreejith, S. *J. Am. Chem. Soc.* **2005**, *127*, 14962.

$5.3 \pm 0.3$ and a $K_a$ yields of $50\,500 \pm 700$ $M^{-1}$. Similar titrations performed between $L_1$ and other divalent ions of Mg, Ca, Mn, Fe, Co, Ni, Zn, and Cd exhibited no significant change in the emission intensities (Figure 1a). At lower and higher pH, viz., 6.0 and 8.0, the fluorescence is further quenched. A change in the anion, viz., $Cu(NO_3)_2$ and $CuCl_2$, indicated no influence of the counteranion on the fluorescence results. Binding of $Cu^{2+}$ with $L_1$ in HEPES buffer was further confirmed by absorption spectral studies (Figure 1b) that provide a $K_a$ of $42\,500 \pm 1000$ $M^{-1}$. However, $Zn^{2+}$ does not show any significant binding in buffer (Figure 1c) (Supporting Information, S4).

Titration of a mixture of $\{L_1 \text{ and } Cu^{2+}\}$ with $M^{2+}$ (Figure 1d) in HEPES buffer resulted in a decrease of fluorescence intensity by ~10% in the case of $Mg^{2+}$, $Ca^{2+}$, $Mn^{2+}$, and $Zn^{2+}$, by ~30% in the case of $Fe^{2+}$, $Co^{2+}$, and $Ni^{2+}$, and by ~45% in the case of $Cd^{2+}$, indicating that there is a net fluorescence increase of $L_1$ by 290−470% when $Cu^{2+}$ is bound in the presence of other biologically relevant metal ions reported here. This can also be gauged by the fluorescence decay constants obtained during the titrations of $\{L_1 \text{ and } Cu^{2+}\}$ with $M^{2+}$, viz., 37 100, 38 000, 40 000, 23 100, and 29 400 $M^{-1}$, respectively, for $Fe^{2+}$, $Co^{2+}$, $Ni^{2+}$, $Cu^{2+}$, and $Cd^{2+}$. Fluorescence studies performed in HEPES buffer by varying the concentration of $Cu^{2+}$ but keeping the $[Cu^{2+}]/[L_1]$ mole ratio at 1:2 clearly indicated that the detection of 580 ppb can be established with an increase in fluorescence by at least 150% (Supporting Information, S4). Thus, $Cu^{2+}$ can be selectively recognized and quantified in HEPES buffer at a physiological pH using $L_1$ to quite low concentrations even in the presence of other biologically relevant metal ions, by eliciting a switch-on fluorescence behavior ($\Phi_{L1} = 0.0005$, $\Phi_{L1}\epsilon_{L1} = 4.7$ $M^{-1}$ $cm^{-1}$; and $\Phi_{L1+Cu} = 0.0035$, $\Phi_{L1+Cu}\epsilon_{L1+Cu} = 34.4$ $M^{-1}$ $cm^{-1}$) with a 7.0-fold increase in quantum yield and a ~7.3-fold increase in brightness ($\Phi_{L1}\epsilon_{L1}$) upon $Cu^{2+}$ addition.
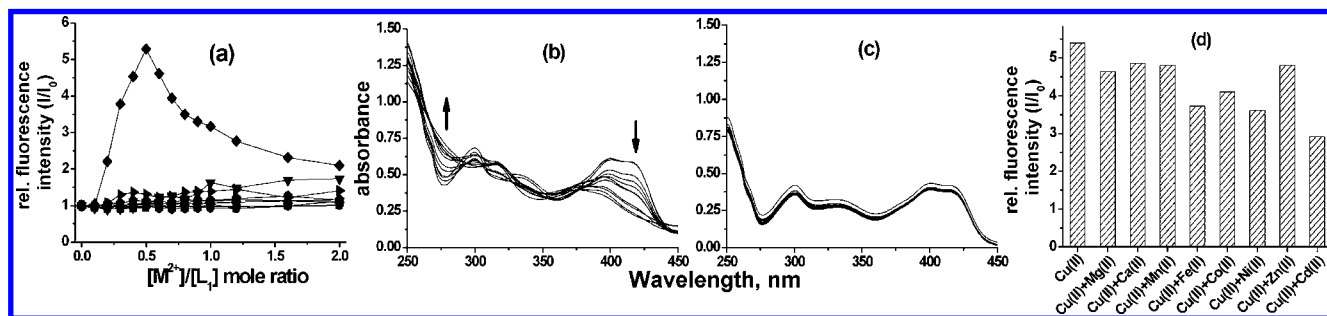
These studies were appropriately compared with those of the synthetic control molecular systems, $L_2$, $L_3$, and $L_4$ (Figure 2, Supporting Information, S1) to establish the role of imine and carbohydrate units in the sensor property of $L_1$.

Titration of $Cu^{2+}$ with $L_2$ in HEPES buffer showed no significant change in the fluorescence intensity, suggesting that the −HC=N− moiety in $L_1$ favors $Cu^{2+}$ binding over that in $L_2$ owing to the formation of a chelate in the case of $L_1$. The effect of such a chelation on the recognition of one metal ion over the other has been recently demonstrated in the case of calix[4]arene derivatives.[4] However, the titration with $Cu^{2+}$ resulted in an increase of $I/I_0$ to only 2.7 in the case of $L_3$ and to 2.3 in the case of $L_4$ (Figure 3a). These data suggest that the marginal increase observed in $I/I_0$ in the case of $L_3$ and $L_4$ can be explained on the basis of the presence of imine and naphthylic −OH moieties suitable for forming six-membered chelate and precludes the involvement of the carbohydrate moiety in $L_4$ in binding at least at the

(4) (a) Dessingou, J.; Joseph, R.; Rao, C. P. *Tetrahedron Lett.* **2005**, *46*, 7967. (b) Kumar, A.; Ali, A.; Rao, C. P. *J. Photochem. Photobiol., A Chem.* **2006**, *117*, 164.

**Figure 1.** (a) Plot of relative fluorescence intensity ($I/I_0$) vs $[M^{2+}]/[L_1]$ mole ratio in HEPES buffer. The symbols refer to: ■ ($Mg^{2+}$), ● ($Ca^{2+}$), ▲ ($Mn^{2+}$), ▼ ($Fe^{2+}$), triangle pointing left ($Co^{2+}$), triangle pointing right ($Ni^{2+}$), ◆ ($Cu^{2+}$), ♠ ($Zn^{2+}$), ● ($Cd^{2+}$). UV−vis absorption spectra measured in the titration of $M^{2+}$ with $L_1$ in HEPES buffer at different $[M^{2+}]/[L_1]$ mole ratios ranging from 0.0 to 2.0: (b) $Cu^{2+}$; (c) $Zn^{2+}$. (d) Histogram showing the relative fluorescence intensity ($I/I_0$) in the titration of $\{L_1 + 0.5$ equiv of $Cu^{2+}\}$ with $M^{2+}$. The concentration of the competitor metal ions used was $0-2.0$ equiv, and at the highest ratio, this comes out to be 4 mol equiv with respect to the copper.
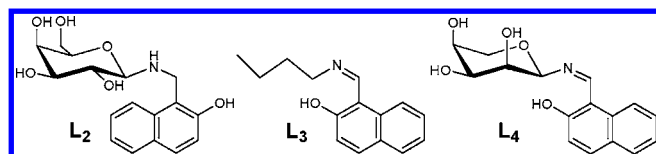


**Figure 2.** Schematic structures of the control molecules $L_2$, $L_3$, and $L_4$.
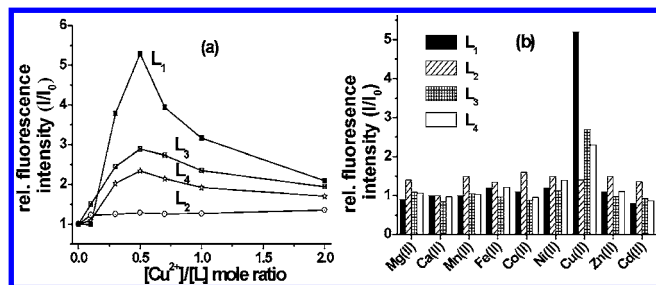


**Figure 3.** (a) Plot of $I/I_0$ vs $[Cu^{2+}]/[L]$ mole ratio in HEPES buffer (pH = 7.2). (b) Histogram indicating $I/I_0$ at the $[M^{2+}]/[L]$ mole ratio of 0.5 in the titration of $L_1$, $L_2$, $L_3$, and $L_4$ with different $M^{2+}$.

$[Cu^{2+}]/[L_4]$ mole ratio of 0.5. The sharp contrast observed in $I/I_0$ between $L_1$ and $L_4$ is attributable to the axial orientation of $C_2-OH$ in the case of ribosyl-based $L_4$. However, at the mole ratio of $[Cu^{2+}]/[L]$ beyond 0.5, a dinuclear copper species is favored in which the carbohydrate-$C_2-OH$ is involved in bridging. Thus, all these results obtained in the titrations of aqueous HEPES buffer support the involvement of the imine and the carbohydrate moieties present in $L_1$ in $Cu^{2+}$ recognition. Further, the titration of $Mg^{2+}$, $Ca^{2+}$, $Mn^{2+}$, $Fe^{2+}$, $Co^{2+}$, $Ni^{2+}$, $Zn^{2+}$, and $Cd^{2+}$ with the sensor molecule, $L_1$, and the control molecules, $L_2$, $L_3$, and $L_4$, under similar conditions in HEPES buffer did not alter the emission intensities to any significant extent (Figure 3b).

Because $Cu^{1+}$ is possible to be present in association with $Cu^{2+}$ in biological systems, the interaction of $Cu^{1+}$ with $L_1$ was studied. Titration of $L_1$ with $Cu^{1+}$ in HEPES buffer shows an increase in the fluorescence of the 356 nm band to an $I/I_0$ value of $3.0 \pm 0.5$, which is comparable with that observed with $Cu^{2+}$. The results of the $Cu^{1+}$ titration were confirmed by repeating the experiment four times. Further, in the titration of $Cu^{1+}$, the 440 nm band also exhibited similar behavior, but the peak $I/I_0$ value was only $1.5 \pm 0.1$, indicating a rather less significant change in this band. Thus, the fluorescence behavior of $Cu^{1+}$ with $L_1$ is almost the same as that of the $Cu^{2+}$ titration. To further confirm this, two additional sets of experiments were carried out. This includes titration of $[L_1 + 0.5$ equiv of $Cu^{2+}]$ with $Cu^{1+}$ and a reverse experiment, viz., titration of $[L_1 + 1.0$ equiv of $Cu^{1+}]$ with $Cu^{2+}$, where the results indicate that both of the ions were behaving similarly. This means that $L_1$ can be used to detect and/or measure the copper ions either as $1+$ or $2+$ or as a mixture. By combining these results, it is possible to conclude that the carbohydrate-based ligand ($L_1$) reported here can detect both $Cu^{2+}$ and $Cu^{1+}$ and hence can be very well suited for application in biological systems.

Titration of $L_3$ and $L_1$ with $Cu^{2+}$ was also carried out using Q-TOF ES MS. In the titration of $L_3$ with $Cu^{2+}$, besides the ligand molecular ion peak ($m/z = 228$), only a 2:1 (ligand/$Cu^{2+}$ ratio, $m/z = 516$) species was present at the 0.2 mole ratio of $Cu^{2+}$. At 0.5 mol equiv of $Cu^{2+}$, the 2:1 species further increased with the appearance of a small portion of 1:1 ($m/z = 289$). However, further addition of $Cu^{2+}$ in the titration exhibits a large increase in the 1:1 species whereas the 2:1 species does not increase any further as shown (Supporting Information, S6); the corresponding species formed are shown in Scheme 2a. Comparison of this with the fluorescence behavior indicates clearly that the fluorescing behavior of these species follows a trend, 1:1 > 2:1. In the titration of $L_3$ with $Cu^{2+}$, no traces of 2:2 species were formed.

In the titration of $L_1$ with $Cu^{2+}$, as the mole ratio of $Cu^{2+}$ increases from 0 to 0.2 to 0.5, the formation of 2:1 (ligand/$Cu^{2+}$ ratio, $m/z = 728$) species is increased considerably and

**Scheme 2** [a]
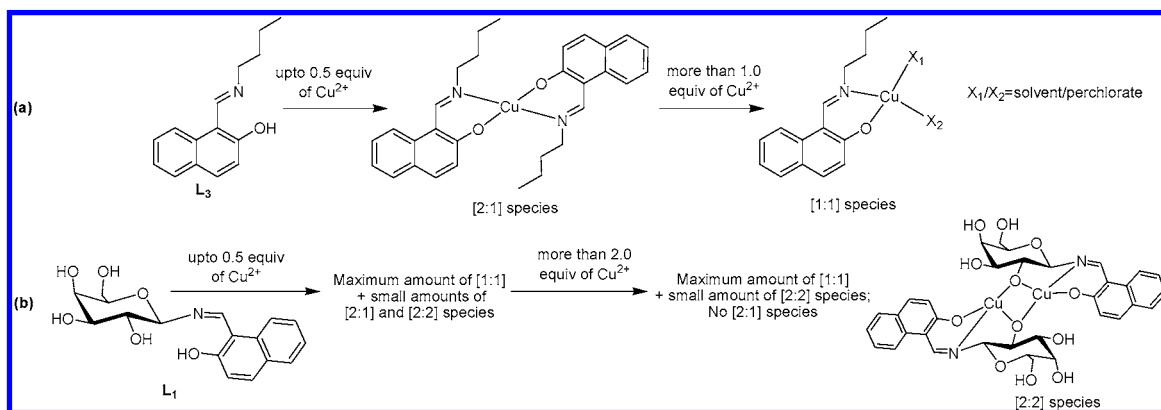
[a] Species formed based on the Q-TOF ES MS experiment: titration of (a) $L_3$ and (b) $L_1$ with $Cu^{2+}$.

decreases thereafter, and the species is completely absent at higher $Cu^{2+}$ mole ratios. On the other hand, the formation of 1:1 ($m/z = 395$) species increases as $Cu^{2+}$ is added and a steep increase is observed beyond the $Cu^{2+}$ mole ratio of 2.0. As the concentration of $Cu^{2+}$ increases, the formation of 2:2 ($m/z = 789$) species also increases, whereas the molecular ion peak of the ligand ($m/z = 334$) decreases progressively and disappears beyond 2 equiv of $Cu^{2+}$ addition. The isotopic pattern of the peaks resulting from the copper-bound species was consistent with the isotopes of copper and their abundance ratio. The extent of all these species can be clearly seen from the Supporting Information (S6), and the species formed are shown in Scheme 2b. Comparison of this with the fluorescence titration indicates clearly that the fluorescing behavior of these species follows a trend, 2:1 ≫ 2:2 > 1:1. The nature of the 1:1 species formed in the case of $L_1$ and $L_3$ could differ in the fact that the coordination in $L_3$ is simply bidentate, whereas $L_1$ can extend a pseudocoordination from the carbohydrate $C_2$−OH additionally. An optimized structure using hybrid density functional theory (B3LYP) with a basis set of LANL2DZ for $Cu^{2+}$ resulted in a $Cu^{2+} \cdots O_{carb}$ distance of 3.26 Å. The $Cu^{2+}$ is coordinatively unsaturated in both the 1:1 species, and to fill the coordination either the anion or the solvent, or both, will be used up. Although $L_1$ can give rise to 2:2 species, $L_3$ does not exhibit any such species. This contrasting behavior observed between $L_1$ and $L_3$ is explainable based on the fact that $L_1$ can form dinuclear species using its carbohydrate $C_2$−OH moiety, whereas $L_3$ cannot, owing to the presence of a butyl moiety instead of the carbohydrate moiety.

Synthetic reactions carried out between $M(OAc)_2 \cdot nH_2O$ and $L_1$ in MeOH resulted in the formation of {Cu($L_1$)(OAc)($H_2O$)$_2$}$_2$, **1**, and {Zn($L_1$)(OAc)(MeOH)$_2$}, **2**, and these exhibited fluorescence characteristics similar to those obtained in the solution titration studies reported here. The dinuclear Cu(II) complex, **1**, exhibits a spectrum that is in agreement with that obtained from the titration studies at the $[Cu^{2+}]/[L_1]$ mole ratio >1.0. Similarly, the absorption spectra of **1** and **2** agree well with those obtained at the

$[M^{2+}]/[L_1]$ mole ratio >1.0 (Supporting Information, S5). The 2:2 dinuclear complex proposed for **1** was supported by crystal structure determinations of 4,6-di-$O$-protected-D-glucopyranosylamine derivatives where the $Cu_2O_2$ core was stabilized by two intramolecular H-bonds utilizing equatorial $C_2$−OH of the carbohydrate.[5] The presence of equatorial $C_2$−OH is still retained in $L_1$ (galactosyl based) but not in $L_4$ (ribosyl based), and hence, $L_1$ stands as a better molecule for sensing $Cu^{2+}$.

Although the carbohydrate-based metal ion sensor molecules are scarce in the literature, $L_1$ stands as a unique molecular system that works well (by exhibiting a 7-fold increase in the quantum yield) in detecting very low concentrations of $Cu^{2+}$ even in the presence of other biological metal ions under physiological pH. Also demonstrated were the merits of $L_1$ against three control molecules, the involvement of the carbohydrate moiety in metal ion recognition, the binding characteristics and the detection of copper-bound species, recognition of $Cu^{1+}$, and the switch-on behavior in the presence of $Cu^{2+}$. Thus, the galactosyl-based $L_1$ may offer its utility for studying $Cu^{2+}$ in biological samples even in association with other metal ions as well as $Cu^{1+}$, as no such synthetic glyco-conjugate sensor is known to date for transition metal ions.

**Supporting Information Available:** Synthesis, characterization, and experimental details (S1); fluorescence and absorption in MeOH (S2 and S3); fluorescence in HEPES buffer (S4); **1** and **2** (S5); and mass spectral data for $Cu^{2+}$ titration (S6). This material is available free of charge via the Internet at http://pubs.acs.org.

OL061274F

(5) (a) Rajsekhar, G.; Sah, A. K.; Rao, C. P.; Guionneau, P.; Bharathy, M.; GuruRow, G. N. *Dalton Trans.* **2003**, 3126. (b) Sah, A. K.; Rao, C. P.; Saarenketo, P. K.; Rissannen, K.; van Albada, G. A.; Reedijk, J. *Chem. Lett.* **2002**, 348.

# Experimental and Computational Studies of Selective Recognition of Hg²⁺ by Amide Linked Lower Rim 1,3-Dibenzimidazole Derivative of Calix[4]arene: Species Characterization in Solution and that in the Isolated Complex, Including the Delineation of the Nanostructures

Roymon Joseph, Balaji Ramanujam, Amitabha Acharya, Anupam Khutia, and Chebrolu P. Rao*

*Department of Chemistry Indian Institute of Technology Bombay, Powai, Mumbai 400076, India*

*cprao@iitb.ac.in*
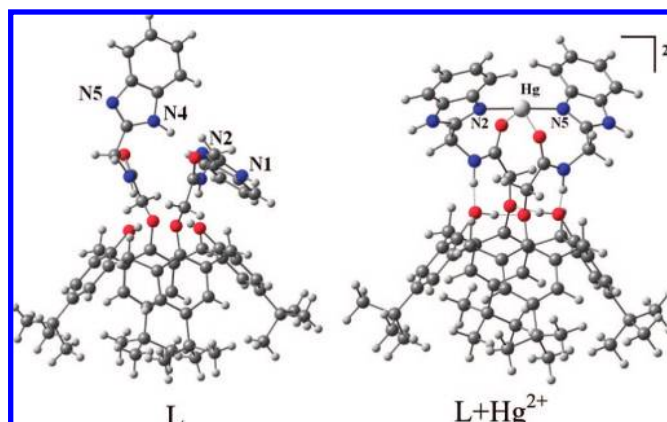
Amide linked lower rim 1,3-dibenzimidazole derivative of calix[4]arene, L has been shown to be sensitive and selective to Hg²⁺ in aqueous acetonitrile solution based on fluorescence spectroscopy, and the stoichiometry of the complexed species has been found to be 1:1. The selectivity of L toward Hg²⁺ has been shown among 11 M²⁺ ions, viz., Mn²⁺, Fe²⁺, Co²⁺, Ni²⁺, Cu²⁺, Zn²⁺, Cd²⁺, Hg²⁺, Pb²⁺, Ca²⁺, and Mg²⁺ studied, including those of the mercury group and none of these ions impede the recognition of Hg²⁺ by L. Role of the solvent on the recognition of Hg²⁺ has been demonstrated. The role of calix[4]arene platform and the benzimidazole moieties in the recognition of Hg²⁺ by L has been delineated upon performing such studies with five different molecules of relevance as reference molecular systems. The binding cores formed by the receptor L and the reference compounds have been established based on the single crystal XRD structures, and the preferential metal ion binding cores have been discussed. The binding of Hg²⁺ with L has been further established based on ¹H and ¹³C NMR, ESI MS, absorption, and fluorescence lifetime measurements. Some of these techniques have been used to establish the stoichiometry of the species formed. The complex species formed between L and Hg²⁺ have been isolated and characterized and found to be 1:1 species even in the isolated complex. Whereas transmission electron microscopy (TEM), atomic force microscopy (AFM), and scanning electron microscopy (SEM) provided the nanostructural behavior of L, the TEM and SEM demonstrated that the mercury complex has different characteristics when compared to L. The TEM, SEM, and powder XRD studies revealed that whereas L is crystalline, that of the mercury complex is not, perhaps a reason for not being able to obtain single crystals of the complex. Binding characteristics of Hg²⁺ toward L have been established based on the DFT computational calculations.

## Introduction

Supramolecular systems like calixarenes[1] functionalized with suitable metal ion binding cores can act as good hosts for the recognition of metal ions.[2] Among these the well studied were those based on calix[4]arene. However, the calix[4]arene based

molecular systems were rather scarce in the literature in detecting toxic, nonradioactive as well as volatile heavy metallic element, such as, mercury.[3] Though there are several other molecular systems for sensing Hg²⁺, calix[4]arene based ones are scarce in the literature and include upper rim functionalized with aryl-azo group[4] and lower rim calix[4]aza-crown derivatives possessing different fluorescent probes including those of dansyl groups.[5] These are generally studied in various organic

**SCHEME 1. Synthesis of the Receptor Molecule, L[a]**
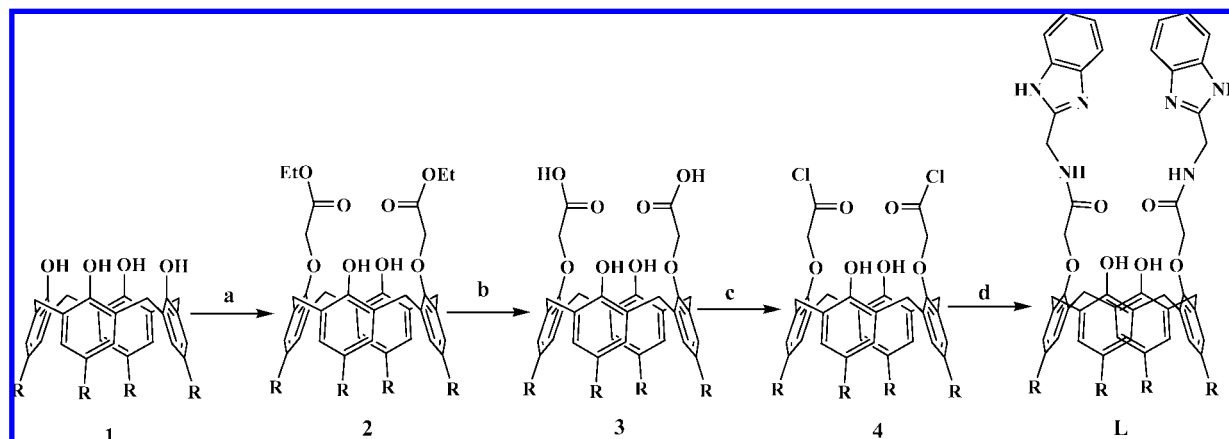


[a] Synthesis of lower rim calix[4]arene-1,3-diderivatives, L: (a) bromoethylacetate/$K_2CO_3$/ acetone; (b) NaOH/$C_2H_5OH$, reflux; (c) $SOCl_2$/benzene, reflux; (d) 2-aminomethylbenzimidazole/$Et_3N$/THF. R = tert-butyl.

solvents and those studied in aqueous medium were limited. Therefore, the development of molecular systems that can selectively recognize $Hg^{2+}$ continues to intrigue researchers. In this regard, we report the development of a biologically relevant benzimidazole attached lower rim 1,3-diderivative of calix[4]arene (L), connected through amide links for the purpose of selectively recognizing $Hg^{2+}$ in aqueous solution. The data has been compared with that of the judiciously selected reference molecules. The binding cores of the receptor and reference molecules have been established by structure determination. The present studies include the delineation of all its properties suitable for selective recognition of $Hg^{2+}$ in aqueous solution, and also the isolation and characterization of the species formed. Nanostructural difference between the L and its mercury complex has been demonstrated. The nature of the mercury complex has been addressed by DFT computational calculations.

## Results and Discussion

The selective recognition of $Hg^{2+}$ by the receptor molecule, L in aqueous solution has been demonstrated primarily using fluorescence spectroscopy and has been further supported by

other techniques, such as, absorption, NMR, and ESI MS. The selectiveness of L has been convincingly demonstrated upon comparing the data obtained from similar studies carried out with appropriately chosen reference molecular systems.

**Receptor Molecule (L).** The receptor molecule, L, has been synthesized in four known steps[6] (Scheme 1). The reaction of **1** with bromoethylacetate results in the formation of 1,3-diester derivative, **2**, and its hydrolysis yielded the corresponding diacid derivative, **3**. The diacid, **3**, when treated with $SOCl_2$ resulted in the formation of diacid chloride, **4**, and this upon coupling with 2-aminomethylbenzimidazole resulted in the receptor molecule, L. All the compounds exhibited satisfactory analytical and spectral data as given in the Experimental section.

**Reference Molecules ($L_1$, $L_2$, $L_3$, $L_4$, and $L_5$).** The reference compounds, $L_1$, $L_2$, $L_3$, $L_4$, and $L_5$ (Figure 1) have been selected keeping in mind the importance or necessity of different chemical units present in L including that of the calixarene platform. Therefore, this resulted in choosing the molecules, such as, simple 2-aminomethyl benzimidazole ($L_1$) without having the calixarene platform, calix-amide without possessing benzimidazole moieties ($L_2$), pyridyl derivative ($L_3$) that could mimic the benzimidazole unit only in part as far as the nitrogen coordination center is concerned, calix-amide derivative possessing only the hydrophobic moiety ($L_4$) but not the coordination centers and the benzimidazole derivative of only p-tert-butylphenol without having the total calixarene framework ($L_5$). Whereas $L_1$ was purchased, $L_2$, $L_3$, and $L_4$ were synthesized by reacting **4** with the appropriate amine moiety, viz., dibenzylamine, 2-aminomethylpyridine and methyl ester of phenylalanine respectively to result in $L_2$, $L_3$, and $L_4$. $L_5$ has been synthesized starting from p-tert-butyl-phenol followed by ester,

(1) (a) Gutsche, C. D. *Calixarenes*; Royal Society of Chemistry: Cambridge, U.K., 1989. (b) Rao, C. P.; Dey, M. *Encycl. Nanosci. Nanotech.* **2004**, *1*, 475.

(2) (a) Lee, Y. O.; Choi, Y. H.; Kim, J. S. *Bull. Korean Chem. Soc.* **2007**, *28*, 1–151. (b) Quang, D. T.; Jung, H. S.; Yoon, J. H.; Lee, S. Y; Kim, J. S. *Bull. Korean Chem. Soc.* **2007**, *28*, 682. (c) Dalbavie, J.-O.; Regnouf-de-Vains, J.-B; Lamartine, R.; Perrin, M.; Lecocq, S.; Fenet, B. *Eur. J. Inorg. Chem.* **2002**, 901. (d) Belhamel, K.; Nguyen, T. K. D.; Benamor, M.; Ludwig, R. *Eur. J. Inorg. Chem.* **2003**, 4110. (e) Kim, S. K.; Kim, S. H.; Kim, H. J.; Lee, S. H.; Lee, S. W.; Ko, J.; Bartsch, R. A.; Kim, J. S. *Inorg. Chem.* **2005**, *44*, 7866. (f) Lee, S. H.; Kim, J. Y.; Ko, J.; Lee, J. Y.; Kim, J. S. *J. Org. Chem.* **2004**, *69*, 2902. (g) Kim, S. K.; Lee, S. H.; Lee, J. Y.; Lee, J. Y.; Bartsch, R. A.; Kim, J. S. *J. Am. Chem. Soc.* **2004**, *126*, 16499. (h) Kim, J. S.; Shon, O. J.; Rim, J. A.; Kim, S. K.; Yoon, J. *J. Org. Chem.* **2002**, *67*, 2348. (i) Kim, J. S.; Noh, K. H.; Lee, S. H.; Kim, S. K.; Kim, S. K.; Yoon, J. *J. Org. Chem.* **2003**, *68*, 597. (j) Lee, J. Y.; Kim, S. K.; Jung, J. H.; Kim, J. S. *J. Org. Chem.* **2005**, *70*, 1463. (k) Choi, J. K.; Kim, S. H.; Yoon, J.; Lee, K.-H.; Bartsch, R. A.; Kim, J. S *J. Org. Chem.* **2006**, *71*, 8011. (l) Kim, J. S.; Kim, H. J.; Kim, H. M.; Kim, S. H.; Lee, J. W.; Kim, S. K.; Cho, B. R. *J. Org. Chem.* **2006**, *71*, 8016. (m) Liang, Zhi.; Liub; Gao, Y *Tetrahedron Lett.* **2007**, *48*, 3587. (n) Banthia, S.; Samanta, A. *Org. Biomol. Chem.* **2005**, *3*, 1428. (o) Chang, K.-C.; Su, I.-H; Senthilvelan, A.; Chung, W.-S. *Org. Lett.* **2007**, *9*, 3363. (p) Ozturk, G.; Akkaya, E. U. *Org. Lett.* **2004**, *6*, 241. (q) Bu, J.-H.; Zheng, Q.-Y.; Chen, C.-F.; Huang, Z.-T *Org. Lett.* **2004**, *6*, 3301. (r) Cao, Y.-D.; Zheng, Q.-Y.; Chen, C.-F.; Huang, Z.-T *Tetrahedron Lett.* **2003**, *44*, 4751. (s) Saiki, T.; Iwabuchi, J.; Akine, S.; Nabeshima, T. *Tetrahedron Lett.* **2004**, *45*, 7007. (t) Kim, S. H.; Choi, J. K.; Kim, S. K.; Simb, W.; Kim, J. S. *Tetrahedron Lett.* **2006**, *47*, 3737. (u) Praveen, L.; Ganga, V. B.; Thirumalai, R.; Sreeja, T.; Reddy, M. L. P.; Varma, R. L. *Inorg. Chem.* **2007**, *46*, 6277. (v) Kim, J. S.; Quang, D. T. *Chem. Rev.* **2007**, *107*, 3780.

(3) (a) Renzoni, A.; Zino, F.; Franchi, E. *Environ. Res.* **1998**, *77*, 68. (b) Boening, D. W. *Chemosphere* **2000**, *40*, 1335.

(4) (a) Kao, T.-L.; Wang, C.-C.; Pan, Y.-T.; Shiao, Y.-J.; Yen, J.-Y.; Shu, C.-M.; Lee, G.-H.; Peng, S.-M.; Chung, W.-S. *J. Org. Chem.* **2005**, *70*, 2912. (b) Ho, I.-T.; Lee, G.-H.; Chung, W.-S. *J. Org. Chem.* **2007**, *72*, 2434.

(5) (a) Talanova, G. G.; Elkarim, N. S. A.; Talanov, V. S.; Bartsch, R. A. *Anal. Chem.* **1999**, *71*, 3106. (b) Choi, M. J.; Kim, M. Y.; Kim, J. R.; Chang, S.-K. *Chem. Lett.* **2000**, 1432. (c) Choi, M. J.; Kim, M. Y.; Chang, S.-K. *Chem. Commun.* **2001**, 1664. (d) Cha, N. R.; Kim, M. Y.; Kim, Y. H.; Choe, J.-I.; Chang, S.-K. *J. Chem. Soc., Perkin Trans.* **2002**, *2*, 1193. (e) Kim, J. H.; Hwang, A.-R.; Chang, S.-K. *Tetrahedron Lett.* **2004**, *45*, 7557. (f) Chen, Q.-Y.; Chen, C.-F. *Tetrahedron Lett.* **2005**, *46*, 165. (g) Me′tivier, R.; Leray, I.; Lebeau, B.; Valeur, B. *J. Mater. Chem.* **2005**, *15*, 2965. (h) Me′tivier, R.; Leray, I.; Valeur, B. *Chem.—Eur. J.* **2004**, *10*, 4480.

(6) Collins, E. M.; McKervey, M. A.; Madigan, E.; Moran, M. B.; Owens, M.; Ferguson, G.; Harris, S. J. *J. Chem. Soc., Perkin Trans. 1* **1991**, 3137.
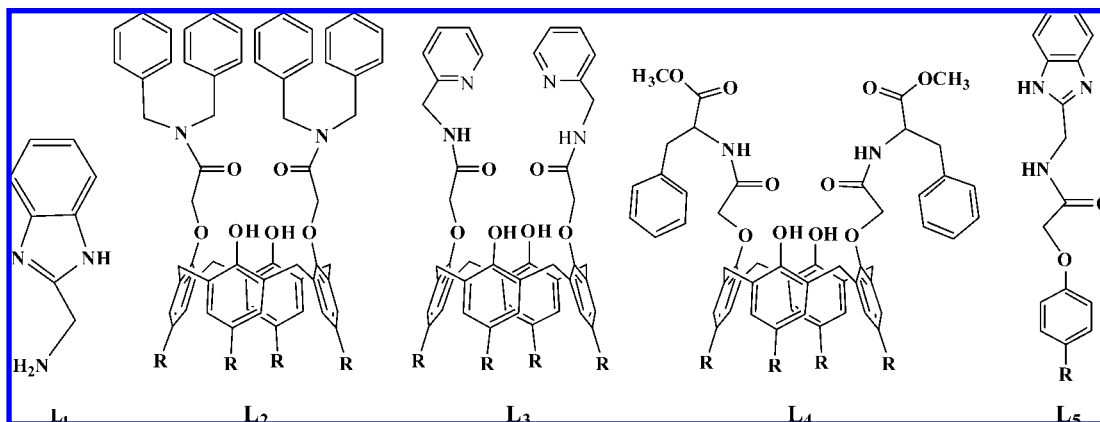
**FIGURE 1.** Schematic structures of reference compounds, $L_1$, $L_2$, $L_3$, $L_4$, and $L_5$. R = tert-butyl.

**TABLE 1. Crystallographic Parameters for the Structure Determination and Refinement**[a]

| | $L_2$ | $L_4$ | L |
|---|---|---|---|
| Empirical Formula | $C_{76}H_{86}N_2O_6 \cdot 2(CHCl_3)$ | $2(C_{68}H_{82}N_2O_{10}) \cdot H_2O$ | $C_{64}H_{74}N_6O_6 \cdot 3(C_2H_5OH)$ |
| Temperature (K) | 293 | 120 | 150 |
| Crystal System | Triclinic | Monoclinic | Triclinic |
| Space group | P$\bar{1}$ (No. 2) | $P2_1$ (No. 4) | P$\bar{1}$ (No. 2) |
| a/Å | 10.164(5) | 14.4663(4) | 13.1060(14) |
| b/Å | 16.251(5) | 26.1325(7) | 13.467(4) |
| c/Å | 23.654(5) | 17.0631(5) | 21.4629(19) |
| $\alpha$/° | 97.756(5) | 90 | 76.369(16) |
| $\beta$/° | 99.898(5) | 96.133(3) | 74.335(9) |
| $\gamma$/° | 96.042(5) | 90 | 73.248(16) |
| Volume/Å³ | 3781(2) | 6413.6(3) | 3441.1(12) |
| Z | 2 | 2 | 2 |
| Reflections collected | 17477 | 66808 | 34518 |
| Independent reflections | 10676 | 22341 | 11985 |
| $R_{int}$ | 0.037 | 0.103 | 0.042 |
| Reflections used[b] | 6350 | 13689 | 6118 |
| Parameters | 873 | 1478 | 797 |
| Final R | 0.0736 | 0.0863 | 0.0710 |
| $R'$[c] | 0.2255 | 0.1814 | 0.2260 |

[a] Structure of $L_3$ has been reported by us earlier (ref 7). [b] = [I > 2.0 σ(I)] [c] = $1/[s^2(F_o^2) + (0.1133P)^2 + 1.8869P]$ where $P = (F_o^2 + 2F_c^2)/3$.

then acid and its coupling to give the amide derivative of benzimidazole. All these derivatives were characterized by NMR, FTIR, and mass spectroscopy as given in the Experimental section. The ¹H NMR data for the receptor and reference compounds clearly suggested cone-conformation for calix[4]arene moiety in case of these derivatives and were further confirmed based on single crystal X-ray structure determinations. The role of calix[4]arene platform in conjunction with the benzimidazole core in the selective recognition of Hg²⁺ by L has been demonstrated in this paper by comparing the results obtained in case of L with those obtained with the reference compounds.
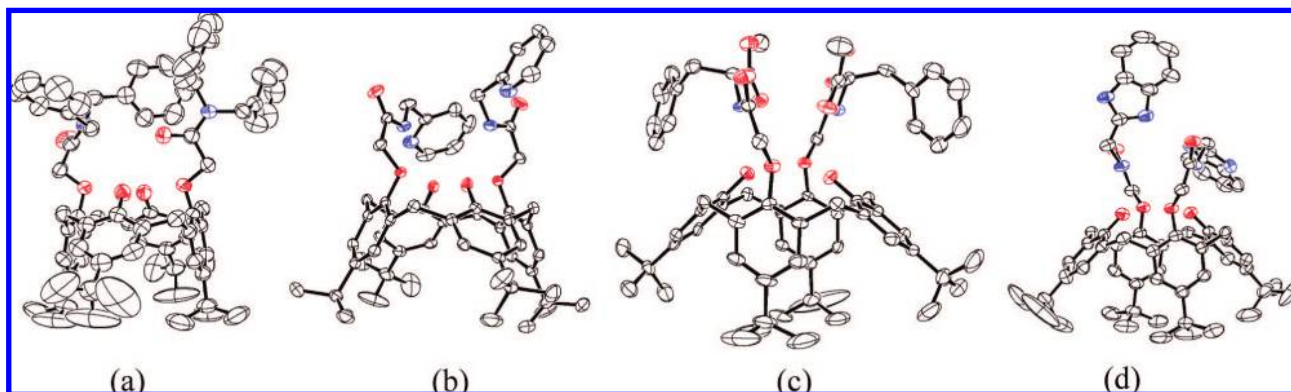
**Single Crystal X-Ray Structures of the Reference and Receptor Molecules.** Single crystal X-ray structural analysis were carried out in case of $L_2$, $L_3$, $L_4$, and L and the corresponding details of the structure determination and refinement are given in Table 1. All the crystal structures confirmed the formation of 1,3- arms through the amide linkages disposed on the same side of the calix[4]arene at the lower rim to result in binding cores and the nature of the conformation of calix[4]arene was found to be the cone, as has also been demonstrated based on NMR studies (Figure 2).

In all these lower-rim diderivatives, there are two intrarim O–H···O hydrogen bonds present to maintain the cone conformational structure. The conformation of the strands in $L_3$, $L_4$, and L are similar up to the amide NH and conformations

do change beyond these among the different structures. $L_2$ cannot show this because the amide group in this case does not have any hydrogen attached to its nitrogen center. The stereoviews and the metric data of all these structures are given in the Supporting Information, S1. The main conformational angles of both the arms are given in Table 2 for $L_2$, $L_3$, $L_4$, and L based on their single crystal XRD structures.

As can be noted from the structure of $L_2$ (Figure 2a), both the arms exhibited different conformations. One of the arms is more bent than the other as can be judged from the intrastrand O···N distances, viz., 3.009 vs 3.561 Å, and also from the intrastrand O–C–C–N dihedral angle, viz., −71.5 vs −159.6°. As a result of this the N to OH(phenolic) distances are 4.26 to 4.50 Å on the bent side and 5.27 to 5.50 Å on the other side, indicating that the strands are reasonably normal to the lower rim and hence are away from extending any H-bond interaction between the N and phenolic-OH moieties. This may be a result of the absence of hydrogen on amide nitrogen.

In the crystal structure of $L_3$[7] (Figure 2b), both the strands were bent to almost the same extent as can be judged from the intrastrand O–C–C-N dihedral angles, viz., 12.2 vs 19.6°, so that N–H of the amide groups form hydrogen bond with the lower-rim phenolic −OH groups. The resulting N–H···O hydrogen bonds have N···O distances of 2.955 and 3.027 Å and N–H···O angle of 171.5 and 172.2°. Molecule $L_3$

**FIGURE 2.** ORTEP views of the molecular structures as obtained from their single crystal XRD: (a) $L_2$; (b) $L_3$, (c) $L_4$, and (d) L.

**TABLE 2.** Selected Dihedral Angles of Both the Arms Based on the Crystal Structures of Receptor and Reference Molecules

| dihedral angle[a] | L | | L₂ | | | L₃ | | L₄ | |
|---|---|---|---|---|---|---|---|---|---|
| D1 | 149.0 | 151.4 | −155.5 | −172.7 | −162.7 | −142.7 | −149.3 | −153.4 | |
| D2 | −9.2 | −21.1 | −71.4 | −159.6 | 19.6 | 12.2 | 19.9 | 19.7 | |
| D3 | −168.5 | −169.7 | 4.3, −174.9 | 177.0, −10.4 | −178.1 | 173.4 | −177.3 | −175.2 | |
| D4 | −62.0 | −179.7 | −102.9, −105.1 | 99.0, 111.7 | −83.6 | −178.3 | −84.1, 151.6 | −96.0, 141.5 | |

[a] The dihedral angles D1 to D4 are sequential ones starting from the calixarene lower rim carbon. D1 = $C_{cal}$–O–$CH_2$–CO; D2 = O–$CH_2$–CO–N; D3 = $CH_2$–CO–N–$CH_2$; D4 = CO–N–C–C.

crystallizes along with a molecule of methanol. The methanol molecule extends a hydrogen bond with the pyridyl nitrogen of one of the arms with a O···N distance of 2.881 Å and O−H···N angle of 173.3° and is also in hydrogen bonding distance with that of the phenolic-OH exhibiting a O···O distance of 3.153 Å. Though both the strands are on the same side, the two strands differ in their $C−N−C−C_{py}$ dihedral angle, viz., −83.6 vs −178.3°, and this results in a large separation between two pyridyl nitrogens, viz., 7.720 Å though the amide nitrogens were disposed close by 3.576 Å, and hence is suited as an $N_4$ binding core. Therefore, a conformational change is a prerequisite if $L_3$ should act as tetradentate ligand which can use four nitrogens for binding to metal ions. On the other hand, each of the strand is independently capable of forming a bidentate $N_2$ binding core to two different metal ions meaning that two different $N_2$ cores being formed instead of an $N_4$ core.

In case of $L_4$, two molecules are present in the asymmetric unit cell where these are related by a pseudo 2-fold axis thereby resulting in a head-to-tail arrangement of these. Both the strands of $L_4$ exhibit similar dihedral angles indicating similar conformation for both the strands and the same is true for the other molecule too. Even $L_4$, like that in $L_3$, both the strands exhibit intramolecular hydrogen bonds between amide N−H and phenolic-OH groups with N···O distances of 3.041 and 2.996 and hydrogen bond angles of 172.8 and 176.9°. As a result of this a $N_2O_2$ core that is suitable for binding metal ion is being formed using the carbonyl oxygens of the ester moieties. The phenyl moieties are oriented away from the core region. Molecule $L_4$ can also exhibit an $N_2O_6$ (Figure 2c) wherein metal ions such as lanthanide may perhaps fit well with some adjustment in the cavity. Thus, there are two possible cores formed in $L_4$: whereas the $N_2O_2$ is at the top portion, the $N_2O_6$ is closer to the lower rim.

In the structure of the receptor molecule, L (Figure 2d), the conformations of the both the strands are different from each other

(7) Rao, P. V.; Rao, C. P.; Kolehmainen, E.; Wegelius, E. K.; Rissanen, K. *Chem. Lett.* **2001**, 1176.

as can be judged from the dihedral angles about C−N−C-C(im) (−179.7 vs −62.1°) and N−C−C(im)-N(H) (−80.1 vs 23.5°). As a result, one of the benzimidazole moieties is aligned along the pseudo 2-fold vertical axis of the calix[4]arene while the other is perpendicular to the axis. Thus while one of the imidazole units is perpendicular to the plane of the lower rim, the other is parallel to it. But the amide N−H in both these is hydrogen bonded to the phenolic O−H groups with N···O distances of 3.050, 3.036 Å and hydrogen bond angle of 163.3 and 169.0°. The two benzimidazole moieties are connected through a strong N−H···N hydrogen bond with N···N distance of 2.863 Å and hydrogen bond angle of 179.8°. This kind of an arrangement results in the formation of $N_4$ core that can be fitted to a distorted tetrahedron, unlike that observed in case of the pyridyl derivative, $L_3$. Formation of an $N_4$ core at the top edge of the calixarene derivative of L is attributed to the presence of two nitrogen centers in the imidazole moiety. At the lower rim, L also exhibits another core of $N_2O_4$ that can accommodate metal ion. Each L is crystallized along with three ethanol molecules. One of these ethanol units extends a O−H···N hydrogen bond with the imidazole nitrogen of one of the strands where the benzimidazole was parallel to the plane of the lower rim.

Thus among all these structures, it is the L that exhibits an $N_4$ based core readily at the lower-rim top portion of the molecule, and a some what less accessible core of $N_2O_2$ is observed with the structure of $L_4$. All others do not have significant cores that can easily accommodate metal ion, however, $L_3$ can accommodate metal ion upon some changes in its conformation wherein the two pyridyl nitrogen centers are brought into the inside of the core. These features are evident from the space filling models shown in Figure 3. Of course all the structures have similar hydrophobic cavity.

Thus, in the structures of these free ligands, the ligation centers arising from the arms are not always oriented well in a fashion to bind to the metal ion directly, rather requires some conformational changes before it can bind to a metal ion. Such arrangement may bring preference in the interaction toward one
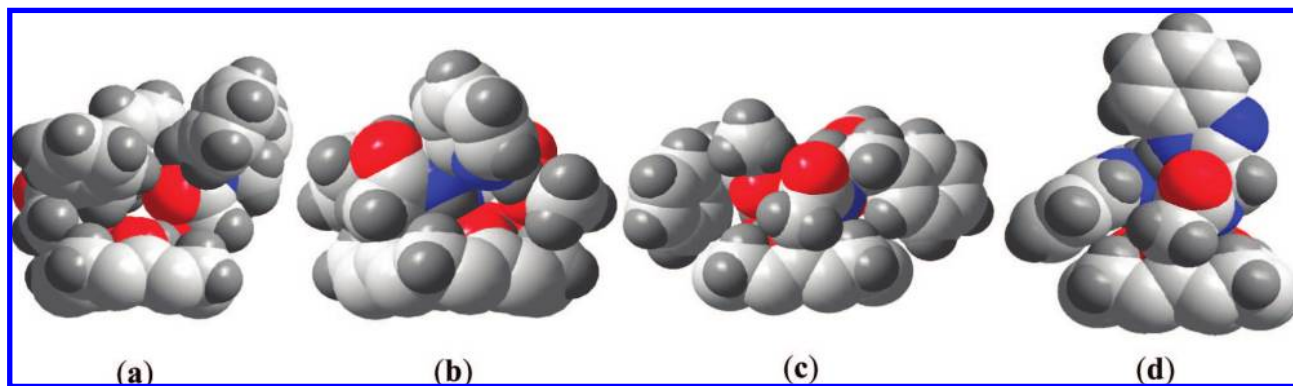
**FIGURE 3.** Space filling models generated from the corresponding crystal structure data: (a) L₂, (b) L₃, (c) L₄, and (d) L. The arene framework of the calixarene base has been removed for clarity.
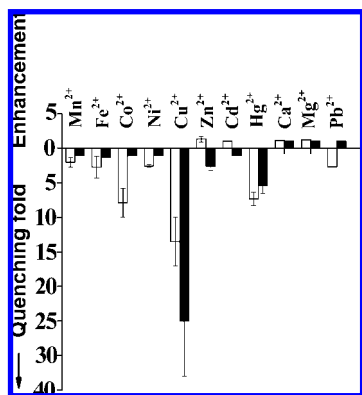


**FIGURE 4.** Histogram showing the number of times of quenching in the fluorescence intensity in case of titration of L with different M²⁺. Open columns are for the CH₃CN and the filled columns are for CH₃OH. Error bars were given based on four different measurements.

metal ion over the other and hence these can be explored for their possible selectivity. Results of the corresponding studies are reported in this paper.

**Solution Metal Ion Binding Studies.** Divalent ions (M²⁺) such as, Mn²⁺, Fe²⁺, Co²⁺, Ni²⁺, Cu²⁺, Zn²⁺, Cd²⁺, Hg²⁺, Pb²⁺, Ca²⁺, and Mg²⁺ were studied for their interaction with the molecular systems reported in this paper by fluorescence spectroscopy. Influence of the solvent on such interactions has also been explored. The receptor selectivity of L was discussed in the light of such data obtained with respect to the reference molecules. Further, the species of selective recognition were characterized both in solution as well as in its isolated state including their nanostructural changes and supported the results of titration.

**Fluorescence Titration of L with M²⁺ in Organic Solvents.** In acetonitrile, when L is excited at 275 nm it exhibits a strong emission maximum around 311 nm. Therefore the fluorescence emission has been used as a handle for studying the interaction of metal ions. The titration of L with M²⁺ in CH₃CN showed fluorescence quenching toward all ions except Zn²⁺, Ca²⁺ and Mg²⁺, wherein the quenching follows a trend, viz., Cu²⁺ ≫ Co²⁺ > Hg²⁺ > Mn²⁺ ≅ Fe²⁺ ≅ Ni²⁺ as reported in Figure 4 (Supporting Information, Figure S2). On the other hand, similar titrations carried out in CH₃OH also exhibited quenching with a number of ions and the trend in the fluorescence quenching has been noted to be Cu²⁺ ≫ Hg²⁺ > Zn²⁺ > Fe²⁺ as given in Figure 4 (Supporting Information, Figure S2). Though L seems to differentiate metal ions better in CH₃OH than in CH₃CN, there is still no selectivity in any of

these solvents toward any one metal ion because either in CH₃OH or in CH₃CN more than one metal ion shows changes in the fluorescence of L. Hence aqueous−organic solutions have been employed for further studies, since such combination is expected to bring changes in the polarity of the medium and the solvation of the metal ion.

**Fluorescence Titration of L with M²⁺ in Aqueous Solutions.** To change the polarity of the acetonitrile, different volume ratios of water was added to result in water to acetonitrile ratios of 1:3, 1:1 and 3:2, and the fluorescence titrations between L and M²⁺ were carried out in these aqueous solutions. Typical fluorescence spectra obtained during the titration of L with Hg²⁺ in 50% aqueous solution and the corresponding fluorescence intensity ratio plot were given in Figure 5a,b. The extent of fluorescence quenching is defined in terms of the quenching fold and the corresponding results obtained from such titrations performed between the L and M²⁺ in aqueous acetonitrile mixtures were shown in Figure 5c (Supporting Information, Figure S3).

In 50% aqueous solution, a 10-fold quenching was observed only in case of Hg²⁺, whereas all other M²⁺ exhibited almost no quenching in fluorescence intensity. However, when the content of water was either low (1:3) or high (3:2), the sensitivity of Hg²⁺ detection decreases and a recognizable response is shown even in case of the Cu²⁺, as a result the selectivity seem to be decreasing at least to some extent (Figure 5c). The species formed between L and Hg²⁺ has been found to be 1:1 based on absorption and ESI MS studies as reported in this paper. Even the Job's plot constructed with the fluorescence data supported the formation of 1:1 complex between Hg²⁺ and L (Supporting Information, Figure S4). Based on the Benesi-Hildebrand equation, the $K_{ass}$ was found to be 20 966 ± 873 M⁻¹. Significant fluorescence intensity changes were observed only in case of the titration of L with Hg²⁺ and not with the other M²⁺ in 1:1 aqueous acetonitrile solution. Hence the 1:1 aqueous solution is well suited for the selective recognition of Hg²⁺ by L. Unlike some of those reported in the literature where a large number of equivalents of Hg²⁺ is required for the formation of 1:1 complex,[5] the present study refers to a stoichiometric titration (Figure 5b). Fluorescence studies performed in 1:1 aqueous solution by varying [Hg²⁺] but keeping the [Hg²⁺]/[L] mole ratio at 1:1 indicated a lower limit detection of 1.4 ± 0.1 ppm or less that is accompanied by a decrease in the fluorescence intensity of L by about 10−12% (Supporting Information, Figure S4). Comparison of the fluorescence data obtained among all these different solvent systems clearly
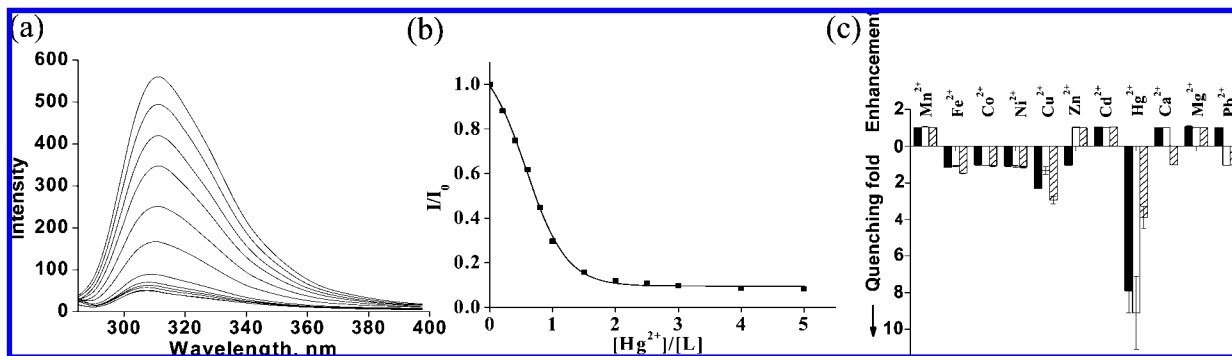
**FIGURE 5.** (a) Fluorescence spectral traces obtained during the titration of L with $Hg^{2+}$ in 1:1 aqueous acetonitrile. (b) Plot of $I/I_0$ as a function of $[Hg^{2+}]/[L]$ mole ratio. (c) Histogram showing the number of times of quenching of fluorescence intensity in case of titration of L with different $M^{2+}$ in aqueous acetonitrile solutions. Open columns are for the data in $H_2O:CH_3CN$ of 1:1. Filled columns are for the data in $H_2O:CH_3CN$ of 1:3. Partially filled columns are for the data in $H_2O:CH_3CN$ of 3:2. Error bars were given based on four different measurements.
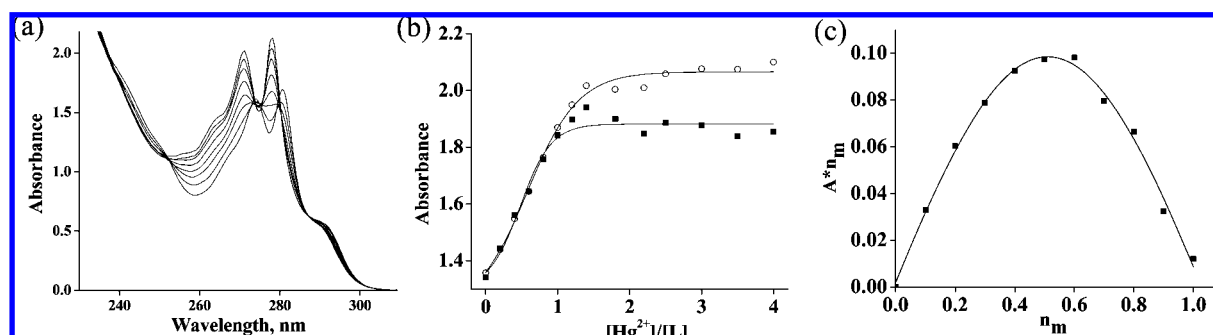


**FIGURE 6.** Titration of L with $Hg^{2+}$ in 50% aqueous acetonitrile: (a) Absorption spectral traces; (b) Plot of absorbance vs mole ratio of $Hg^{2+}$ added, 271 nm band (○), 277 nm band (■), (c) Job's plot of $n_m$ vs $A*n_m$, where $n_m$ is mole fraction of the metal ion added and $A$ is absorbance.
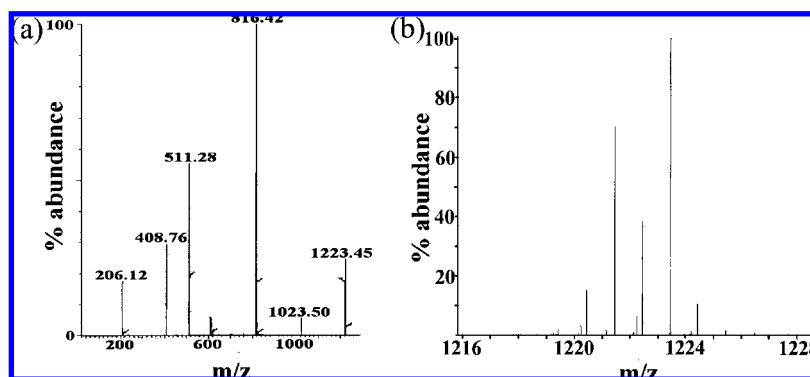


**FIGURE 7.** (a) ESI mass spectrum showing the molecular ion peak for the 1:1 complex formed between L and $Hg^{2+}$ during titration. (b) Expansion of the molecular ion peak.

suggest that while L retained its sensitivity toward $Hg^{2+}$ in all the aqueous acetonitrile solutions, it is highly selective in 50% aqueous solution implying that L can be a selective receptor for $Hg^{2+}$ in aqueous solution. The binding of $Hg^{2+}$ with L has been further confirmed based on the titrations performed using absorption, ESI MS, and NMR.

**Absorption Spectral Studies of L with $Hg^{2+}$.** To confirm the binding of $Hg^{2+}$ with L, absorption spectral studies were carried out for the titration of $Hg^{2+}$ with L in 1:1 aqueous solution. The spectral changes and the isosbestic point observed at 252 and 286 nm in the titration clearly indicate transition between the ligand and the complexed species. Quantitative changes observed in two absorption bands are suggestive of stoichiometric reaction between L and $Hg^{2+}$. The corresponding Job's plot fits very well with the formation of 1:1 complex (Figure 6).

**Electrospray Mass Spectral Studies of L with $Hg^{2+}$.** The complex formed between L and $Hg^{2+}$ has been further confirmed to be 1:1 based on ESI MS. The mass spectra yielded a molecular ion peak for 1:1 complex at $m/z$ of 1223.5, where its isotopic peak pattern supports the presence of $Hg^{2+}$ (Figure 7).

**NMR Studies of the Titration of L with $Hg^{2+}$.** During the titration of L with $Hg^{2+}$, $^1H$ NMR spectra showed no change in the cone conformation, however, showed marginal to considerable downfield shifts in the δ of C- and N- bound protons of the pendant, amide and benzimidazole moieties to different extents as can be seen from the spectra given in Figure 8. The N−H protons of the benzimidazole showed a downfield shift of ∼2.5 ppm and the other benzene protons of the benzimidazole moiety indeed exhibited large downfield shifts. Corresponding metal ion induced shifts for different protons
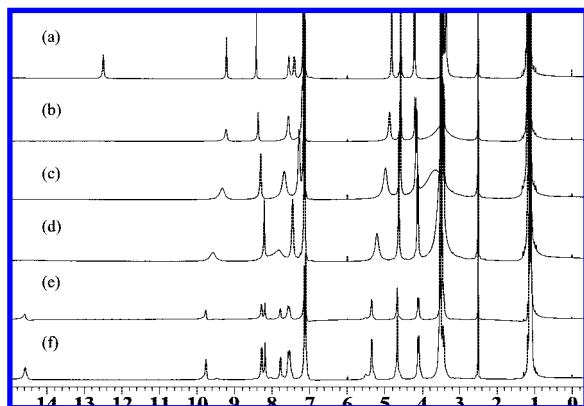
**FIGURE 8.** ¹H NMR spectra measured during the titration of L with Hg²⁺ (in DMSO d6). (a) L, (b) L + 0.25 equiv Hg²⁺, (c) L + 0.5 equiv Hg²⁺, (d) L + 1 equiv Hg²⁺, (e) L + 1.5 equiv Hg²⁺, (f) L + 2 equiv Hg²⁺.
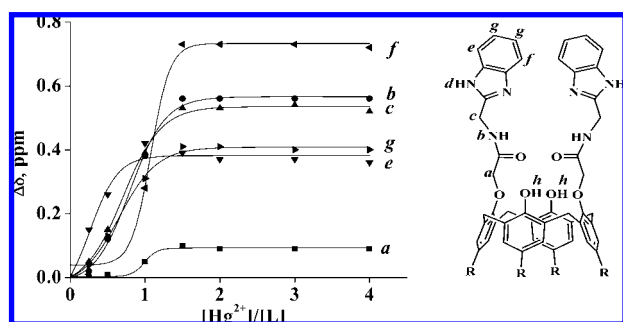


**FIGURE 9.** Metal ion-induced downfield shifts $\Delta\delta$ ($\Delta\delta = \delta_{(L+Hg^{2+})} - \delta_L$) observed with different protons of L at various mole ratios of [Hg²⁺]/[L]. The labeling for various protons can be seen from the structure given here.

are plotted in Figure 9 and the data indicate that the Hg²⁺ ion mainly interacts with the benzimidazole part of the calix[4]arene derivative. Hg²⁺ induced downfield shifts have also been noticed with the benzimidazole carbons in ¹³C NMR spectrum (Supporting Information, Figure S5). Such downfield shifts were also noticed in the literature in case of some Hg²⁺ bound complexes.[8] Thus the NMR study clearly supports the binding of Hg²⁺ to benzimidazole moieties in L.

To find whether other metal ions of the mercury group, viz., Zn²⁺ and Cd²⁺, bind to L or not, absorption titrations were carried out with these ions and found that there are no changes in the absorption spectra of L during the titration with these ions, in aqueous acetonitrile solution (Figure 10). On the other hand, formation of the complex was very clear from the absorption spectra when L was titrated with Hg²⁺ as reported
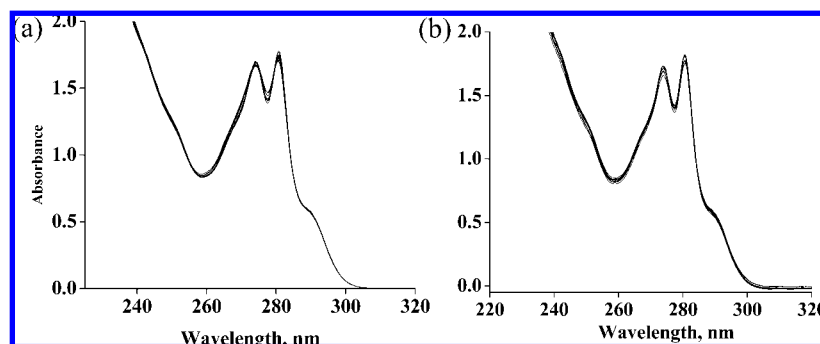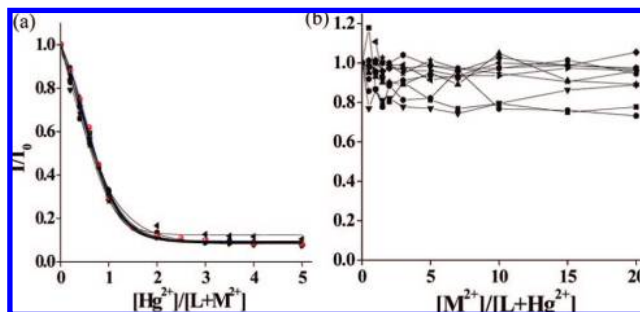


**FIGURE 11.** Plots of relative fluorescence intensity (I/I₀): (a) Titration of {L + 5*M²⁺} by Hg²⁺; (b) Titration of {L + 2*Hg²⁺} by M²⁺. The symbols correspond to, ■ = Mn²⁺; ● = Fe²⁺; ▲ = Co²⁺; ▼ = Ni²⁺; solid triangle pointing left = Cu²⁺; solid triangle pointing right = Zn²⁺; ◆ = Cd²⁺; pentegon = Ca²⁺; ⬡ = Mg²⁺; ★ = Pb²⁺; and red ● = Hg²⁺.

in this paper. Even the ¹H NMR titration carried out between L and Zn²⁺ exhibited only marginal shifts, viz., 0.02 to 0.08 ppm, whereas the shifts are in the range of ∼0.1 to 0.8 ppm in case of the titration of L with Hg²⁺, suggesting that there is no complex formation between L and Zn²⁺ (Supporting Information, Figure S6). Thus all this data clearly support the selective binding of Hg²⁺ even among its group elements (i.e., among Zn²⁺, Cd²⁺ and Hg²⁺) to benzimidazole moieties in L.

**Competitive Metal Ion Titrations.** To establish whether L can selectively recognize Hg²⁺ even in the presence of other metal ions, two types of competitive metal ion titrations were carried out in 1:1 aqueous solution. While in one, it is the Hg²⁺ bound L was titrated with the other M²⁺, viz., {L + 2*Hg²⁺} by M²⁺, in the second case it was the reverse type of titration, viz., {L + 5*M²⁺} by Hg²⁺. Such study was expected to reveal the possible use of L in the selective recognition of Hg²⁺. Based on the two titrations, it is noticed that no M²⁺ has any affect on Hg²⁺ sensing by L as can be seen from the fluorescence intensity ratio plots (Figure 11a and b). Because L has benzimidazole as well as amide moieties, the role of each of these units has also been addressed by extending the titration studies with the reference compounds, viz., L₁, L₂, L₃, L₄, and L₅.

**Fluorescence Studies of the Reference Compounds.** The fluorescence data obtained with L₁ clearly indicate that more than one M²⁺ quenches the fluorescence and hence is not selective to any M²⁺ (Figure 12a). No change in fluorescence is observed in case of the titration of L₂ with any M²⁺ (Figure 12b), and hence, L₂ is sensitive to any metal ion. Even L₃ does not show any significant changes in the fluorescence by all the M²⁺, except the Hg²⁺ (Figure 12c), which shows only a partial quenching beyond 10 equivalents and hence does not exhibit much sensitivity toward Hg²⁺. The L₄ do not show any response



**FIGURE 10.** Absorption spectra during the titration of L with M²⁺ in 1:1 H₂O:CH₃CN mixture: (a) Zn²⁺ and (b) Cd²⁺.
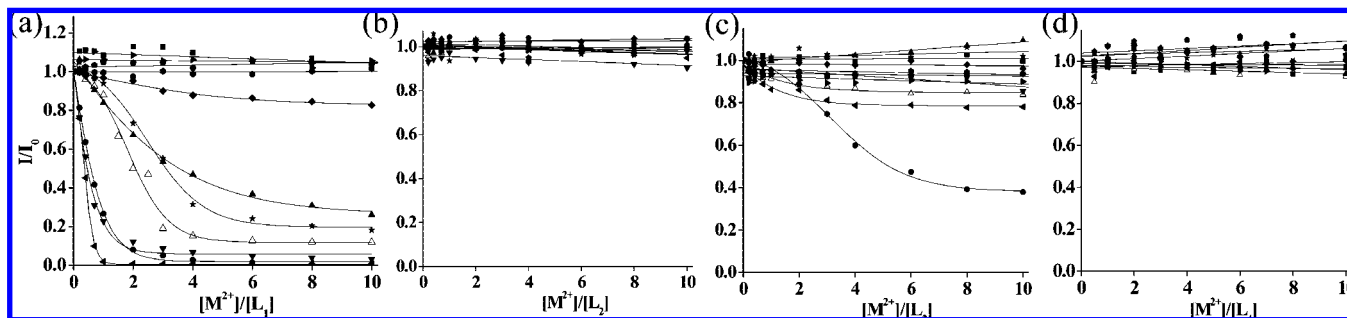
**FIGURE 12.** Fluorescence titration data for reference compounds in 50% aqueous acetonitrile solution except for (b) which is in 25% aqueous acetonitrile solution: (a) $L_1$, (b) $L_2$, (c) $L_3$, and (d) $L_4$. The symbols correspond to, ■ = $Mn^{2+}$; △ = $Fe^{2+}$; ▲ = $Co^{2+}$; ▼ = $Ni^{2+}$; solid triangle pointing left = $Cu^{2+}$; solid triangle pointing right = $Zn^{2+}$; ◆ = $Cd^{2+}$; pentegon = $Ca^{2+}$; ⬤ = $Mg^{2+}$; ★ = $Pb^{2+}$; and ● = $Hg^{2+}$.
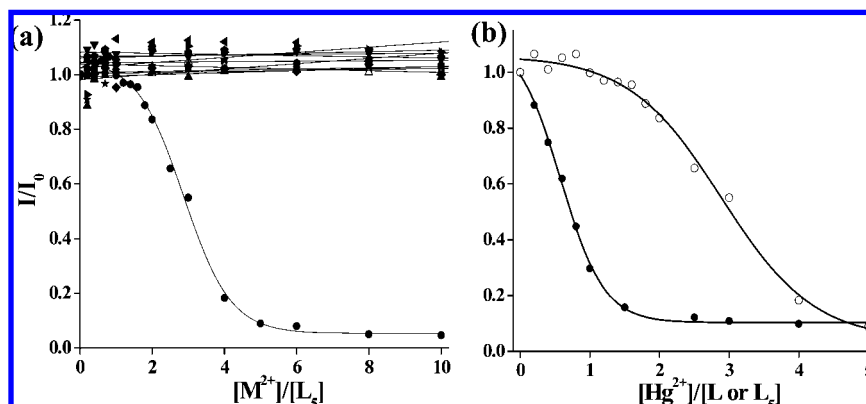


**FIGURE 13.** Plots of $(I/I_0)$ as a function of metal to the ligand mole ratio during the fluorescence titration studied in aqueous acetonitrile: (a) titration of $L_5$ with $M^{2+}$ (symbols carry same meaning as those given in Figure 12); (b) titration of L (●) and $L_5$ (○) with $Hg^{2+}$.

to $M^{2+}$ including $Hg^{2+}$ (Figure 12d) and hence is neither sensitive nor selective in aqueous solution toward any metal ion. Comparison of the fluorescence titration data of {L + $M^{2+}$} with that of {$L_1$ + $M^{2+}$} clearly suggest that the presence of benzimidazole moiety alone, as in $L_1$, is not sufficient enough for the recognition of $Hg^{2+}$. Although $L_5$ is sensitive only toward $Hg^{2+}$ among all the different $M^{2+}$ studied (Figure 13a), total fluorescence quenching of $L_5$ occurs only beyond four equivalents of $Hg^{2+}$ indicating that the rate of quenching of fluorescence is much slower with $L_5$ as compared to L. Comparison of $I/I_0$ plots of the titration of L and $L_5$ (Figure 13b) with $Hg^{2+}$ clearly differentiate the species formed in case of $L_5$ from that formed with L besides suggesting the binding of benzimidazole moiety to $Hg^{2+}$. Whereas L forms 1:1 species with $Hg^{2+}$, in case of $L_5$, at least two or three molecules are required to form the $Hg^{2+}$ complex. All this indicates that the receptor molecule, L is more sensitive toward $Hg^{2+}$ than the reference molecule, $L_5$, by using both its benzimidazole arms simultaneously wherein the calixarene moiety acts as a platform.

Comparison of the fluorescence titration data of all the reference systems with that of L clearly indicate that though the benzimidazole moiety is definitely required for binding, none of the reference compounds except $L_5$ is selective toward $M^{2+}$ under the conditions studied and hence supports the role of calix[4]arene as a necessary platform and the benzimidazole moieties as binding units besides providing hydrophobic zone in the recognition of $Hg^{2+}$. However, $L_5$ has lower sensitivity toward $Hg^{2+}$ as compared to the receptor molecule, L. Our recent study of simple diamino derivative of calix[4]arene having no benzimidazole moiety showed

response to $Hg^{2+}$ in fluorescence but does not show any selectivity, as the ion tends to go into the cavity in the absence of any preferential binding core.[9] We have also demonstrated that a binding core having chelation capability can substantially improve $M^{2+}$ recognition at the lower rim.[10]

**Fluorescence Lifetime Measurements of Mercury Binding.** The fluorescence decay data of L (Figure 14a) in 50% aqueous solution can be primarily fitted to a single exponential species (98%) having lifetime of 0.45 ns that is characteristic of the benzimidazole component. Titration of this with 1 equivalent of $Hg^{2+}$ brought significant changes in the fluorescence decay pattern that can be fitted with biexponential yielding two life times, viz., 0.55 and 0.15 ns with species ratio of 25% and 75% respectively. Further, the titration of this mixture with one additional equivalent of $Hg^{2+}$ (a total of 2 equiv of $Hg^{2+}$) did not bring much change in the decay behavior by exhibiting two species with life times of 0.63 and 0.16 ns and a species ratio of 12% and 88% respectively. Thus the lifetime of the major species present in $Hg^{2+}$ bound case results in a decrease by 3-fold. Similar trends in lifetimes were noticed between simple $L_1$ (Figure 14b) (0.09 ns, 93%) and {$L_1$ + $Hg^{2+}$} (0.03 ns, 100%). The difference in the lifetime of L (0.45 ns) and that of $L_1$ (0.09 ns) is indicative of the constricted mobility of the benzimidazole moiety when tethered to the calix[4]arene as in L. For the same reason, it is also evident from the steady state fluorescence data that while different $M^{2+}$ quench the fluorescence in case of $L_1$, only $Hg^{2+}$ quenches in case of L.

(8) (a) Wang, J.; Qian, X. *Org. Lett.* **2006**, *8*, 3721. (b) Kim, J. S.; Choi, M. G.; Song, K. C.; No, K. T.; Ahn, S.; Chang, S.-K. *Org. Lett.* **2007**, *9*, 1129.

(9) Joseph, R.; Gupta, A.; Rao, C. P. *J. Photochem. Photobiol. A* **2007**, *188*, 325.
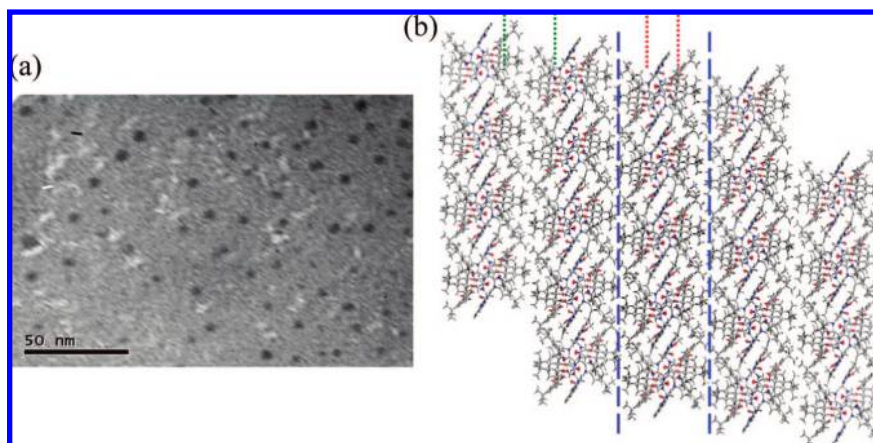
(10) (a) Dessingou, J.; Joseph, R.; Rao, C. P. *Tetrahedron Lett.* **2005**, *46*, 7967. (b) Kumar, A.; Ali, A.; Rao, C. P. *J. Photochem. Photobiol. A* **2006**, *177*, 164.
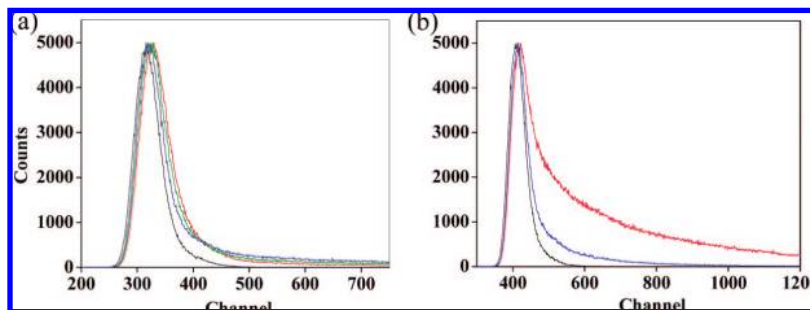
**FIGURE 14.** Fluorescence decay plots during the titration of Hg²⁺: (a) in case of L, prompt (black), no Hg²⁺ but only L (red), L + 1 equiv Hg²⁺ (green), and L + 2 equiv of Hg²⁺ (blue); (b) in case of L₁, prompt (black), no Hg²⁺ but only L₁ (red), and L₁ + 2 equiv of Hg²⁺ (blue).
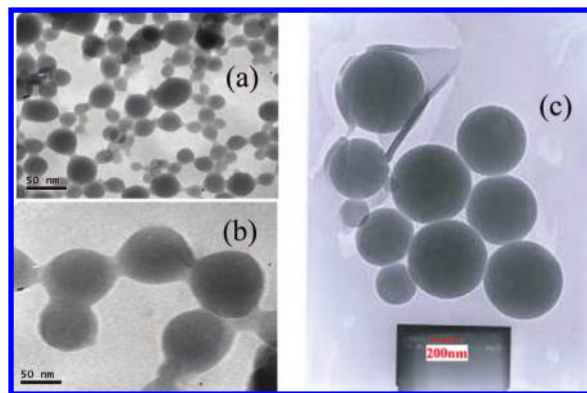


**FIGURE 15.** (a) TEM micrographs for the ligand L in ethanol. (b) Lattice diagram of L: hydrophobic region ∼16Å (green dots), Hydrophilic region ∼8 Å (red dots), and bilayer of hydrophilic and hydrophobic region ∼2.4 nm (blue dashes).

Thus the fluorescence lifetime measurements clearly suggest that the Hg²⁺ ion binds to benzimidazole moieties and thereby demonstrate the advantage of these moieties when connected to the calix[4]arene platform.

To further understand the nature of the complex formed between Hg²⁺ and L, the complex has been isolated and characterized by different techniques including the study of its nanostructure in comparison with L. The Hg²⁺ binding characteristics have been further addressed based on DFT computational calculations.

**Isolation and Characterization of Hg²⁺ Complex of L.** From a synthetic scale reaction carried out between L and Hg²⁺, a light-yellow product was isolated and the elemental analysis including that of Hg²⁺ suggested the formation of a complex with composition, viz., [HgL](ClO₄)₂·4C₂H₅OH, and was further characterized by UV−vis, ¹H NMR, and ESI MS. The ¹H NMR spectrum of this complex agrees well with that obtained during the titration of L with Hg²⁺ as reported earlier in this paper. The absorption spectrum of the complex clearly differs from that of the ligand. ESI mass spectrum exhibited molecular ion peak at 1231.77 corresponding to [M + Hg + Li]⁺ where in the authenticity of this peak could be established based on the isotopic peak pattern indicating the presence of mercury in the molecular ion. Thus, all the characterization data supports the formation of the complex as well as the formulation satisfactorily as given in the experimental. The nanostructural behavior of this complex has been established based on different microscopy techniques, viz., transimission electron microscopy (TEM), scanning electron microscopy (SEM) and atomic force microscopy (AFM) and the results were compared with that of the ligand data.



**FIGURE 16.** TEM micrographs for the mercury complex of L: (a) and (b) in ethanol; (c) in aqueous acetonitrile solution. Corresponding scales are shown in the figure.

**Nanostructural Studies of L and Its Complex with Hg²⁺.** In TEM, the ligand (L) sample prepared from ethanol indicated the formation of reasonably uniform and well separated spherical clusters of 5−10 nm size as can be seen from the micrograph given in Figure 15a. The lattice structure of L derived based on single crystal XRD showed formation of lower rim head-to-head dimers resulting in hydrophilic core. Extension of such dimers resulted in the formation of layers of hydrophobic (16 Å) and hydrophilic (8 Å) regions where the distance between the two such adjacent layers turns out to be 2.4 nm (Figure 15b) and hence could result in the formation of nanostructures as observed in TEM.

On the other hand, in TEM the Hg²⁺ complex of L exhibit spherical clusters of sizes higher than that found for L, viz., 40−70 nm and are connected together to form chains with some
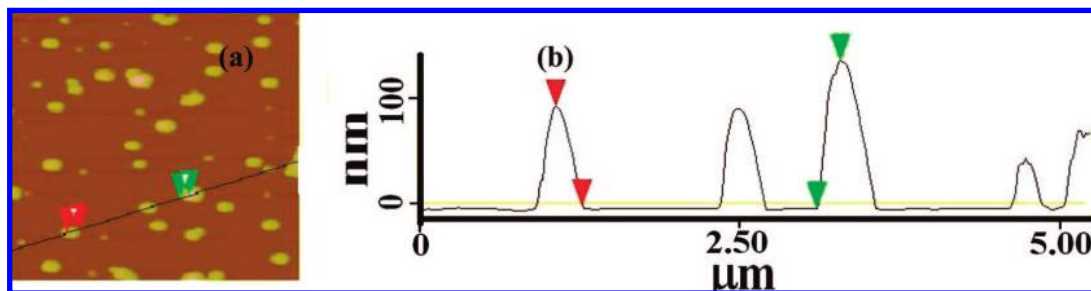
**FIGURE 17.** (a) Atomic force microscopy image of L in ethanol. (b) Height measurements for two particles shown in (a) with red and green markers.

branching (Figure 16a). A closer view of these chains clearly indicate that there is a reasonable overlap between the adjacent spheres so as to form a dumb-bell shaped units connected together, resulting in the distortion of the spherical nature (Figure 16b). The nanostructural behavior of mercury complex has also been found to be different from that of the simple mercury acetate studied under the same conditions. Such dumb-bell structures were reported with pyrogallol-based calix[4]arene derivative.[11] Thus the nanostructures observed in case of the $Hg^{2+}$ complex of L in the present case may provide hinge for future studies. Since the ligand is selective toward $Hg^{2+}$ in aqueous acetonitrile solution, TEM studies were also carried out from the samples of the mercury complex prepared from this solution. The micrographs observed in this case (Figure 16c) exhibited large size spherical nanostructures ranging from 200 to 400 nm size. A close look at these micrographs reveals that there is hardly any overlap between the spheres unlike that observed in case of the ethanol samples. This suggests that the solvent plays a role in the nanocluster formation and the self-aggregation is more in the aqueous solution system. Each of these spherical units present in the TEM micrographs of the complex may be the result of the manifestation of $Hg^{2+}$ leading to aggregates at the molecular level formed through the connectivity of their hydrophilic mercury containing lower rim terminals and an ensemble of such units interacting through their hydrophobic upper rim terminals appropriately resulting in recognizable nanostructures in the complex.

The simple ligand in ethanol medium gives spherical particles which are well spread all over the mica sheets in AFM studies as can be noted from the micrographs given in Figure 17a. The particle height distribution can be noted from Figure 17b. The individual particle heights are found to be in the range of 90−150 nm. However, we were unable to get the AFM pictures for the mercury complex due to heavy roughness. This leads to the conclusion that in presence of $Hg^{2+}$ the particle sizes are quite big and hence the probe-surface interaction is high enough to give large roughness.

The ligand shows high crystallinity in scanning electron micrographs whereas the mercury complex does not show any crystalline nature (Figure 18). The noncrystalline nature of the mercury complex has also been evidenced from electron diffraction of a particle in TEM studies.

It can be noted from the X-ray diffractogram that the ligand L (Figure 19) is highly crystalline, as can also be understood from the single crystal structure reported in this paper. However, the powder diffractogram of the mercury complex of L showed a broad hump in the $2\theta$ region of 10−40° indicating that the mercury complex is noncrystalline.

Thus, the TEM clearly indicated that there exists a difference in the nanostructure formed by L when compared to its $Hg^{2+}$



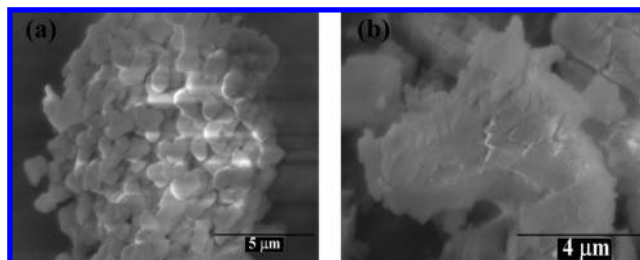**FIGURE 18.** SEM micrographs: (a) L and (b) mercury complex of L.
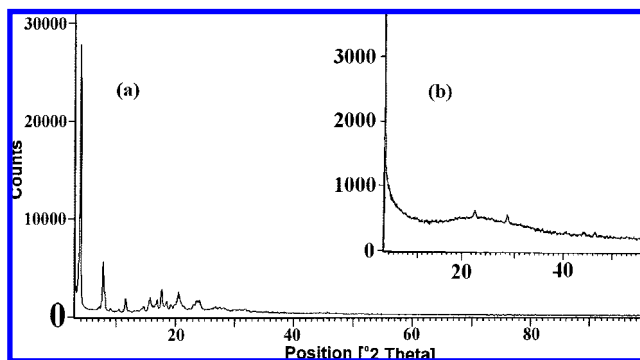


**FIGURE 19.** Powder X-ray diffractograms: (a) for the ligand, L and (b) for the mercury complex of L.

complex. The noncrystalline nature of the mercury complex of L has been delineated based on microscopy as well as the diffraction data, and thus, the microscopy studies seem to be useful in differentiating the complex from that of the ligand.

Because there was no crystal structure of the $Hg^{2+}$ complex available, the complexation was modeled by density functional theory (DFT) based computational studies.

**Computational Optimization of the $Hg^{2+}$ Complex of L.** All the computational calculations reported here were performed using Gaussian 03 package.[12] The crystal structure of the ligand L has been taken as the initial guess and was optimized to highest level of HF/6−31G through a cascade process, viz., AM1 → HF/STO-3G → HF/3−21G → HF/6−31G. The initial guess for the mercury complex was obtained by taking the optimized structure of L from HF/6−31G and simply placing the $Hg^{2+}$ ion well above the binding core so that there are no interactions present between $Hg^{2+}$ and L. This initial guess structure for the mercury complex was optimized using DFT

(11) Heaven, M. W.; Cave, G. W. V.; McKinlay, R. M.; Antesberger, J.; Dalgarno, S. J.; Thallapally, P. K.; Atwood, J. L. *Angew. Chem., Int. Ed.* **2006**, *45*, 6221.

(12) Frisch, M. J. *Gaussian 03*, revision C.02; Gaussian, Inc.: Wallingford, CT, 2004. The full reference is listed in the Supporting Information S8.
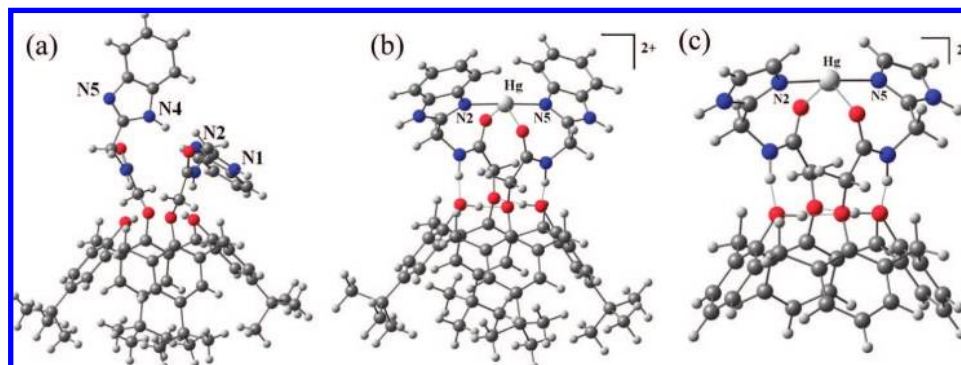
**FIGURE 20.** (a) Crystal structure of L being optimized in HF/6−31G. (b) B3LYP/CEP-121G optimized structure of the [HgL]$^{2+}$ (c) B3LYP/CEP-121G optimized structure of the [HgL′]$^{2+}$. The large gray sphere is mercury ion.

**TABLE 3.** Dihedral Angles of Both the Arms of the Structures Optimized by B3LYP/CEP−121G[a]

| dihedral angle | L | | Hg−L | | L′ | | Hg−L′ | |
|---|---|---|---|---|---|---|---|---|
| D1 | 131.2 | 118.4 | 141.3 | 141.3 | 131.9 | 126.6 | 141.0 | 140.9 |
| D2 | −1.9 | 17.6 | −29.3 | −29.4 | −4.6 | 4.5 | −26.6 | −26.5 |
| D3 | −174.6 | −178.4 | −153.1 | −153.1 | −177.3 | 179.0 | −153.1 | −153.1 |
| D4 | −123.4 | −126.7 | −101.3 | −101.2 | −128.7 | −127.1 | −102.3 | −102.1 |

[a] Dihedral angles D1−D4 have the same meaning as in Table 2.

computations (Supporting Information, S7) by going through B3LYP/CEP-31G followed by B3LYP/CEP-121G.[13] The optimization study resulted in the formation of a linearly coordinated species of the type N2···Hg···N5 (178.6°) with Hg···N distance of 2.092 Å (Figure 20a). Such linear coordination was proposed in case of a tetra-4-picolyl derivative of calix[4]arene in the literature.[14] In addition the structure also reveals weak interaction with the amide carbonyl oxygens where the Hg···O distance was found to be 2.7 Å. Weak interactions present between the Hg$^{2+}$ and oxygen have been reported in the literature.[15] Comparison of the benzimidazole arms in L (Figure 20a) with those present in the complex (Figure 20b) suggests that the corresponding dihedral angles have to be changed to bring N$_2$ and N$_5$ in line to form coordination with Hg$^{2+}$ when compared to that present in the free ligand (Table 3). As the computational times involved with L was enormously high, initial calculations were performed using mutilated ligand, L′ wherein the L′ was generated from L simply by replacing the tertiary butyl groups and the benzene portion of the benzimidazole by hydrogens. Thus the computational optimizations were also done with [HgL]$^{2+}$ as well as with [HgL′]$^{2+}$. In both the ligands, viz., L and L′, the conformations of the arms were found to be similar (Table 3). Also the geometry about the Hg$^{2+}$ was found to be exactly same in both the complexes, viz., [HgL]$^{2+}$ and [HgL′]$^{2+}$ (Figure 20).

The stabilization energies were computed using the formula, $\Delta E_s = \Delta E_{complex} - (\Delta E_{lig} + \Delta E_{M^{2+}})$. On the basis of these calculations, gas phase stabilization energies were found to be −355.2 and −393.9 Kcal/mol, respectively, for the complexes [HgL]$^{2+}$ and [HgL′]$^{2+}$. Single point energy of these optimized complexes were computed in presence of acetonitrile and water solvent dielectric fields and the corresponding average stabilization energies were computed to be −187.9 and −291.7 kcal/mol for [HgL]$^{2+}$ and [HgL′]$^{2+}$, respectively.

**Conclusions**

Selective recognition of Hg$^{2+}$ by calix[4]arene derivative has been addressed by us in this paper both from the point view of organic fine-tuning of the lower rim arm derivatization as well as to understand its capacity in recognizing Hg$^{2+}$ even in the presence of other M$^{2+}$. To achieve this goal, identification of the species of recognition is of utmost importance both in solution phase and also in its isolated form. In effect the studies related to these are being addressed in this paper both by experimental as well as by computational approaches. Synthetic modification in the arms at the lower rim resulted in different derivatives which can be used as reference compounds. The reference compounds were chosen in such a way that there is a similarity between these molecules and receptor molecule only in one feature at a time and there is a smooth change in the features of one reference molecule to the other.

Thus, the receptor L has been shown to be sensitive (1.4 ± 0.1 ppm) and selective to Hg$^{2+}$ among 11 divalent metal ions studied as well as 5 different reference compounds compared with, and further found that aqueous acetonitrile was best suited solvent combination for sensing Hg$^{2+}$ by L through the formation a 1:1 complex. Even the other ions from the same group, viz., Zn$^{2+}$ and Cd$^{2+}$, do not bind to L. None of the M$^{2+}$ impedes the interaction of Hg$^{2+}$ with L. Thus L is very sensitive and selective toward Hg$^{2+}$ even in the presence of other M$^{2+}$ ions. All the data obtained based on L, comparison of this with that obtained for L$_1$ to L$_5$, suggested the necessity of the calix[4]arene platform, benzimidazole binding core as well as the presence of hydrophobic moiety in the vicinity of the binding core for the recognition of Hg$^{2+}$. Examination of the crystal structures of the receptor molecule, viz., L, with those of the reference molecules, viz., L$_2$, L$_3$, L$_4$, and L$_5$, clearly demonstrated the advantage of the benzimidazole moiety in forming a binding core that would easily respond to the metal ion

(13) Jian, F. F.; Zhao, P. S.; Ma, H. B. *Struct. Chem.* **2005**, *16*, 469.
(14) de Namor, A. F. D.; Cornejo, A. A.; Sonalhi, R.; Shehab, M.; Nolan, K. B.; Ouazzani, N.; Mandi, L. *J. Phys. Chem. B* **2005**, *109*, 14735.
(15) (a) Hossain, G. M. G.; Amoroso, A. J.; Banu, A.; Malik, K. M. A. *Polyhedron* **2007**, *26*, 967. (b) Lourenco, L.; Marques, L. L.; Lang, E. S.; Fennera, H.; Castellano, E. E. *Z. Anorg. Allg. Chem* **2005**, *631*, 745. (c) Meyer, G. Nockemann, Peter. *Z. Anorg. Allg. Chem.* **2003**, *629*, 1447. (d) Garcia-Raso, A.; Fiol, J. J.; Rigo, S.; Lopez-Lopez, A.; Molins, E.; Espinosa, E.; Borras, E.; Alzuet, G.; Borras, J.; Castineiras, A. *Polyhedron* **2000**, *19*, 991.

presence. The observed difference in the sensitivity and selectivity toward $Hg^{2+}$ by L and $L_3$, the two closely related derivatives, may be addressed owing to the presence of two nitrogen centers per arm in the former while it is only one nitrogen center in the latter besides the difference in their coordinating ability of their nitrogen centers. This has provided additional advantage for L to sense as well as to select metal ion better than the $L_3$ and also better than the other reference molecules. Though $L_5$ is also sensitive toward $Hg^{2+}$, it requires higher equivalents of $Hg^{2+}$ for quenching the fluorescence of $L_5$ as compared that required for L and hence L is more sensitive toward $Hg^{2+}$ than the reference molecule, $L_5$.

Thus the present study clearly provided a molecular design approach for calix[4]arenes for their sensing toward $Hg^{2+}$. The complex species formed between L and $Hg^{2+}$ has been further proven in solution by absorption, NMR, ES MS and fluorescence lifetime measurements. To further understand the nature of the complex formed between $Hg^{2+}$ and L, the complex has been isolated and characterized and its composition has been established to be 1:1 complex. Transmission electron microscopy indicated that there exists a clear-cut difference in the nanostructure formed by L when compared to its $Hg^{2+}$ complex indicating that the TEM can provide a means to differentiate L from its mercury complex. Both the SEM and powder XRD studies demonstrated the crystallinity difference between the L and its mercury complex, wherein the mercury complex is amorphous, perhaps a reason for us not been able to obtain single crystals of the mercury complex. Detailed studies of microscopy of such receptor systems and their metal ion complexes are currently underway in our laboratory. The structure of the mercury complex has been further demonstrated based on DFT computational calculations performed with B3LYP/CEP-121G using $[HgL]^{2+}$ and $[HgL']^{2+}$.

## Experimental Section

All the perchlorate salts were procured from Sigma Aldrich Chemical Co., U.S.A. All the solvents used were dried and distilled by usual procedures immediately before use. Distilled and deionized water was used in the studies. $^1H$ and $^{13}C$ NMR spectra were measured on a Varian Mercury NMR spectrometer working at 400 MHz. The mass spectra were recorded on Q-TOF micromass (YA-105) using electrospray ionization method. The time-resolved single photon counting (TCSPC) was measured on fluorocube time-resolved fluorescence spectrometer from IBH, UK. Steady state fluorescence spectra were measured on Perkin-Elmer LS55. The absorption spectra were measured on Shimadzu UV2101 PC. The elemental analyses were performed on ThermoQuest microanalysis. FT IR spectra were measured on Perkin-Elmer spectrometer using KBr pellets. Single crystal X-ray diffraction data were measured on OXFORD XCALIBUR-S CCD machine. TEM experiments were performed on a JEOL 1200 EX transmission electron microscope operating at 80−120kV. AFM studies were performed in multimode Veeco Dimensions 3100 SPM with Nanoscope IV controller instrument. SEM was performed on a Hitachi S3400 cold-cathode Field Emission Scanning Electron Microscope (Hitachi High Technologies America, Inc., Pleasanton, CA). All the computational calculations were performed using Gaussian 03 package.

**Synthesis and Characterization Data for the Receptor Molecule L. 1**. The p-tert-butyl-calix[4]arene, **1**, is synthesized by the condensation of *p*-tert-butyl-phenol with formaldehyde in presence of NaOH as per the procedure given by Gutsche and coworkers (ref: *J. Am. Chem. Soc.*, **1981**, *103*, 3782).

**2.** A mixture of **1** (10 g, 15.4 mmol), potassium carbonate (4.26 g, 30.8 mmol), and ethyl bromoacetate (5.14 mL, 30.8 mmol) were taken in dry acetone (1.6 L) and stirred and heated at reflux for 15 h under nitrogen atmosphere. The cooled reaction mixture was filtered through a bed of celite and the filtrate and dichloromethane washings of the celite were combined and concentrated to dryness. Recrystallization of the residue from ethanol yielded the diester. Yield (9.86 g, 78%). $^1H$ NMR (CDCl$_3$, $\delta$ ppm): 0.98 (s, 18H, C(CH$_3$)$_3$), 1.26 (s, 18H each, C(CH$_3$)$_3$), 1.34 (t, 6H, CH$_2$−CH$_3$, $J$ = 7.02 Hz), 3.32 (d, 4H, Ar−CH$_2$-Ar, $J$ = 13.4 Hz), 4.30 (q, 4H, CH$_2$−CH$_3$), 4.45 (d, 4H, Ar−CH$_2$-Ar, $J$ = 13.2 Hz), 4.73 (s, 4H, OCH$_2$CO), 6.82 (s, 4H, Ar−H), 7.02 (s, 4H, Ar−H), 7.06 (s, 2H, OH).

**3.** A mixture of the diester, **2**, (10 g, 12.2 mmol) and 15% aq. sodium hydroxide (32 mL) in ethanol (500 mL) was stirred and heated under reflux for 24 h and the reaction mixture was evaporated under reduced pressure to yield a white residue. The residue was diluted (suspension) with cold water (500 mL), and hydrochloric acid (3 N) was added with vigorous mixing until pH 1 was reached. The solid was filtered, dried in air, and further dissolved in chloroform. The solution was washed with hydrochloric acid (3 N) and brine, dried, and concentrated to afford the diacid product, **3**. **3** was recrystallized from aq. acetone (acetone:water, 7:3 v/v). Yield (7.92 g, 85%). $^1H$ NMR (CDCl$_3$, $\delta$ ppm): 1.10 (s, 18H each, C(CH$_3$)$_3$), 1.30 (s, 18H each, C(CH$_3$)$_3$), 3.46 (d, 4H, Ar−CH$_2$−Ar, $J$ = 13.74 Hz), 4.13 (d, 4H, Ar−CH$_2$−Ar, $J$ = 13.44 Hz), 4.70 (s, 4H, OCH$_2$CO), 6.99 (s, 4H, Ar−H), 7.07 (s, 4H, Ar−H).

**4.** To dry benzene (100 mL), p-tert-butylcalix[4]arene diacid, **3**, (4.0 g) and SOCl$_2$ (6 mL) were added and refluxed under nitrogen atmosphere for 4 h. The solvent and residual SOCl$_2$ were removed under reduced pressure, and this yielded diacid chloride **3** as off white solid and was used *in situ* for the preparation of L.

**5,11,17,23-Tetra-tert-butyl-25,27-bis((2-aminomethylbenzimidazole)carbonylmethoxy)-26,28-dihydroxycalix[4]arene, L.** A suspension of 2-(aminomethyl)benzimidazole. 2HCl (2.73 g, 12.4 mmol) and Et$_3$N (6 mL, 43.1 mmol) was stirred in dry THF (100 mL) under argon atmosphere. Diacid chloride, **4** (4.32 g, 5.34 mmol) in dry THF (50 mL) was added dropwise to this reaction mixture. Immediately, a yellowish precipitate was formed and stirring was continued for 48hrs at room temperature. After filtration, the filtrate was concentrated to dryness. A yellow solid was obtained which was extracted with CHCl$_3$, washed with water and then with brine and the organic layer was dried with anhydrous MgSO$_4$. Filtrate was concentrated to dryness and recrystallized from EtOH/CHCl$_3$ to get **L** as a white solid. Yield (55%, 2.95 g) C$_{64}$H$_{74}$N$_6$O$_6$ (1023.29): Anal. (% found) C 67.58, H 7.50, N 6.76, C$_{64}$H$_{74}$N$_6$O$_6$. 2C$_2$H$_5$OH. CHCl$_3$ (% requires) C 67.11, H 7.11, N 6.80). FTIR: (KBr, cm$^{-1}$): 1679 $\nu_{C=O}$, 3380 $\nu_{OH}$. $^1H$ NMR: (CDCl$_3$, $\delta$ ppm): 0.98 (s, 18H, (C(CH$_3$)$_3$), 1.25 (s, 18H, (C(CH$_3$)$_3$), 3.28 (d, 4H, Ar−CH$_2$−Ar, $J$ = 13.30 Hz), 3.96 (d, 4H, Ar−CH$_2$−Ar, $J$ = 13.30 Hz), 4.40 (s, 4H, −CH$_2$CONH−), 4.88 (d, 4H, −CONHCH$_2$−, $J$ = 5.50 Hz), 6.8 (s, 4H, Ar-H), 7.03 (s, 4H, Ar−H), 7.23−7.25 (m, 4H, benzimidazole), 7.53−7.55 (m, 4H, benzimidazole), 7.45 (s, 2H, −OH), 8.95 (t, 2H, −NH, $J$ = 5.19). $^{13}C$ NMR: (CDCl$_3$, 400 MHz $\delta$ ppm): 31.10, 31.8 (C(CH$_3$)$_3$), 32.1(Ar−CH$_2$−Ar), 34.0, 34.2 (C(CH$_3$)$_3$), 37.3 (CH$_2$−benzimidazole), 73.8 (OCH$_2$CO), 114.9, 124.1, 125.5, 126.1, 127.4, 135.5, 135.9, 142.7, 148.1, 149.2, 149.8, 152.0, (benzimidazole and calix-Ar-C), 170.6 (C=O). m/z (ES-MS) 1023.72 ([M]$^+$ 100%), 1024.7 ([M+H]$^+$ 35%,). Single crystals of L were obtained by slow evaporation of the solvent mixture (EtOH/CHCl$_3$) at room temperature to give single crystals of L.

**Synthesis and Characterization Data for the Reference Compounds, L$_1$, L$_2$, L$_3$, L$_4$, and L$_5$. L$_1$.** 2-Aminomethylbenzimidazole, L$_1$ is being procured as 2HCl salt from Sigma Aldrich Chemical Co. and was used in the reactions. The fluorescence studies of this molecule in presence of M$^{2+}$ were carried out upon neutralizing the HCl salt by using Et$_3$N.

**L$_2$.** A suspension of dibenzylamine (2.55 g, 12.4 mmol) and Et$_3$N (3 mL, 21.57 mmol) was stirred in dry THF (100 mL) under argon atmosphere. Diacid chloride, **3** (4.32 g, 5.34 mmol) in dry THF (50 mL) was added dropwise to this reaction mixture. Immediately a yellowish precipitate was formed and stirring was continued for

48 h at room temperature. After filtration, the filtrate was concentrated to dryness. A yellow solid was obtained, which was extracted with CHCl₃ and washed with water and then with brine, and the organic layer was dried with anhydrous MgSO₄. Filtrate was concentrated to dryness and recrystallized from EtOH/CHCl₃ to get **L₂** as white crystalline solid. Yield (3.5 g, 60%.). C₇₆H₈₆N₂O₆· CHCl₃ (1242): Anal. (% found) C 74.90, H 7.59, N 2.36, (% requires) C 74.43, H 7.01, N 2.26. FTIR: (KBr, cm⁻¹): 1667 $\nu_{C=O}$, 3371 ($\nu_{OH}$). ¹H NMR: (CDCl₃, δ ppm): 0.97 (s, 18H, C(C**H₃**)₃), 1.26 (s, 18H, C(C**H₃**)₃), 3.26 (d, 4H, Ar−C**H₂**−Ar, *J* = 13.30 Hz), 4.37 (d, 4H, Ar−C**H₂**−Ar, *J* = 13.30 Hz), 4.60, 4.70 (s, 4H, N−C**H₂**) 4.82 (s, 4H, −OC**H₂**CO), 6.87 (s, 4H, Ar-**H**), 7.00 (s, 4H, Ar−**H**), 7.24 (s, 2H, −O**H**), 7.31 (m, 10H, benzyl-**H**).. ¹³C NMR: (CDCl₃, δ ppm): 31.2, 31.8 (C(**C**H₃)₃), 32.0(Ar−**C**H₂−Ar), 33.9, 34.0 (**C**(CH₃)₃), 49.4, 48.6 (−N**C**H₂), 74.1 (O**C**H₂CO), 125.1, 125.8, 126.8, 127.4, 127.7, 127.9, 128.7, 129.1, 133.0, 136.5, 137.0, 141.3, 147.2, 150.7, 151.16 (Ar−**C**), 168.8 (**C**=O). ES-MS: *m/z* (intensity (%), fragment) 1146.53 (40, [M + Na]⁺). ¹H and ¹³C NMR spectra are given in the Supporting Information, Figure S9.

**L₃.** This compound was synthesized by following the procedure given for L except using 2-(aminomethyl)pyridine (1.40 g, 12.94mmol), Et₃N (2.18 g, 21.57mmol), and diacid chloride (4.32 g, 5.34 mmol), in dry THF (150 mL). The crude product was recrystallized by slow evaporation of the solvent from C₂H₅OH/ CHCl₃. Yield (2.69 g, 52%.) FTIR: (KBr, cm⁻¹): 1682 ($\nu_{C=O}$), 3338 ($\nu_{OH}$). ¹H NMR: (CDCl₃, δ ppm): 0.91 (s, 18H, (C(C**H₃**)₃), 1.20 (s, 18H, (C(C**H₃**)₃), 3.28 (d, 4H, Ar−C**H₂**−Ar, *J* = 13.48 Hz), 3.98 (d, 4H, Ar−C**H₂**−Ar, *J* = 13.48 Hz), 4.45 (s, 4H, −OC**H₂**), 4.61 (d, 4H, −NH−C**H₂**, *J* = 5.15 Hz), 6.76 (s, 4H, Ar−**H**), 6.96 (s, 4H, Ar−**H**), 7.07 (t, 2H, Py−**H**, *J* = 6.10 Hz), 7.14 (s, 2H, −O**H**), 7.32 (d, 2H, Py−**H**, *J* = 7.53 Hz), 7.56 (t, 2H, Py−**H**, *J* = 7.73 Hz), 8.31 (d, 2H, Py−**H**, *J* = 4.76 Hz), 9.10 (t, 2H, N**H**CO, *J* = 5.15 Hz) ¹³C NMR: (CDCl₃, δ ppm): 31.1, 31.7 (C(**C**H₃)₃), 32.1(Ar−**C**H₂−Ar), 34.0, 34.2 (**C**(CH₃)₃), 45.4 (−N**C**H₂), 74.9 (O**C**H₂CO), 122.4, 122.4, 125.6, 126.2, 127.2, 132.2, 136.7, 142.9, 148.3, 149.2, 149.4, 149.7, 156.9 (Ar−**C**), 168.62 (**C**=O). ESI-MS: *m/z* (intensity (%), fragment) 946.6 (30, [M + 1]⁺).

**L₄.** In 50 mL of THF solution of **3** (1.0 g, 1.3 mmol), 1-hydroxybenztriazol (0.392 g, 2.9 mmol) and DCC (0.598 g, 2.9 mmol) were stirred at room tempreture. To this, L-phenylalanine methyl ester hydrochloride (0.625 g, 2.9 mmol) and triethyl amine (1.5 mL) in 30 mL THF were added dropwise. Stirring was continued for 48 h. Solvent was evaporated under reduced pressure. The solid was redissolved in CH₂Cl₂. The reaction mixture was washed with 1 N HCl followed by brine and the organic layer was collected and dried with anhydrous Na₂SO₄. After filtration, the solvent was removed under reduced pressure. The pure product was obtained as white powder (0.75 g, 56.0%). C₆₈H₈₂N₂O₁₀· (1086): Anal. (% found) C 74.75, H 7.20, N 2.75, (% requires) C 75.14, H 7.55, N 2.58. FTIR (KBr, cm⁻¹): 3458, 3304 ($\nu_{NH/OH}$), 1752 ($\nu_{C=O}$, COOMe), 1670 ($\nu_{C=O}$, CONH). ¹H NMR (CDCl₃, δ ppm): 1.02, 1.30 (s, 36H, C(C**H₃**)₃), 3.02−3.15 (m, 6H, Ar−C**H₂**−Ar, and Cᵝ**H₂**−Ph), 3.47 (d, 2H, Ar−C**H₂**−Ar, *J* = 13.76 Hz), 3.64 (s, 6H, OC**H₃**), 4.06 (d, 2H, Ar−C**H₂**−Ar, *J* = 12.9 Hz), 4.10 (d, 2H, Ar−C**H₂**−Ar, *J* = 14.2 Hz), 4.14 (d, 2H, O−C**H₂**−CO, *J* = 15.2 Hz), 5.03 (d, 2H, O−C**H₂**−CO, *J* = 15.0 Hz), 5.10 (q, 2H, Cᵅ**H**, *J* = 7.8, 7.0 Hz), 6.87 (d, 4H, Ar−**H**), 7.03 (m, 14H, Ar−**H**, Ph−**H**), 7.73 (s, 2H, O**H**), 9.51 (d, 2H, N**H**, *J* = 8.3). ¹³C NMR (CDCl₃, 400 MHz,): δ 30.9, 31.7 (C(**C**H₃)₃), 32.0, 32.5 (Ar−**C**H₂−Ar), 33.9, 34.0 (tert-**C**), 39.0 (**C**H₂−Ph), 52.1 (O**C**H₃), 52.8 (**C**H), 74.9 (O-**C**H₂−CO), 124.7, 125.3, 125.8, 126.4, 126.5, 126.7, 127.6, 128.1, 128.9, 132.6, 136.1, 142.3, 147.8, 149.7, 150.0 (aromatic carbons), 168.8 (**C**ONH), 171.8 (**C**OOMe) ppm. ES-MS: *m/z* = 1087 ([M + H]⁺, 100%). ¹H and ¹³C NMR spectra are given in Supporting Information, Figure S9.

**L₅.** Reference compound L₅ has been synthesized as shown in Scheme 2. ¹H and ¹³C NMR spectra are given in the Supporting Information, Figure S9.

**SCHEME 2. Synthesis of L₅ᵃ**
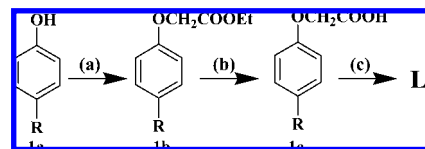


ᵃ (a) bromoethylacetate/K₂CO₃/ acetone; (b) KOH/C₂H₅OH/Water, reflux; (c) EDCI/ Et₃N/ HOBT/2-aminomethyl benzimidazole. R = tert-butyl.

**1b:** A mixture of *p-tert*-butyl phenol, **1a** (2.00 g, 13.3 mmol), potassium carbonate (2.40 g, 17.3 mmol), and ethyl bromoacetate (1.77 mL, 15.99 mmol) was taken in dry acetone (150 mL), and the reaction mixture was stirred and heated at reflux for 12 h under nitrogen atmosphere. The cooled reaction mixture was concentrated under reduced pressure. The residue was dissolved in CHCl₃ and washed with 1N HCl. The organic layer was separated and washed with brine followed by drying using MgSO₄. After filtration, solvent was evaporated by drying under vacuum to result in a yellow oil. Yield (3.20 g, 97%). ¹H NMR (CDCl₃, δ ppm): 1.29 (s, 9H, C(C**H₃**)₃), 1.30 (t, 3H, CH₂(C**H₃**)₃), 4.28 (q, 2H, C**H₂**−CH₃, *J* = 7.33 Hz), 4.59 (s, 2H, OC**H₂**CO), 6.84 (d, 2H, Ar−**H**, *J* = 8.86 Hz), 7.30 (d, 2H, Ar−**H**, *J* = 8.85 Hz).

**1c:** A mixture of the **1b**, (3.20 g, 13.55 mmol) and potassium hydroxide (1.6 g, 28.46mmol) in 120 mL of ethanol:water (2:1 v/v) mixture were stirred and heated under reflux for 12 h and the reaction mixture was evaporated under reduced pressure to yield a white residue. The residue was taken in 1 N HCl (100 mL) and CHCl₃ (250 mL). The organic layer was washed with water and dried over MgSO₄. All the organic solvent was evaporated to yield white solid as pure product. Yield (2.00 g, 71%). ¹H NMR (CDCl₃, δ ppm): 1.29 (s, 9H each, C(C**H₃**)₃), 4.66 (s, 2H, OC**H₂**CO), 6.86 (d, 2H, Ar−**H**, *J* = 8.86 Hz), 7.32 (d, 2H, Ar−**H**, *J* = 8.85 Hz).

**L₅:** To a solution of **1c** (0.3 g, 1.44mmol) in CH₂Cl₂ (75 mL) was added Et₃N (1.00 mL, 7.21mmol), 1-ethyl-(3-dimethylaminopropyl)-3-carbodiimide hydrochloride (EDCI.HCl) (0.41 g, 2.16mmol) and catalytic amount of 1-hydroxybenzotriazole (HOBT) and stirred the solution at 0 °C for 30 min under N₂ atmosphere. 2-Aminomethyl benzimidazole (0.48 g, 2.16mmol) was added to this reaction mixture and stirred at room temperature for overnight. The resulting mixture was washed with water followed by saturated NaHCO₃ and brine. The product can be purified either by using silica gel column with chloroform-methanol as eluant or alternatively by dissolving the impurities in dichloromethane and filtering off the product, to give white solid. Yield (0.36 g, 74%). C₂₀H₂₃N₃-O₂.CH₃OH· (369.45): Anal. (% found) C 67.82, H 7.10, N 10.94, (% requires) C 68.27, H 7.36, N 11.37. FTIR: (KBr, cm⁻¹): 1654 ($\nu_{C=O}$). ¹H NMR (DMSO-d₆, δ ppm): 1.24 (s, 9H, C(C**H₃**)₃), 4.56 (s, 2H, OC**H₂**), 4.58 (s, 2H, NC**H₂**), 6.92 (d, 2H, Ar-**H**, *J* = 8.86 Hz), 7.14 (m, 2H, Benz-**H**), 7.30 (d, 2H, Ar-**H**, *J* = 8.86 H), 7.51 (br, 2H, Benz-**H**), 8.78 (t, 1H, CON**H**, *J* = 5.80 Hz), 12.31 (s, 1H, Benz-N**H**). ¹³C NMR: (DMSO-d₆, δ ppm): 31.4, 33.8, 36.9, 67.0, 79.3, 114.3, 121.4, 126.1, 143.4, 152.1, 155.6, 168.4. ESI MS: *m/z* (intensity (%), fragment) 338.3 (100, [M + H]⁺).

**Synthesis, Isolation, and Characterization of the Hg²⁺ Complex of L.** Metal salt, Hg(ClO₄)₂ (0.094 g, 0.235 mmols) was dissolved in CH₃OH (5 mL) and was added to the ligand, L (0.20 g, 0.196 mmols) in CHCl₃. The solution was stirred overnight followed by refluxing for 12 h. The resulting solution was concentrated, washed with minimum amount of methanol and dried under vacuum. Yield (80%, 0.22 g). ¹H NMR: (CDCl₃, 400 MHz δ ppm): 1.10 (s, 18H, C(C**H₃**)₃), 1.14 (s, 18H, C(C**H₃**)₃), 3.43 (d, 4H, Ar−C**H₂**−Ar, *J* = 12.50 Hz), 4.10 (d, 4H, Ar−C**H₂**−Ar, *J* = 12.50 Hz), 4.65 (s, 4H, −C**H₂**CONH−), 5.33 (s, 4H, −CON-HC**H₂**−), 7.10 (s, 4H, Ar−**H**), 7.13 (s, 4H, Ar−**H**), 7.52 (m, 4**H**, benzimidazole), 7.76 (s, 2**H**, benzimidazole), 8.19 (s, 2H, −O**H**), 8.27 (m, 2H, benzimidazole), 9.75 (s, 2H, CON**H**), 14.56 (s, 2H, −N**H**-benzimidazole). Anal. (% found) C 53.02, H 6.41, N 5.57, Hg 12.92. C₆₄H₇₄N₆O₆. 4C₂H₅OH. Hg(ClO₄)₂ (% required) C 53.41,

H 6.10, N 5.21, Hg 12.49. ES MS 1231.77 ($[M + Hg + Li]^+$) UV−vis spectral data $\lambda$, nm ($\varepsilon$, mole.lit$^{-1}$.cm$^{-1}$): 263 (13932); 270 (18314); 277 (17753); 292 (5168).

**Details of Solution Studies.** All the metal salts used for the titrations were as their perchlorate salts (Caution: perchlorate salts may explode under some conditions) with a formula, $M(ClO_4)_2.xH_2O$. All the solvents used were of analytical grade and were purified and dried by routine procedures immediately before use.

**Fluorescence Studies.** Fluorescence emission spectra were measured on Perkin-Elmer LS55 by exciting the solutions at 275 nm and the emission spectra were recorded in the 285−400 nm range. Different solvent or solvent combinations were used for fluorescence studies are $CH_3OH$, $CH_3CN$, $H_2O:CH_3CN$ (1:1), $H_2O:CH_3CN$ (1:3), and $H_2O:CH_3CN$ (3:2). The fluorescence studies performed in $CH_3OH$ solution uses always a 50 $\mu$L of chloroform solution of L (i.e., the 3 mL solution contains 2.950 mL of $CH_3OH$ and 0.050 mL of $CHCl_3$). All the measurements were made in 1 cm quartz cell and maintained a final L concentration of 10 $\mu$M. During the titration, the concentration of metal perchlorate was varied accordingly to result in requisite mole ratios of metal ion to L and the total volume of the solution was maintained constant at 3 mL in each case by adding appropriate solvent or solvent mixtures. Normalized emission (relative fluorescence) intensities ($I/I_0$) (where, $I_0$ is the intensity with no metal ion addition; $I$ is the intensity at different metal ion to L mole ratios) were plotted against the mole ratio of metal ion to the L. The association constant of the mercury complex formed in the solution has been estimated using the standard Benesi-Hildebrand equation, viz.,

$$\frac{1}{I - I_0} = \frac{1}{I_1 - I_0} + \frac{1}{(I_1 - I_0)K_a[M^{2+}]} \tag{1}$$

where $I_0$ is the intensity of L, $I$ is the intensity in the presence of $M^{2+}$, $I_1$ is intensity upon saturation with $M^{2+}$ and $K_a$ is the association constant of the complex formed.

The same procedure was followed in the case of the $M^{2+}$ titration of $L_2$. Whereas in the case of $L_1$, the hydrochloride salt of $L_1$ was first dissolved in water and neutralized with $Et_3N$ prior to the titration.

**Absorption Studies.** L (0.00303 M) was dissolved in $CH_3CN$, and $Hg(ClO_4)_2$ (0.00303 M) taken in $H_2O:CH_3CN$ (1:1) were used for titrations. Titrations were carried out by varying the equivalents of metal ion between 0 and 4.0 using the additions of 0, 20, 40, 60, 80, 100, 120, 160, 180, 220, 250, 300, 350, and 400 $\mu$L stock solution and by fixing the ligand concentration as constant at 100

$\mu$L and all the solutions were diluted to 3 mL using $H_2O:CH_3CN$ (1:1) solvent system before used for the study. Same procedure was followed for recording the absorption spectra of the titration of metal ions $Zn^{2+}$ and $Cd^{2+}$ with L.

**NMR Titration Experiments.** (a) $Hg^{2+}$ titration with L. L (0.0245 M) was dissolved in 0.4 mL of DMSO-$d_6$ and recorded the $^1H$ NMR spectra. Metal ion titrations were carried out by adding different volumes of, viz., 10, 20, 30, 40, 60, 80, 120, and 160 $\mu$L of bulk $Hg(ClO4)_2$ (0.245 M) solution to a solution of L to result in $[Hg^{2+}]/[L]$ mole ratio of 0−4 (b) $Zn^{2+}$ titration with L. Same procedure as in (a) was followed in the titration of $Zn^{2+}$ with L.

**Microscopy Studies.** TEM experiments were performed on a JEOL 1200 EX transmission electron microscope operating at 80−120kV. Carbon coated copper grids of 300 mesh were used as substrate for the sample. Stock solutions of the samples were prepared by dispersing the weighed sample in appropriate solvent followed by sonicating the mixture for 30 min to result in a concentration of $\sim$6 × 10$^{-4}$ M. Different sample blocks were made by placing 5−10 $\mu$L of the sample solution on the copper grid and allowing it to dry in air at room temperature. AFM studies were performed in multimode Veeco Dimensions 3100 SPM with Nanoscope IV controller instrument. Contact mode with non conductive silicon nitride probe having sharp fine tip at the end was used in all the cases. Sample preparation was identical with TEM sample preparation. Mica sheets were used as substrate for the studies. SEM was performed on a Hitachi S3400 cold-cathode Field Emission Scanning Electron Microscope (Hitachi High Technologies America, Inc., Pleasanton, CA). SEM experiment grids were prepared by gold coating.

**Supporting Information Available:** Single crystal X-ray structural information (Figure S1), fluorescence titration data (Figures S2−S4), NMR titration data (Figures S5 and S6), computational data (Figure S7), full reference of Gaussian 03 (Figure S8), and NMR spectra for $L_2$ and $L_4$, $L_5$ (Figure S9). This material is available free of charge via the Internet at http://pubs.acs.org.

JO800073G

# Lower Rim 1,3-Di{bis(2-picolyl)}amide Derivative of Calix[4]arene (L) as Ratiometric Primary Sensor toward Ag$^+$ and the Complex of Ag$^+$ as Secondary Sensor toward Cys: Experimental, Computational, and Microscopy Studies and INHIBIT Logic Gate Properties of L[‡]

Roymon Joseph, Balaji Ramanujam, Amitabha Acharya, and Chebrolu P. Rao*

*Bioinorganic Laboratory, Department of Chemistry, Indian Institute of Technology Bombay, Mumbai 400 076, India*

*cprao@iitb.ac.in*
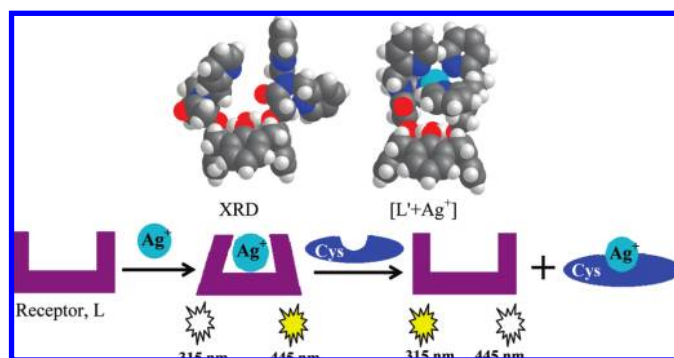
A structurally characterized lower rim 1,3-di{bis(2-picolyl)}amide derivative of calix[4]arene (L) exhibits high selectivity toward Ag$^+$ by forming a 1:1 complex, among nine other biologically important metal ions, *viz*., Na$^+$, K$^+$, Mg$^{2+}$, Ca$^{2+}$, Mn$^{2+}$, Fe$^{2+}$, Co$^{2+}$, Ni$^{2+}$, and Zn$^{2+}$, as studied by fluorescence, absorption, and $^1$H NMR spectroscopy. The 1:1 complex formed between L and Ag$^+$ has been further proven on the basis of ESI mass spectrometry and has been shown to have an association constant, $K_a$, of $11117 \pm 190$ M$^{-1}$ based on fluorescence data. L acts as a primary ratiometric sensor toward Ag$^+$ by *switch-on* fluorescence and exhibits a lowest detectable concentration of 450 ppb. DFT computational studies carried out in mimicking the formation of a 1:1 complex between L and Ag$^+$ resulted in a tetrahedral complex wherein the nitrogens of all four pyridyl moieties present on both arms are being coordinated. Whereas these pyridyls are located farther apart in the crystal structure, appropriate dihedral changes are induced in the arms in the presence of silver ion in order to form a coordination complex. Even the nanostructural features obtained in TEM clearly differentiates L from its Ag$^+$ complex. The *in situ* prepared silver complex of L detects Cys ratiometrically among the naturally occurring amino acids to a lowest concentration of 514 ppb by releasing L from the complex followed by formation of the cysteine complex of Ag$^+$. These were demonstrated on the basis of emission, absorption, $^1$H NMR, and ESI mass spectra. The INH logic gate has also been generated by choosing Ag$^+$ and Cys as input and by monitoring the output signal at 445 nm that originates from the excimer emission of L in the presence of Ag$^+$. Thus L is a potential primary sensor toward Ag$^+$ and is a secondary sensor toward Cys.

## Introduction

Recognition of metal ions and amino acids are of prime interest in the context of metalloproteins and metallo-enzymes, where Ag$^+$ and Cys are not exceptions. Though the Ag$^+$ is not a biologically essential element, its complexes are used in medicine and agriculture.[1] The antimicrobial

(1) (a) Jung, W. K.; Koo, H. C.; Kim, K. W.; Shin, S.; Kim, S. H.; Park, Y. H. *Appl. Environ. Microbiol.* **2008**, *74*, 2171. (b) Silver, S.; Phung, L. T.; Silver, G. *J. Ind. Microbiol. Biotechnol.* **2006**, *33*, 627.

action of silver mainly takes place through its interactions with sulfur in the case of amino acids and peptides,[2] and Ag$^+$ ions are inactive toward other amino acids. A side effect of silver originating from its prolonged use is irreversible darkening of the skin and mucous membrane.[3] Accumulation of silver by microbial species could also act as a source for this element.[4] Among the 20 naturally occurring amino acids, Cys plays an important role in living cells.[5] Both the deficiency and excess accumulation of Cys are detrimental to life.[6] Therefore, the detection and sensing of silver and Cys, by a single molecular system with dual functionality, are certainly challenging and are intriguing to the current researchers. Owing to the ubiquitous nature of calix[4]arenes[7] by possessing hydrophilic and hydrophobic characters together in the same structure, these molecules can act as good mimics of enzymes[8] and also provide a suitable platform for building appropriate binding cores. There are some reports in the literature for the selective recognition of silver either by potentiometry,[9] by $^1$H NMR,[10] or by fluorescence technique[11] using calix[4]arene derivatives. Similarly, amino acid

recognition by calix[4]arene derivatives is rather limited, and the recognitions were mainly carried out by mass spectroscopy,[12] calorimetry,[13] $^1$H NMR studies,[13b,c,14] and HPLC;[15] detection by fluorescence spectroscopy[16] is scarce. Coleman et al. reported several *p*-sulfonatocalix[4]arenes for amino acid recognition and were able to establish the structure of these calixarene amino acid complexes even in the solid state.[17] There are few reports available in the literature in which amino acid recognition was achieved by chemo sensing ensemble.[12b,18] Though there are several receptors to recognize Ag$^+$ and Cys individually, to the best of our knowledge, there has been no report of any calix[4]arene molecular system that would detect selectively Ag$^+$ followed by Cys by acting as primary as well as secondary sensor. Thus the present paper reports the synthesis, characterization, and ratiometric silver-sensing properties of a lower rim functionalized calix[4]arene possessing dipicolyl moiety connected through an amide linkage (L) and the recognition of Cys by the corresponding silver complex. Thus L acts as a primary sensor toward Ag$^+$ and as a secondary sensor toward Cys and thereby exhibits INH logic gate properties. The sensor property of L toward Ag$^+$ has been proven to be due to the formation of the complex on the basis of different experimental and computational studies. Experimental evidence has also been provided for the release of L from the reaction of Cys with the silver complex.

## Results and Discussion

**Receptor Molecule L.** The receptor molecule, L, has been synthesized by four known steps starting from *p-tert*-butyl calix[4]arene as given in Scheme 1,[19] (see also Experimental Section). The acid chloride derivative **4** was prepared by reacting **3** with SOCl$_2$, followed by coupling with bis(2-picolyl)-amine to result in the receptor molecule, L. All of these molecules including L were characterized satisfactorily by $^1$H NMR, $^{13}$C NMR, ESI MS, FTIR, and elemental analysis. The cone conformation of L has been confirmed by $^1$H NMR spectroscopy and also by the structure determined on the basis of single crystal X-ray diffraction, as reported in this paper.

**Crystal Structure of L.** The ligand L was crystallized by slow diffusion of diethyl ether into a solution containing L in a mixture of methanol and chloroform, and the structure was determined by single crystal XRD (Supporting Information, S01).

(2) Mcdonnell, G.; Russell, D. A. *Clin. Microbiol. Rev.* **1999**, *12*, 147.

(3) (a) Butkus, M. A.; Labare, M. P.; Starke, J. A.; Moon, K.; Talbot, M. *Appl. Environ. Microbiol.* **2004**, *70*, 2848. (b) Petering, H. G. *Pharmaolc. Ther. A* **1976**, *1*, 127. (c) Russell, A. D.; Hugo, W. B. *Prog. Med. Chem.* **1994**, *31*, 351.

(4) Slawson, R. M.; Van Dyke, M. I.; Lee, H.; Trevors, J. T. *Plasmid* **1992**, *27*, 72.

(5) (a) Ball, R. O.; Courtney-Martin, G.; Pencharz, P. B. *J. Nutr.* **2006**, *136*, 1682S. (b) Griffith, W. *Method Enzymol.* **1987**, *143*, 366.

(6) (a) Shahrokhian, S. *Anal. Chem.* **2001**, *73*, 5972. (b) Heafield, M. T.; Fearn, S.; Steventon, G. B.; Waring, R. H.; Williams, A. C.; Sturman, S. G. *Neurosci. Lett.* **1990**, *110*, 216. (c) Puka-Sundvall, M.; Eriksson, P.; Nilsson, M.; Sandberg, M.; Lehmann, A. *Brain Res.* **1995**, *705*, 65.

(7) (a) Gutsche, C. D. *Acc. Chem. Res.* **1983**, *16*, 161. (b) Shinkai, S. *Tetrahedron* **1993**, *49*, 8933.

(8) (a) Izzet, G.; Douziech, B.; Prange, T.; Tomas, A.; Jabin, I.; Mest, Y. L.; Reinaud, O. *Proc. Natl. Acad. Sci. U.S.A.* **2005**, *102*, 6831. (b) Rondelez, Y.; Bertho, G.; Reinaud, O. *Angew. Chem., Int. Ed.* **2002**, *41*, 1044. (c) Cacciapaglia, R.; Casnati, A.; Mandolini, L.; Reinhoudt, D. N.; Salvio, R.; Sartori, A.; Ungaro, R. *J. Am. Chem. Soc.* **2006**, *128*, 12322. (d) Molenveld, P.; Engbersen, J. F. J.; Reinhoudt, D. N. *J. Org. Chem.* **1999**, *64*, 6337. (e) Molenveld, P.; Stikvoort, W. M. G.; Kooijman, H.; Spek, A. L.; Engbersen, J. F. J.; Reinhoudt, D. N. *J. Org. Chem.* **1999**, *64*, 3896. (f) Molenveld, P.; Engbersen, J. F. J.; Reinhoudt, D. N. *Angew. Chem., Int. Ed.* **1999**, *38*, 3189.

(9) (a) Kumar, M.; Mahajan, R. K.; Sharma, V.; Singh, H.; Sharma, N.; Kaur, I. *Tetrahedron Lett.* **2001**, *42*, 5315. (b) Zeng, X.; Weng, L.; Chen, L.; Leng, X.; Zhang, Z.; He, X. *Tetrahedron Lett.* **2000**, *41*, 4917. (c) Zeng, X.; Weng, L.; Chen, L.; Leng, X.; Ju, H.; He, X.; Zhang, Z.-Z. *J. Chem. Soc., Perkin Trans. 2* **2001**, 545.

(10) (a) Creaven, B. S.; Deasy, M.; Flood, P. M.; McGinley, J.; Murray, B. A. *Inorg. Chem. Commun.* **2008**, *11*, 1215. (b) Wong, M. S.; Xia, P. F.; Zhang, X. L.; Lo, P. K.; Cheng, Y.-K.; Yeung, K.-T.; Guo, X.; Shuang, S. *J. Org. Chem.* **2005**, *70*, 2816. (c) Struck, O.; Chrisstoffels, L. A. J.; Lugtenberg, R. J. W.; Verboom, W.; van Hummel, G. J.; Harkema, S.; Reinhoudt, D. N. *J. Org. Chem.* **1997**, *62*, 2487. (d) Kim, S. K.; Lee, J. K.; Lee, S. H.; Lim, M. S.; Lee, S. W.; Sim, W.; Kim, J. S. *J. Org. Chem.* **2004**, *69*, 2877. (e) Wong, M. S.; Xia, P. F.; Lo, P. K.; Sun, X. H.; Wong, W. Y.; Shuang, S. *J. Org. Chem.* **2006**, *71*, 940. (f) Zeng, X.; Sun, H.; Chen, L.; Leng, X.; Xu, F.; Li, Q.; He, X.; Zhang, W.; Zhang, Z.-Z. *Org. Biomol. Chem.* **2003**, *1*, 1073. (g) Kim, J. S.; Yang, S. H.; Rim, J. A.; Kim, J. Y.; Vicens, J.; Shinkai, S. *Tetrahedron Lett.* **2001**, *42*, 8047. (h) Budka, J.; Lhotak, P.; Stibor, I.; Michlova, V.; Sykora, J.; Cisarova, I. *Tetrahedron Lett.* **2002**, *43*, 2857.

(11) Kim, J. S.; Noh, K. H.; Lee, S. H.; Kim, S. K.; Kim, S. K.; Yoon, J. *J. Org. Chem.* **2003**, *68*, 597.

(12) (a) Stone, M. M.; Franz, A. H.; Lebrilla, C. B. *J. Am. Soc. Mass Spectrom.* **2002**, *13*, 964. (b) Perret, F.; Morel-Desrosiers, N.; Coleman, A. W. *J. Supramol. Chem.* **2002**, *2*, 533.

(13) (a) Zielenkiewicz, W.; Marcinowicz, A.; Cherenok, S.; Kalchenko, V. I.; Poznanski, J. *Supramol. Chem.* **2006**, *18*, 167. (b) Arena, G.; Casnati, A.; Contino, A.; Magri, A.; Sansone, F.; Sciotto, D.; Ungaro, R. *Org. Biomol. Chem.* **2006**, *4*, 243. (c) Douteau-Guével, N.; Perret, F.; Coleman, A. W.; Morel, J.-P.; Morel-Desrosiers, N. *J. Chem. Soc., Perkin Trans. 2* **2002**, 524. (d) Douteau-Guével, N.; Coleman, A. W.; Morel, J.-P.; Morel-Desrosiers, N. *J. Chem. Soc., Perkin Trans. 2* **1999**, 629.

(14) (a) Douteau-Guevel, N.; Coleman, A. W.; Morel, J.-P.; Morel-Desrosiers, N. *J. Phys. Org. Chem.* **1998**, *11*, 693. (b) Da Silva, E.; Coleman, A. W. *Tetrahedron* **2003**, *59*, 7357. (c) Arena, G.; Contino, A.; Gulino, F. G.; Magri, A.; Sansone, F.; Sciotto, D.; Ungaro, R. *Tetrahedron Lett.* **1999**, *40*, 1597. (d) Frish, L.; Sansone, F.; Casnati, A.; Ungaro, R.; Cohen, Y. *J. Org. Chem.* **2000**, *65*, 5026. (e) Casnati, A.; Fabbi, M.; Pelizzi, N.; Pochini, A.; Sansone, F.; Ungaro, R. *Bioorg. Med. Chem. Lett.* **1996**, *6*, 2699. (f) Baldini, L.; Casnati, L.; Sansone, F.; Ungaro, R. *Chem. Soc. Rev.* **2007**, *36*, 254. (g) Ikeda, A.; Shinkai, S. *Chem. Rev.* **1997**, *97*, 1713. (e) Casnati, A.; Sansone, F.; Ungaro, R. *Acc. Chem. Res.* **2003**, *36*, 246.

(15) Kalchenko, O. I.; Da Silva, E.; Coleman, A. W. *J. Inclusion Phenom. Macrocyclic Chem.* **2002**, *43*, 305.

(16) (a) Lu, J. Q.; Zhang, L.; Sun, T. Q.; Wang, G. X.; Wu, L. Y. *Chin. Chem. Lett.* **2006**, *17*, 575. (b) Li, H.; Wang, X. *Photochem. Photobiol. Sci.* **2008**, *7*, 694.

(17) (a) Perret, F.; Lazar, A. N.; Coleman, A. W. *Chem. Commun.* **2006**, 2425. (b) Selkti, M.; Coleman, A. W.; Nicolis, I.; Douteau-Guével, N.; Villain, F.; Tomas, A.; de Rango, C. *Chem. Commun.* **2000**, 161. (c) Lazar, A. N.; Danyluk, O.; Suwinska, K.; Coleman, A. W. *J. Mol. Struct.* **2006**, *825*, 20.

(18) Ait-Haddou, H.; Wiskur, S. L.; Lynch, V. M.; Anslyn, E. V. *J. Am. Chem. Soc.* **2001**, *123*, 11296.

(19) Joseph, R.; Ramanujam, B.; Acharya, A.; Rao, C. P. *Tetrahedron Lett.* **2009**, *50*, 2735.

**SCHEME 1.** Synthesis of Lower Rim Calix[4]arene-1,3-di-derivatives, L, and Its XRD Structure[a]
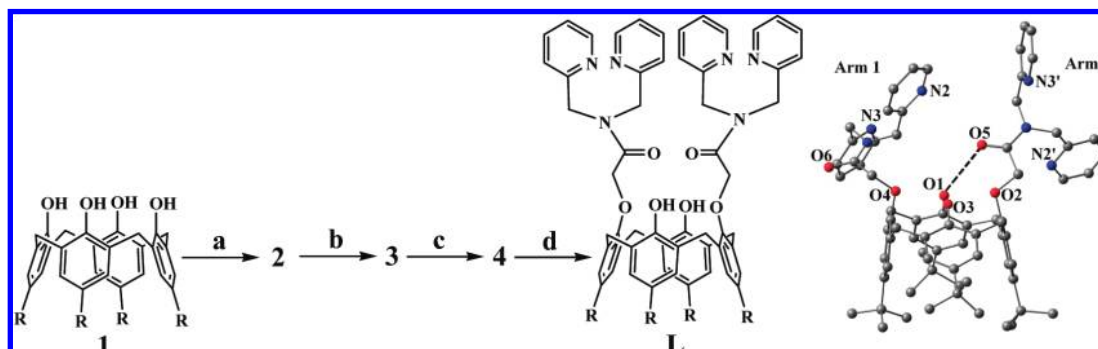


[a]Reagents and conditions: (a) bromoethylacetate/$K_2CO_3$/acetone; (b) NaOH/$C_2H_5OH$, reflux; (c) $SOCl_2$/benzene, reflux; (d) bis(2-picolyl)amine/$Et_3N$/ THF. R = *tert*-butyl.
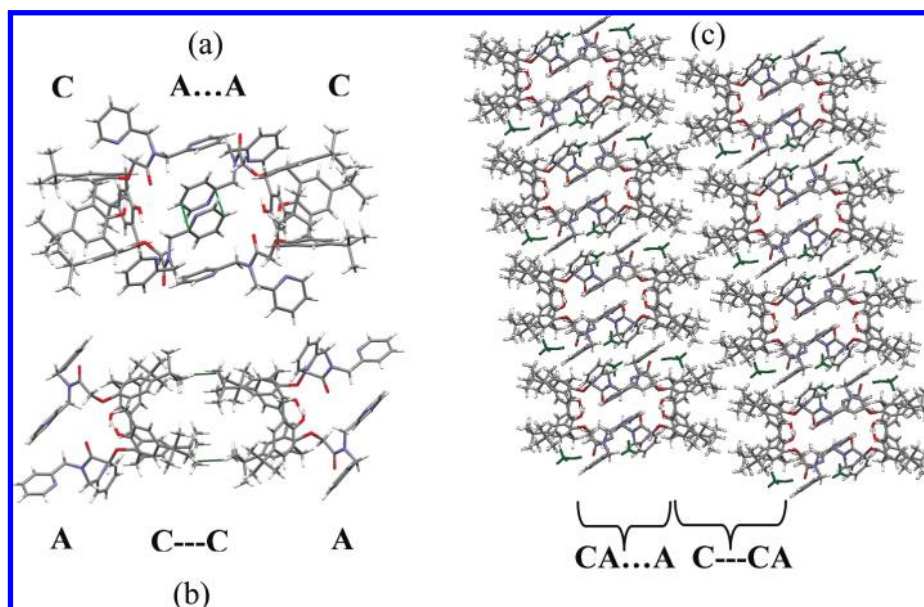


**FIGURE 1.** From the crystal structure of L: (a) dimer formed by the arms of L (i.e., CA···AC type), (b) dimer formed by the hydrophobic arene cavity (i.e., AC---CA type), and (c) lattice structure of L where methanols are shown in green. "A" is the arms portion, and "C" is the arene cavity.

In the asymmetric unit cell of the centrosymmetric triclinic system, two methanol molecules were crystallized along with one molecule of L. The two O−H···O intramolecular hydrogen bonds {H···O, O···O distances (Å) and O−H···O angle (deg) are 1.820, 2.844, 169 and 2.014, 2.784, 147} observed at the lower rim fixes the calix[4]arene in a cone conformation. Because of the presence of a hydrogen bond between amide CO and phenolic OH (2.362 Å, 3.010 Å, 131°), one of the amide CO is projected inside the cavity of calix[4]arene (Arm 2, Scheme 1), while lack of the hydrogen bonding makes the other amide CO to point outside the calix[4]arene cavity (Arm 1, Scheme 1). The nitrogen atoms present in the pyridyl moiety generates possible binding cores in L (based on arms, $N_4$ and $N_4O_2$; arms + phenolic OH, $O_4$ and $N_4O_6$). Among these, the nitrogen-rich pyridyl core is best suited for transition metal ions.[19,20] The details of the structure determination and the refinement as well as some important bond lengths, bond angles, and hydrogen

bond data are given in Supporting Information, S01. However, the two arms are disposed in space farther apart by exhibiting inter-arm N···N distances ranging from 5.1 to 8.9 Å and intra-arm N···N distances ranging from 4.9 to 5.4 Å. Hence, L needs to undergo some conformational changes if the arms are to be involved in binding to a metal ion through coordination.

**Lattice Structure.** In the lattice, L forms a dimer through the interactions extended between the arms of both partners in a head-to-head fashion. These are through $\pi-\pi$ interactions extended between the pyridyl moieties of similar type of arms of the two partners (Figure 1a). Such head-to-head dimers form a supramolecular column through arene−arene interactions extended between the hydrophobic cavities of the two neighbor dimers via the *tert*-butyl groups, where the shortest distance between the *tert*-butyl carbons being ∼3.45 Å (Figure 1b). Thus the column is a repetition of ---CA···AC---CA···AC---CA···AC---CA···, where "C" represents the hydrophobic cavity portion possessing the *tert*-butyl groups and "A" represents the arms portion. These columns are further connected through weak H-bond

(20) Joseph, R.; Ramanujam, B.; Pal, H.; Rao, C. P. *Tetrahedron Lett.* **2008**, *49*, 6257.
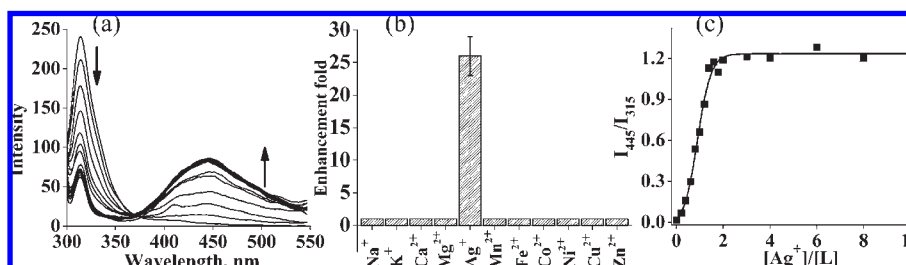
**FIGURE 2.** (a) Fluorescence spectral traces of L (10 $\mu$M) during titration with Ag$^+$; (b) histogram representing the relative fluorescence intensity ($I/I_0$) observed at 445 nm; (c) plot of relative fluorescence intensity ratio, *viz.*, $I_{445}/I_{315}$ vs [Ag$^+$]/[L] mole ratio.
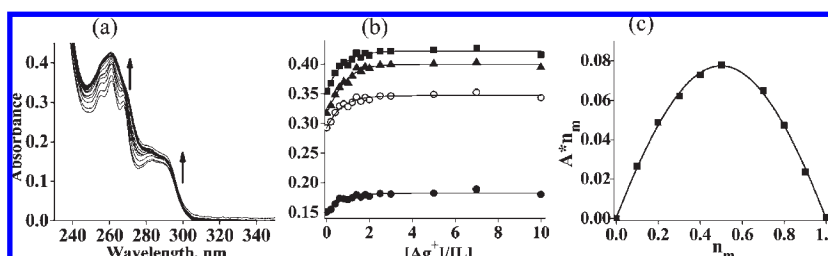


**FIGURE 3.** Absorption spectral titration of L with Ag$^+$: (a) spectral traces observed during the titration in the region 230−350 nm; (b) plots of absorbance versus mole ratio of [Ag$^+$]/[L] for different bands ($\bullet$ = 282, $\circ$ = 268, $\blacksquare$ = 261, and $\blacktriangle$ = 255 nm); and (c) Job's plot of $n_m$ versus $A*n_m$, where $n_m$ is the mole fraction of the metal ion added and $A$ is the absorbance.

interactions offered by the solvent methanol molecules present in the lattice resulting in the structure shown in Figure 1c.

**A. Primary Sensor Properties of L in the Selective Recognition of Ag$^+$. Fluorescence Titration Studies.** Calix[4]arene derivative L has been studied for its interaction with Ag$^+$ by exciting the solutions at 285 nm and by following the emission bands observed at 315 and 445 nm, which shows fluorescence quenching and enhancement, respectively, as the concentration of added Ag$^+$ increases. This resulted in the formation of an iso-emissive point at 375 nm (Figure 2a). Moreover the ligand L showed a fluorescence enhancement of ∼25-fold during the titration with Ag$^+$ (Figure 2b). None of the other M$^{n+}$ ions, *viz.*, Na$^+$, K$^+$, Mg$^{2+}$, Ca$^{2+}$, Mn$^{2+}$, Fe$^{2+}$, Co$^{2+}$, Ni$^{2+}$, Cu$^{2+}$, and Zn$^{2+}$, showed fluorescence changes except Cu$^{2+}$, which shows changes only in the 315 nm band, suggesting that the changes observed in this band alone can be used for selective recognition of Cu$^{2+}$ as reported by us recently,[19] while Ag$^+$ can be selectively recognized by ratiometric variation of the fluorescence intensity, *viz.*, [$I_{445}/I_{315}$] as reported in this paper (Figure 2c). The new emission band at 445 nm originates from the excimer formation of pyridyl moieties in the excited state, suggesting that the silver ion brings the pyridyl moieties together during the metal ion binding. Such excimer formation has been reported in the literature for a tetra-derivative of calix[4]arene containing pyridyl moieties at its lower rim.[21] The binding constant of L with Ag$^+$ was calculated by the Benesi−Hildebrand equation, and the corresponding association constant $K_a$ was found to be 11117 ± 190 M$^{-1}$. The minimum concentration at which L can detect Ag$^+$ has been found to be 450 ppb (Supporting Information, S02).

**Absorption Titration Studies.** To get further support for the metal ion binding, absorption titration has also been

carried out between L and Ag$^+$. The ligand L exhibited four absorption bands centered at 261, 285, 255, and 268 nm; all of these bands showed an increase in the absorbance upon addition of Ag$^+$ (Figure 3a); and saturation in absorbance was observed at ≥2 equiv (Figure 3b). The stoichiometry of the complex formed between L and Ag$^+$ has been derived to be 1:1 on the basis of a Job's plot (Figure 3c), and the $K_a$ value was found to be 11941 M$^{-1}$.

**Electrospray Mass Spectrometry.** ESI MS spectrum obtained during the titration of L with Ag$^+$ results in a 100% molecular ion peak at $m/z$ = 1235.5 corresponding to a 1:1 complex. The isotopic peak pattern observed for Ag$^+$ closely resembles that of the calculated one, supporting the presence of metal ion and hence the complex formation (Figure 4).
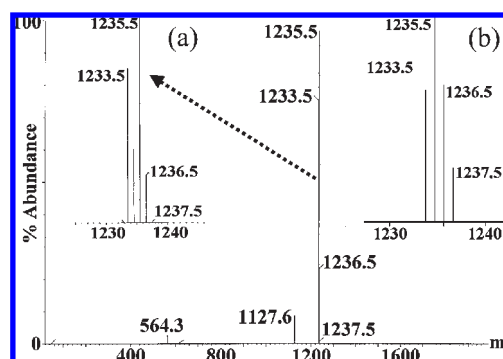


**FIGURE 4.** ESI MS spectrum obtained in the titration of L with Ag$^+$. Insets: (a) expanded peak of the complex; (b) calculated isotopic pattern for the complex of [L+Ag$^+$].

**$^1$H NMR Titration of L with Ag$^+$.** Interaction between L and Ag$^+$ was studied by NMR spectroscopy in DMSO-$d_6$. During the titration, the concentration of L was kept constant and the added [Ag$^+$] mole ratio was varied, *viz.*, 0.5, 1, 1.5, 2.0, 2.5, 3.5,

(21) Souchon, V.; Maisonneuve, S.; David, O.; Leray, I.; Xie, J.; Valeur, B. *Photochem. Photobiol. Sci.* **2008**, *7*, 1323.
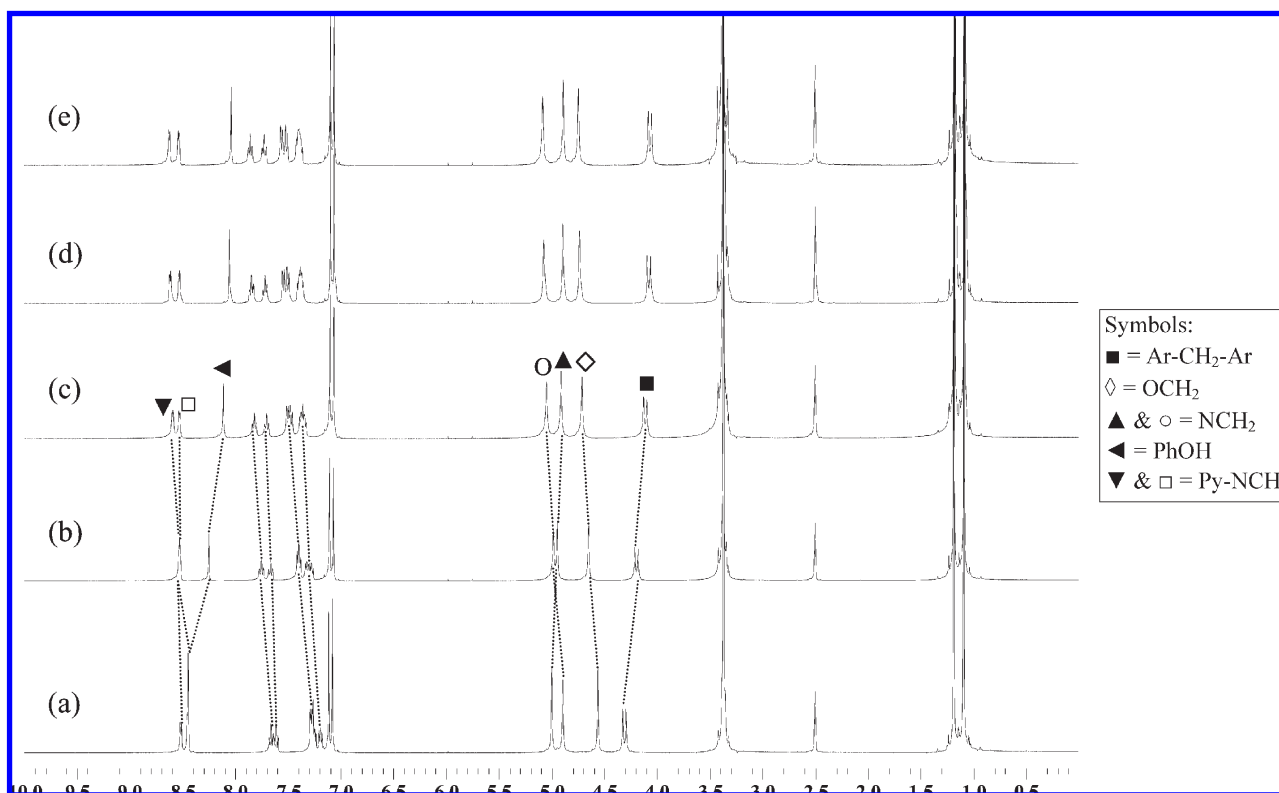
**FIGURE 5.** $^1$H NMR spectra measured during the titration of L with different mole ratios of $Ag^+$ (in DMSO-$d_6$): (a) 0; (b) 0.5; (c) 1.0; (d) 1.5; (e) 2.0.

and 4.5 equiv (Figure 5). $^1$H NMR studies showed minimal to marginal changes in the $\delta$ values of pyridyl, phenolic-OH, and bridged -CH$_2$ protons (Figure 6). Absence of any changes observed in the chemical shift of aromatic and/or *tert*-butyl protons rules out any interaction between the arene and $Ag^+$. If the $Ag^+$ were to be interacting with the arene cavity of the calixarene, the aromatic protons would show corresponding shifts as reported in the literature by Shinkai and co-workers.[22] The downfield shift observed in the pyridyl and the arm -NCH$_2$ protons is suggestive of the binding of $Ag^+$ in the pyridyl core through nitrogens. The upfield shift observed in the bridged -CH$_2$ and the phenolic -OH groups of calix[4]arene are suggestive of the breakage and/or weakening of lower rim H-bond interactions to result in conformational changes as reported for calix[4]arene derivatives in the literature in the presence of $Ag^+$ ion[10f] (Figure 6).
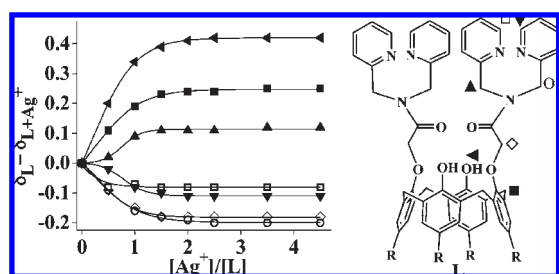


**FIGURE 6.** Metal-ion-induced shift ($\Delta\delta = \delta_L - \delta_{L+Ag^+}$) observed with different protons of L at various mole ratios of $[Ag^+]/[L]$ as taken from Figure 5. Symbols are the same as in Figure. 5.

(22) Ikeda, A.; Tsuzuki, H.; Shinkai, S. *J. Chem. Soc., Perkin Trans. 2* **1994**, 2073.

**Competitive Metal Ion Titrations.** To find out whether L can detect $Ag^+$ selectively even in the presence of other metal ions, competitive metal ion titrations were carried out. A 1:5 mole ratio mixture of L and $M^{n+}$ were titrated against different equivalents of $Ag^+$, and the corresponding fluorescence emission spectra were recorded. It was found that $Ag^+$ can replace all the other $M^{n+}$ ions except $Cu^{2+}$, as can be seen from Figure 7. Thus, while $Ag^+$ ion can be detected quantitatively in the presence of a number of biologically relevant $M^{n+}$ ions except $Cu^{2+}$, the $Cu^{2+}$ indeed can be quantified by L in the presence of all of these.
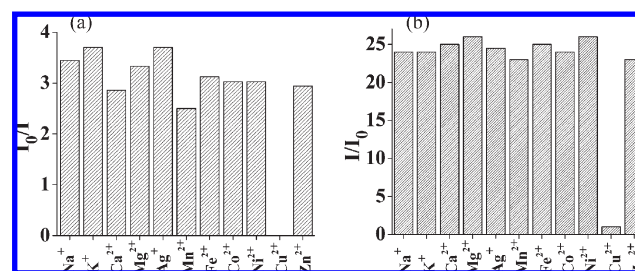


**FIGURE 7.** Relative fluorescence intensity of L upon addition of 3 equiv of $Ag^+$ in the presence of 5 equiv of $M^{n+}$ ions at (a) 315 and (b) 445 nm.

**Control Molecules.** To substantiate the role of the calix-[4]arene platform and the presence of a nitrogen core in the recognition process of L, several related molecular systems, *viz.*, $L_1$, $L_2$, $L_3$, and $L_4$, shown in Figure 8 have been subjected to similar titration studies by emission spectroscopy. These were chosen for the following reasons: (a) $L_1$
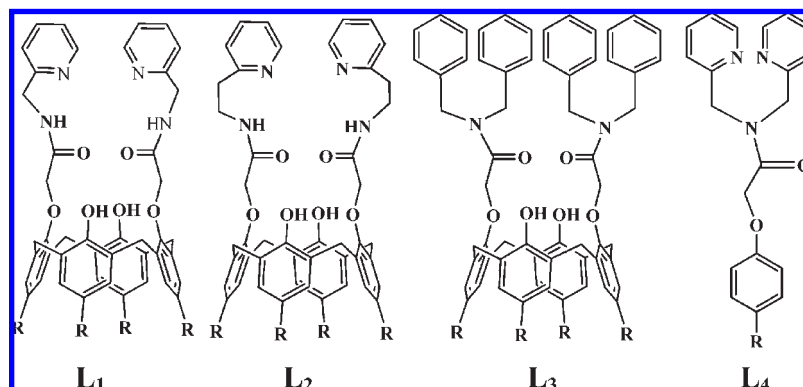
**FIGURE 8.** Schematic representation of the control molecules, $L_1$, $L_2$, $L_3$, and $L_4$. R = *tert*-butyl.

contains one methyl pyridyl moiety instead of the two present in L; (b) the binding core present in $L_2$ has one additional $CH_2$ group but one less pyridyl group, providing a different binding core compared to that of L; (c) the pyridyl moieties in L have been replaced by noncoordinating benzyl moieties in $L_3$; (d) the calix[4]arene platform present in L has been replaced by a single strand in $L_4$ while retaining the binding arm.

Synthesis and characterization details of the control molecules, $L_1$ and $L_3$, have been discussed by us earlier.[19] $L_2$ was prepared by coupling a diacid chloride derivative of calix[4]arene, **4** (given in Scheme 1), with 2-amino ethyl pyridine, and the product formed was purified and characterized by spectral techniques (Supporting Information, S03). A single strand derivative having *p-tert*-butyl phenol instead of calix-[4]arene has been synthesized by coupling the acid chloride derivative of *p-tert*-butyl phenol with bis(2-picolyl)amine moiety as shown in Scheme 2 (Supporting Information, S03). The product formed has been purified by silica gel

**SCHEME 2. Synthesis of $L_4$[a]**
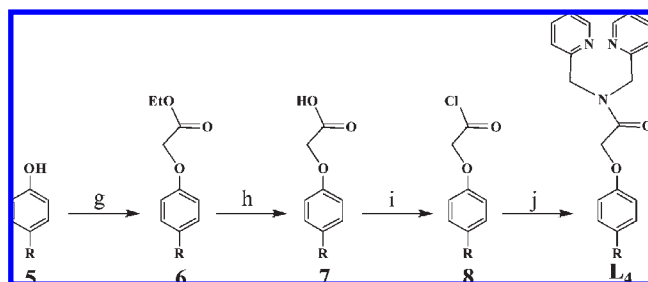


[a]Reagents and conditions: (g) bromoethylacetate/$K_2CO_3$/acetone; (h) KOH/$C_2H_5OH$/water, reflux; (i) $SOCl_2$/benzene, reflux; and (j) bis(2-picolyl)amine/$Et_3N$/THF. R = *tert*-butyl.

column chromatography and was characterized by different analytical and spectral techniques.

The control molecules, $L_1$, $L_2$, $L_3$, and $L_4$, have been studied for their binding ability toward $Ag^+$ ion, and it was found that none of these show any fluorescence change, indicating their noninteractive nature with $Ag^+$ ion (Figure 9).

**Computational Modeling of the $Ag^+$ Complex of L.** As the stiochiometry of the complex formed between $Ag^+$ and L was found to be 1:1 based on emission, absorption, and ESI
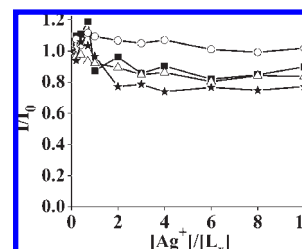


**FIGURE 9.** Plot of relative fluorescence intensity ($I/I_0$) versus mole ratio of $Ag^+$ added to the control molecules: $L_1$ (■), $L_2$ (△), $L_3$ (○), and $L_4$ (★).

MS studies, the nature of $Ag^+$ coordination with L was studied by computational studies using the Gaussian03 software package.[23] The initial geometry for L was taken from the single crystal XRD structure. As the number of atoms present in L was too large, L′ was generated from L by replacing the *tert*-butyl groups present at the upper rim with hydrogens. Such changes made in calixarene systems to reduce the computational times exhibited no influence on the conformation of the arm as shown by us earlier.[20,24] L′ is chemically and structurally similar to L and hence was used in the calculations to reduce the computational times. The geometry optimizations for L and L′ were done in a cascade fashion starting from semiempirical PM3 followed by *ab initio* HF to DFT B3LYP by using various basis sets, *viz.*, PM3 → HF/STO-3G → HF/3-21G → HF/6-31G → B3LYP/STO-3G → B3LYP/3-21G → B3LYP/6-31G. The optimization at the DFT level showed considerable change in the dihedral angles of the arms when

(23) Frisch, M. J.; Trucks, G. W.; Schlegel, H. B.; Scuseria, G. E.; Robb, M. A.; Cheeseman, J. R.; Montgomery, J. A., Jr.; Vreven, T.; Kudin, K. N.; Burant, J. C.; Millam, J. M.; Iyengar, S. S.; Tomasi, J.; Barone, V.; Mennucci, B.; Cossi, M.; Scalmani, G.; Rega, N.; Petersson, G. A.; Nakatsuji, H.; Hada, M.; Ehara, M.; Toyota, K.; Fukuda, R.; Hasegawa, J.; Ishida, M.; Nakajima, T.; Honda, Y.; Kitao, O.; Nakai, H.; Klene, M.; Li, X.; Knox, J. E.; Hratchian, H. P.; Cross, J. B.; Adamo, C.; Jaramillo, J.; Gomperts, R.; Stratmann, R. E.; Yazyev, O.; Austin, A. J.; Cammi, R.; Pomelli, C.; Ochterski, J. W.; Ayala, P. Y.; Morokuma, K.; Voth, G. A.; Salvador, P.; Dannenberg, J. J.; Zakrzewski, V. G.; Dapprich, S.; Daniels, A. D.; Strain, M. C.; Farkas, O.; Malick, D. K.; Rabuck, A. D.; Raghavachari, K.; Foresman, J. B.; Ortiz, J. V.; Cui, Q.; Baboul, A. G.; Clifford, S.; Cioslowski, J.; Stefanov, B. B.; Liu, G.; Liashenko, A.; Piskorz, P.; Komaromi, I.; Martin, R. L.; Fox, D. J.; Keith, T.; Al-Laham, M. A.; Peng, C. Y.; Nanayakkara, A.; Challacombe, M.; Gill, P. M.W.; Johnson, B.; Chen, W.; Wong, M. W.; Gonzalez, C.; Pople, J. A. *Gaussian 03, revision C.02*; Gaussian, Inc.: Wallingford, CT, 2004.
(24) Joseph, R.; Ramanujam, B.; Acharya, A.; Khutia, A.; Rao, C. P. *J. Org. Chem.* **2008**, *73*, 5745.
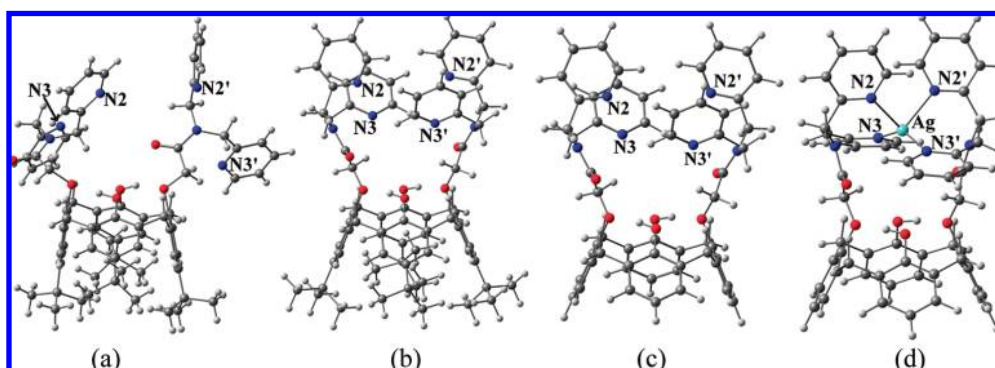
**FIGURE 10.** (a) Molecular structure of L from single crystal XRD, (b) L optimized through B3LYP/6-31G, (c) L′ optimized through B3LYP/6-31G, and (d) DFT optimized structure of [Ag-L′]. The bond distance (Å) and bond angles (deg) in the coordination sphere are Ag−N2 = 2.517, Ag−N3 = 2.326, Ag−N2′ = 2.517, Ag−N3′ = 2.326 Å and N2−Ag−N3 = 109.7, N2−Ag−N2′ = 98.9, N2−Ag−N3′ = 91.8, N3−Ag−N2′ = 91.8, N3−Ag−N3′ = 147.1, N2′−Ag−N3′ = 109.7°.
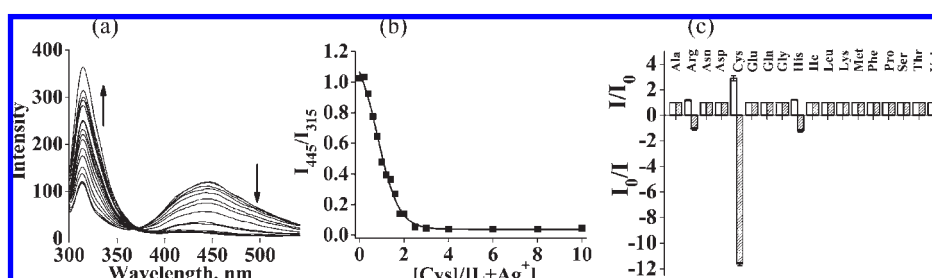


**FIGURE 11.** (a) Fluorescence spectral traces obtained during the titration of [L+Ag$^+$] with cysteine, (b) plot of relative fluorescence intensity ($I_{445}/I_{315}$) versus mole ratio of cysteine, and (c) histogram representing the effect of various amino acids on the fluorescence behavior of [L+Ag$^+$]. Filled columns = 445 nm, open columns = 315 nm.

compared to the crystal structure (Supporting Information S04). As a result of this, the inter-arm N···N distances are shortened from 5.1−8.9 Å to 4.7−5.5 Å, and intra-arm N···N distances are shortened from 4.9−5.4 Å to 3.73 Å; thus the arms are well poised for metal ion binding in the optimized L. The conformational changes of the arms are exactly same in both L and L′ (Figure 10, Supporting Information S04), and hence their coordination features are exactly same.

To study the binding characteristics of Ag$^+$, a starting model was generated by taking the DFT optimized L′ and placing the silver ion well above the core of pyridyl moieties at a non-interacting distance. This model was then optimized initially using HF/3-21G level of calculations, and the output structure from this was taken as input for DFT calculations performed using B3LYP with SDDAll basis set for Ag$^+$ and 6-31+G(d) for all other atoms in the complex. The optimized complex of Ag$^+$ with L′ at this stage showed a distorted tetrahedral geometry around Ag$^+$ where all four pyridyl nitrogens are bonded to the central ion with Ag−N distances of 2.326 and 2.517 Å (Figure 10, Supporting Information S04). These Ag−N distances are comparable with the experimental ones reported in the literature.[25] However, the geometry about Ag$^+$ is significantly distorted by exhibiting coordination angles in the range 91.8−147.1°.

**B. Secondary Sensor Behavior of [L+Ag$^+$] and Selective Recognition of Cys among Naturally Occurring Amino Acids.** Since L recognizes Ag$^+$ ratiometrically, the utility of [L+Ag$^+$] complex toward selective recognition of amino acid has been studied so that this complex can act as a secondary sensor.

**Fluorescence Titration.** The chemosensing ensemble used in these titrations was prepared *in situ* by mixing L and Ag$^+$ in a 1:2 ratio. Out of 20 amino acids studied for their interaction, only Trp and Tyr did not yield interpretable results owing to their strong emission that overlaps with the emission of L. The chemosensing mixture was titrated with all of the remaining naturally occurring 18 amino acids, where the fluorescence spectrum of [L+Ag$^+$] is altered only in the presence of Cys and not with the other 17 amino acids. During the titration of [L+Ag$^+$] with Cys, the emission band at 315 nm enhances and that observed at 445 nm quenches. This is exactly reverse to what happens when L is titrated with Ag$^+$, as reported in this paper (Figure 2), indicating that the Ag$^+$ is being removed from the complex by Cys to release free L (Figure 11) and thus the recognition of Cys by [L+Ag$^+$] complex as a secondary sensor. The release of L in the titration of Cys is followed by the formation of Cys complex of Ag$^+$ as it can form a stable complex with the thiol functionality. The necessity of -SH function and the formation of a Cys complex of Ag$^+$ were further proven on the basis of the emission studies performed on control molecular systems as reported in this paper. The detection limit of Cys by [L+Ag$^+$] complex has been found to be 514 ppb (Supporting Information, S05).

(25) Munakata, M.; Wen, M.; Suenaga, Y.; Kuroda-Sowa, T.; Maekawa, M.; Anahata, M. *Polyhedron* **2001**, *20*, 2321.

**Titration with Control and Analogous Molecules.** Since fluorescence changes occur only in the presence of Cys and not with the other amino acids, the role of the -SH function in Ag$^+$ binding was further confirmed by studying the fluorescence response of [L+Ag$^+$] with different sulfur-containing systems, *viz.*, cysteine ethyl ester, cysteamine, glutathionine reduced (GSH), and glutathionine oxidized (GSSG) (Figure 12). All of these, except GSSG, exhibited changes in the fluorescence owing to the presence of the -SH functionality, whereas in GSSG the -SH is oxidized to -S-S-. Even Met does not show changes in the fluorescence owing to the presence of R-S-Me and not the -SH function. This experiment clearly suggests that Ag$^+$ mainly interacts through the -SH function of cysteine, and hence the [L+Ag$^+$] chemoensemble acts as a sensor for the thiol functionality.
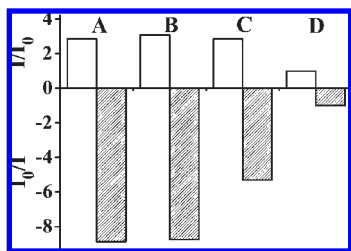


**FIGURE 12.** Histogram representing the enhancement and quenching fold exhibited by sulfur-containing (*viz.*, -SH and -S-S-) molecules, where A = cysteine ethyl ester, B = cysteamine, C = glutathionine reduced (GSH), and D = glutathionine oxidized (GSSG). Filled and open columns correspond to 445 and 315 nm emission bands, respectively.

**ESI MS Titration of [L+Ag$^+$] with Cys.** To provide further proof for the release of L and the formation of a Cys complex of Ag$^+$, ESI MS titration was carried out. The spectrum exhibited two major *m/z* peaks (Figure 13). Whereas the peak observed at 240.2 is assignable to [2Cys + 2Ag + Na − H]$^{2+}$, that observed at 1128 is assignable to [L + H]$^+$. The first peak is from the Ag$^+$ complex of Cys, and the second peak is from simple L. All this clearly supports the release of L as well as the formation of the Ag$^+$ complex of Cys, i.e., {[L+Ag$^+$] + Cys → L + [Cys+Ag$^+$]}. Even the absorption spectral studies clearly demonstrate the release of L when Cys is added to [L+Ag$^+$] (Supporting Information, S06).
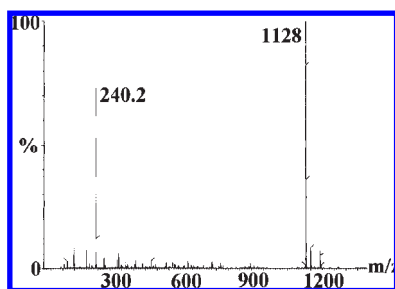


**FIGURE 13.** ESI mass spectrum obtained in the titration of [L+Ag$^+$] with Cys.

**$^1$H NMR Titration of [L+Ag$^+$] with Cysteine and Cysteamine.** The release of L and the formation of the complex of Ag$^+$ have been further proven through $^1$H NMR titration carried out between [L+Ag$^+$] and Cys/cysteamine. The titration of

[L+Ag$^+$] with Cys could not be continued beyond 1 equiv owing to precipitation (Supporting Information, S07); therefore, the detailed titrations were carried out using cysteamine instead of Cys, as the fluorescence behavior of both of these was found to be same. During the titration, as the concentration of cysteamine increases, the proton signals of bridged-CH$_2$, -OCH$_2$, -NCH$_2$, pyridyl, and lower rim phenolic-OH are shifted and moved toward simple L (Supporting Information, S07). Quantitative changes observed in the chemical shift can be seen from the plots given in Figure 14. Thus it has been found that cysteamine removes Ag$^+$ from the binding core of calix[4]arene using its -SH function, resulting in the recovery of simple L from the [L+Ag$^+$]. On the other hand the formation of the Ag$^+$ complex with Cys has been identified based on ESI MS.
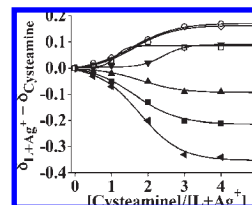


**FIGURE 14.** (a) Cysteamine-induced chemical shifts $\Delta\delta$ ($\Delta\delta = \delta_{(L+Ag^+)+cysteamine} - \delta_{(L+Ag^+)}$) observed with different protons of L at various mole ratios of [cysteamine]/[L+Ag$^+$] as noted in Supporting Information, S07. For symbols refer to Figure 5.

**TEM Studies.** To determine whether the release of L from the reaction of [L+Ag$^+$] with Cys is reflected in their nanostructural features, TEM studies were performed with L, [L+Ag$^+$], and {[L+Ag$^+$]+Cys}, and the corresponding micrographs and particle size distributions are shown in Figure 15. The micrographs show spherical particles in the case of L. The smaller size particles are in the range of 90−150 nm, whereas the bigger clusters have diameters of 180−270 nm. The interconnectivity present in these particles is similar to that observed in case of the complexation of Hg$^{2+}$ with amide-linked benzimidazole-1,3-di-derivative of calixarene as reported by us recently.[24] When AgClO$_4$ is added to L, the size of the particles is reduced drastically to 15−35 nm and the shape is changed to nonspherical, indicating the complexation of L with Ag$^+$ where the complex possessing silver ions exhibits dark spots. Thus, both the size and shape of the particles differ between L and [L+Ag$^+$], suggesting that it is possible to identify the complex formation between L and Ag$^+$ by using nanostructural features.
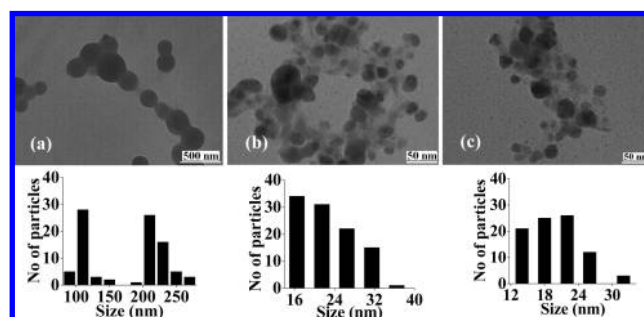


**FIGURE 15.** TEM images of (a) L, (b) [L+Ag$^+$], and (c) {[L+Ag$^+$]+Cys} and their particle size distribution plots (bottom). Number of particles analyzed ranges from 100 to 150 in each case.

However, the micrographs also show background images corresponding to the unreacted AgClO$_4$. Upon addition of Cys to the complex, the micrographs are filled with particles arising from L, [L+Ag$^+$], AgClO$_4$, and [Cys·Ag$^+$] complex. Therefore, it is difficult to clearly distinguish the particles of L alone from all of these because the particles containing the Ag$^+$ dominate as dark spots, and hence the lighter spots expected from L cannot be easily distinguished as these are buried in the background. (Supporting Information S08)

**Dynamic Light Scattering (DLS) Studies.** In DLS, all of the species have shown solvo-dynamic diameters of more than 10 $\mu$m. The simple ligand L is shown to have an average diameter much higher than that of its [L+Ag$^+$] complex as well as that observed from the reaction mixture of {[L+Ag$^+$] + Cys}. The trend observed in solvo-dynamic diameters is in line with the particle size distribution of the individual species observed in TEM (Supporting Information, S09).

**C. INH Logic Gate Properties of L with Ag$^+$ and Cys.** In the present case, the logic gate properties of L have been studied using two input signals as Ag$^+$ and Cys, respectively, by monitoring the emission of L at 445 nm (Figure 16). From the perspective of logic functions, the emission of L has been determined only by the presence of single input, *viz.*, Ag$^+$, and not with the cysteine, as Cys is insensitive to L. This means that the emission of L is switched on only in the presence of Ag$^+$ (25 fold fluorescence enhancement of 445 nm band of L) and in the absence of Cys. Under the conditions where Ag$^+$ is absent and Cys is present, no emission is observed in the 445 nm band of L (Supporting Information, S10). Similarly in the presence of 2 equiv of Ag$^+$ and Cys, the fluorescence emission of L at 445 nm was quenched and no significant output signal was observed. From these studies, it has been found that L can be used as a INHIBIT (INH) logic gate toward Ag$^+$ in the absence of Cys by observing the emission at 445 nm. The truth table and the pictorial representation for the corresponding INH are given in Figure 16.
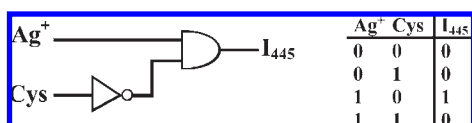


**FIGURE 16.** (a) INH logic gate represented using a conventional gate notation; an active output signal is obtained when Ag$^+$ = 1 and Cys = 0. (b) Truth table for the INH logic gate; Ag$^+$ and Cys are inputs to the system; I$_{445}$ is the output signal of L at 445 nm.

**Conclusions and Correlations**

A structurally characterized lower rim 1,3 diamide-bis-(2-picolyl)-derivative of calix[4]arene (L) exhibits high selectivity toward Ag$^+$. The selectivity has been demonstrated by fluorescence, absorption, and ESI MS spectroscopy. Interaction of Ag$^+$ with L enhances the fluorescence emission at 445 nm and quenches the fluorescence at 315 nm, thus exhibiting a ratiometric behavior. L is sensitive and selective toward Ag$^+$ over nine other biologically important ions studied, *viz.*, Na$^+$, K$^+$, Mg$^{2+}$, Ca$^{2+}$, Mn$^{2+}$, Fe$^{2+}$, Co$^{2+}$, Ni$^{2+}$, and Zn$^{2+}$, as demonstrated by individual as well as competitive metal ion titrations. L can detect up to 450 ppb by switch-on fluorescence at 445 nm; thus L is a ratiometric primary sensor for Ag$^+$. The necessity of the pyridyl moieties

and the calix[4]arene platform in the recognition of Ag$^+$ has been demonstrated by comparing the fluorescence results obtained from several control molecules.

Whereas the fluorescence and absorption spectroscopy provided information for the formation of 1:1 complex between Ag$^+$ and L, *viz.*, [LAg$^+$], the ESI MS confirmed the same unambiguously by exhibiting an isotopic peak pattern for the presence of silver in the complex. The complex formation between L and Ag$^+$ has been further followed by measuring $^1$H NMR spectra as a function of added silver perchlorate concentration. Comparison of the changes observed in the chemical shifts of different protons, in terms of downfield and upfield, suggests Ag$^+$ binding in the pyridyl-nitrogen core (N$_4$ core) associated with some conformational changes in the calixarene platform. It has been demonstrated by transmission electron microscopy that the nanostructural features of L and its complex of Ag$^+$ differ substantially to differentiate the complex from that of simple L.

Therefore, the silver-binding capabilities of the nitrogen-binding core of pyridyl moieties available in L has been examined by computational calculations at the DFT level. The arms are found to be quite farther apart in the crystal structure of L as can be judged from the intra- and inter-arm N···N distances. Therefore, the binding of metal ions can take place only when considerable dihedral changes take place particularly in the arms of L. Indeed the computational calculations performed on L (or its shorter version, L′) in the presence of Ag$^+$ clearly demonstrated substantial changes in the dihedral angles. Comparison of the orientation of the arms and the binding cores present in the crystal structure of L, the optimized structure of L, and its Ag$^+$ complex clearly suggest that the arm undergoes conformational changes along with some rotation about the pyridyl moiety so as to bring all four pyridyl nitrogens in a manner to bind to the central Ag$^+$ in a tetrahedral fashion (Figure 17). The tetrahedral geometry observed about Ag$^+$ is highly distorted as can be judged on the basis of the wide range (91.8−147.1°) of coordination sphere angles observed.
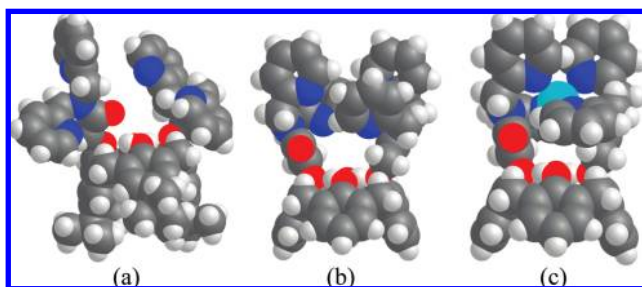


**FIGURE 17.** Space-filling model for (a) molecular structure of L from XRD, (b) L′ optimized at DFT (B3LYP/6-31G), and (c) [L′+Ag$^+$] optimized at DFT {B3LYP with mixed basis set SDDAll(Ag) and 6-31+G(d) for other atoms}. Ag$^+$ is in cyan.

The *in situ* prepared silver complex of L, *viz.*, [L+Ag$^+$], was able to detect Cys ratio-metrically in a manner exactly reverse to what happens when Ag$^+$ is added to L in fluorescence spectroscopy. Thus, upon addition of Cys to [L+Ag$^+$], the 445 nm band intensity decreases and that of the 315 nm band increases, suggesting the release of L from the silver complex. The release of L has also been further proven on the basis of NMR titration. The present studies also demonstrate the

necessity of the -SH function in removing the $Ag^+$ from its complex of L based on several analogous and control molecules. The removal of $Ag^+$ by cysteine (or other -SH molecules) and the formation of a $Ag^+$ complex of Cys has been proven on the basis of ESI mass spectrometry. Thus the *in situ* generated $[L+Ag^+]$ complex selectively recognizes Cys among the naturally occurring amino acids to a lowest concentration of 514 ppb, and hence L acts as secondary sensor toward Cys. The characteristic changes observed in the fluorescence spectroscopy during the sensing of $Ag^+$ as well Cys are represented schematically in Scheme 3 to express the primary and secondary sensor properties of L.

**SCHEME 3. Schematic Representation of the Primary and Secondary Sensing Properties of L**
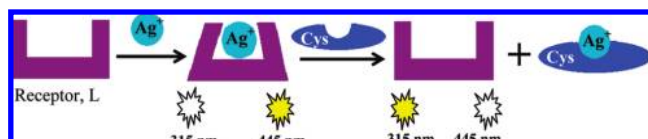


The INH logic gate has been generated by choosing $Ag^+$ and Cys as inputs and by monitoring the output signal at 445 nm that originated from the excimer emission of L in the presence of $Ag^+$. Thus L is a potential primary sensor toward $Ag^+$ and is a secondary sensor toward Cys, and both act ratiometrically.

## Experimental Section

All the perchlorate salts, *viz.*, $Mn(ClO_4)_2 \cdot 6H_2O$, $Fe(ClO_4)_2 \cdot xH_2O$, $Co(ClO_4)_2 \cdot 6H_2O$, $Ni(ClO_4)_2 \cdot 6H_2O$, $Cu(ClO_4)_2 \cdot 6H_2O$, $Zn(ClO_4)_2 \cdot 6H_2O$, $Ag(ClO_4) \cdot xH_2O$, $NaClO_4 \cdot H_2O$, $KClO_4$, $Ca(ClO_4)_2 \cdot 4H_2O$, and $Mg(ClO_4)_2 \cdot 6H_2O$, were procured from Sigma Aldrich Chemical Co., USA. All solvents used were dried and distilled by usual procedures immediately before use. Distilled and deionized water was used in the studies. The synthesis procedures and the characterization data of all molecules used in this paper are given in Supporting Information S03. Original NMR spectra of all these molecules are given in Supporting Information S03. The details of the instruments used for all studies are discussed in Supporting Information S11.

**Ligand L.** A suspension of bis(2-picolyl)amine (0.59 g, 2.96 mmol) and $Et_3N$ (0.55 g, 5.43 mmol) was stirred in dry THF (30 mL) under argon atmosphere. Diacid chloride **4** (1.08 g, 1.35 mmol) in dry THF (30 mL) was added dropwise to this reaction mixture. Immediately, a yellowish precipitate was formed, and stirring was continued for 48 h at room temperature. After filtration, the filtrate was concentrated to dryness. A yellow solid was obtained that was extracted with $CHCl_3$ and washed with water and then with brine, and the organic layer was dried with anhydrous $MgSO_4$. Filtrate was concentrated to dryness and purified by column chromatography to give L as white

solid. Yield (35%, 0.52 g). Anal. Calcd for $C_{72}H_{82}N_6O_6 \cdot C_2H_5OH$: C, 75.74; H, 7.56; N, 7.16. Found: C, 75.18; H, 7.34; N, 7.34. FTIR (KBr, $cm^{-1}$): 1641 ($\nu_{C=O}$), 3394 ($\nu_{OH}$). $^1H$ NMR ($CDCl_3$, $\delta$ ppm): 0.93 (s, 18H, $C(CH_3)_3$), 1.27 (s, 18H, $C(CH_3)_3$), 3.27 (d, 4H, Ar-$CH_2$-Ar, $J = 13.14$ Hz), 4.34 (d, 4H, Ar-$CH_2$-Ar, $J = 13.14$ Hz), 4.71, 4.94 (s, 8H, $NCH_2$), 4.97 (s, 4H, $OCH_2$), 6.76 (s, 4H, Ar-**H**), 7.02 (s, 4H, Ar-**H**), 7.04 (t, 2H, Py-**H**, $J = 6.40$ Hz), 7.13 (t, 2H, Py-H, $J = 6.42$ Hz), 7.25 − 7.27 (m, 2**H**, Py-**H**), 7.40 (d, 2H, Py-**H**, $J = 7.90$ Hz), 7.51−7.58 (m, 6H, Py-**H** and O**H**), 8.41 (d, 2H, Py-**H**, $J = 4.88$ Hz) 8.52 (d, 2H, Py-**H**, $J = 4.88$ Hz). $^{13}C$ NMR ($CDCl_3$, 100 MHz $\delta$ ppm): 31.1, 31.8 ($C(CH_3)_3$), 31.9 (Ar-$CH_2$-Ar), 33.9, 34.0 (**C**($CH_3)_3$), 51.4, 52.2 (N$CH_2$), 74.5 ($OCH_2CO$), 122.2, 122.3, 122.5, 125.1, 125.7, 127.9, 132.7, 136.7, 136.9, 141.3, 147.1, 148.9, 149.9, 150.8, 156.4, 157.3 (Py-*C* and calix-Ar-**C**), 169.2 (**C**=O). $m/z$ (ES-MS) 1127.78 ($[M]^+$ 70%), 1128.80 ($[M + H]^+$ 40%,).

**Solutions for Spectroscopy.** The fluorescence and absorption titrations were carried out in methanol. The concentration of L and its reference molecules were kept constant at $10 \mu M$ for the fluorescence titrations and at $20 \mu M$ for the absorption titrations. The amino acids were dissolved in $500 \mu L$ of water and diluted further using methanol to get the required concentration. $^1H$ NMR titrations, *viz.*, $Ag^+$ and cysteamine with L (0.011 M), were carried out in DMSO-$d_6$ ($400 \mu L$) except for the cysteine titration, where the amino acid was dissolved in $D_2O$ ($200 \mu L$).

**Solutions and Sample Preparation for TEM and DLS Studies.** Ligand L and silver perchlorate solutions were made in methanol. Cys solution was made by dissolving the amino acid in $\sim 500 \mu L$ deionized water and then the volume was made up by methanol. The final concentration of the solutions was kept $\sim 6 \times 10^{-4}$ M. TEM and DLS studies of L were carried out by using a solution of $50 \mu L$ in 3.0 mL of methanol, which results in $10 \mu M$ as also used in case of fluorescence studies. For the silver complexation studies $50 \mu L$ of L was mixed with $100 \mu L$ of $Ag^+$. Similarly for the reaction with Cys, $100 \mu L$ of Cys was added to the silver complex. Different sample blocks for TEM were made by placing $20-30 \mu L$ of the sonicated (15 min) sample solution on the copper grid and allowing it to dry in air at room temperature.

**Supporting Information Available:** Single crystal X-ray structural information (S01), minimum detection limit (S02 and S05), synthesis and characterization (S03), computational data (S04), absorption data (S06), $^1H$ NMR titration data (S07), TEM and DLS data (S08 and S09), fluorescence titration data (S10), and instrumental details (S11). This material is available free of charge via the Internet at http://pubs.acs.org.

# Nanofibers Formed Through $\pi\cdots\pi$ Stacking of the Complexes of Glucosyl-*C2*-salicyl-imine and Phenylalanine: Characterization by Microscopy, Modeling by Molecular Mechanics, and Interaction by α-Helical and β-Sheet Proteins

**Amitabha Acharya, Balaji Ramanujam, Atanu Mitra, and Chebrolu P. Rao\***

Department of Chemistry, Indian Institute of Technology Bombay, Powai, Mumbai -400 076, India

**ABSTRACT** This paper deals with the self-assembly of the 1:1 complex of two different amphiphiles, namely, a glucosyl-salicyl-imino conjugate (L) and phenylalanine (Phe), forming nanofibers over a period of time through $\pi\cdots\pi$ interactions. Significant enhancement observed in the fluorescence intensity of L at ~423 nm band and the significant decrease observed in the absorbance of the ~215 nm band are some characteristics of this self-assembly. Matrix-assisted laser desorption ionization/time of flight titration carried out at different time intervals supports the formation of higher aggregates. Atomic force microscopy (AFM), transmission electron microscopy, and scanning electron miscroscopy results showed the formation of nanofibers for the solutions of L with phenylalanine. In dynamic light scattering measurements, the distribution of the particles extends to a higher diameter range over time, indicating a slow kinetic process of assembly. Similar spectral and microscopy studies carried out with the control molecules support the role of the amino acid moiety over the simple —COOH moiety as well as the side chain phenyl moiety in association with the amino acid, in the formation of these fibers. All these observations support the presence of $\pi\cdots\pi$ interactions between the initially formed 1:1 complexes leading to the fiber formation. The aggregation of 1:1 complexes leading to fibers followed by the formation of bundles has been modeled by molecular mechanics studies. Thus the fiber formation with L is limited to phenylalanine and not to any other naturally occurring amino acid and hence a polymer composed of two different biocompatible amphiphiles. AFM studies carried out between the fiber forming mixture and proteins resulted in the observation that only BSA selectively adheres to the fiber among the three α-helical and two β-sheet proteins studied and hence may be of use in some medical applications.

Molecular self-assembly attracts a great deal of attention of scientists and technologists in recent times because of its use in the design and fabrication of nanostructures that lead to the development of advanced materials.[1,2] Among this, peptide amphiphiles (PAs), possessing both hydrophobic and hydrophilic segments[3] are one class of molecules that plays an important role in bioactivity and sensing studies.[4−6] These segments lead to ordered arrangements to minimize the interfacial energies with solvent to result in the formation of different nanoarchitectures, such as, spheres,[7] tubes,[8] and cylinders.[9,10] Because such molecular scaffolds are biocompatible, they present a great potential as self-assembling materials for drug delivery[11] and as bioactive scaffolds for cell signaling.[12] Some examples of this include (a) the formation of glyco-conjugate nanoribbons from the self-assembly of PAs possessing both the peptide moiety as well as the carbohydrate moiety;[13] (b) the architectural changes brought about in the formation of nanofibers of the PAs conjugated with polydiacetylenes upon photoirradiation;[3] (c) the formation of different architectures from hydrophilic dextran-derived polymers with cationic and anionic derivatizations;[14] and so on. The first example of this is the result of a $\pi\cdots\pi$ interaction exhibited between the phenyl moieties of the Phe residues of the neighbor molecules. The role of the aromatic side chain in the fiber formation of amyloids has already been

reported in the literature.[15−17] Similarly, some carbohydrate derivatives were reported to form fibers when attached to aromatic side chains.[18,19] Though the formation of nanofibers was reported from the interaction of two different amphiphiles in the literature,[20−28] none of these is between a glycoconjugate and an amino acid. Therefore, this article deals with the formation of nanofibers from two different amphiphiles,
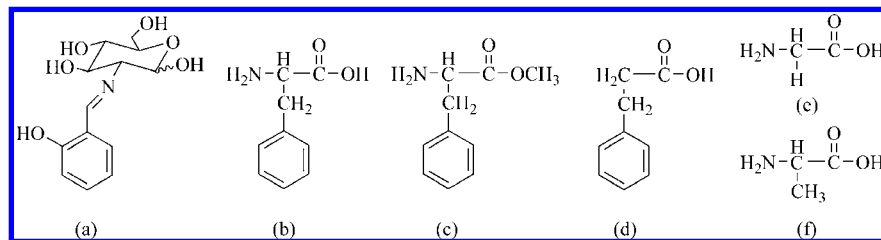
**Figure 1.** Schematic structures of the amphiphiles: (a) glucosyl-salicyl-imino conjugate (L) and (b) phenylalanine. Schematic structures of the control molecules: (c) methyl ester of phenylalanine (Phe-OMe), (d) 3-phenylpropionic acid, (e) glycine, and (f) alanine.

namely, Phe possessing a side chain phenyl moiety and a glucosyl-salicyl-imine conjugate possessing a salicyl moiety. To the best of our knowledge, this is the first report where two different biocompatible amphiphiles, a glycoconjugate and an amino acid, were shown to form nanofibers.

### RESULTS AND DISCUSSION

The glucosyl-C2-salicyl-imine conjugate amphiphile, 1-(D-glucopyranosyl-2′-deoxy-2′-iminomethyl)-2-hydroxybenzene (L), possessing both hydrophilic carbohydrate moiety and the hydrophobic phenyl moiety, was synthesized by reacting glucosylamine hydrochloride with salicylaldehyde in a 1:1 ratio in the presence of 1.2 equivalents of triethylamine as base in one step in 87% yield. The L has been characterized by $^1$H NMR, ESI-MS, and elemental analysis (Supporting Information, SI 01). The schematic structures of the amphiphiles, namely, L and phenylalanine, are shown in Figure 1, along with the control molecules used in the present study.

**Fluorescence Titration Studies.** When phenylalanine (Phe) is added to L in methanol (Experimental Section) and excited at 320 nm, the emission band emerges at ~435 nm owing to the presence of the imine moiety in conjunction with the aromatic moiety, as also found by us in the case of glyco- and calix-imino-conjugates.[29−35] The fluorescence intensity of the emission peak increases slowly as a function of time (Supporting Information, SI 02) (even after subtracting the background emission from Phe) as a result of the complexation enhanced fluorescence when the amino acid complexes with L. A total saturation in fluorescence intensity is attained over a period of 1 day (Figure 2a). With this, the overall enhancement in the fluorescence intensity was found to be (47 ± 5)-fold, though it is only (6 ± 1)-fold immediately when Phe was added to L. The enhancement in the fluorescence intensity has also been found to increase further when the mole ratio of the added Phe increases (Figure 2b) and attains saturation around ≥2 equivalents by exhibiting same enhancement ratio. Such fluorescence enhancement is expected only when Phe interacts with L, where the interactions can be either through hydrogen bonding or through hydrophobic (or $\pi \cdots \pi$ type) or through a combination of these.

To establish the involvement of −COOH, −NH$_2$, or phenyl moiety of Phe on the observed fluorescence enhancement, experiments were carried out with methyl ester of phenylalanine (Phe-OMe), 3-phenylpropionic acid (3-PPA), glycine (Gly), and alanine (Ala) (Figure 1). While it is the −COOH moiety that was converted to ester in Phe−OMe, it is the −NH$_2$ group that was replaced by −H in 3-PPA to study the importance of −COOH and −NH$_2$ moieties, respectively. On the other hand, the studies carried out using Gly and Ala, provides the importance of the side chain phenyl moiety present in Phe. The titrations carried out between L and Phe-OMe exhibited fluorescence enhancement similar to that observed in the titration of L with simple Phe suggesting that the −COOH present in Phe is not critical for the interaction (Figure 2c). Similar titrations carried out between L and 3-PPA resulted in no change in the fluorescence intensity of L, suggesting that the amine moiety present in Phe is indeed necessary for the interaction.
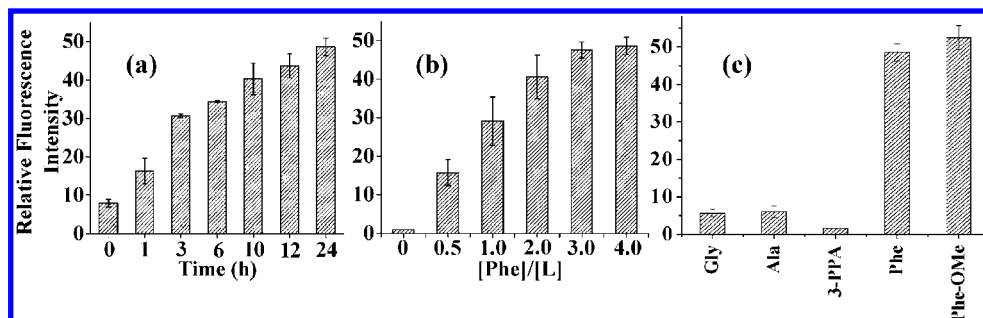


**Figure 2.** Relative fluorescence intensity observed during the titration of L with Phe: (a) as a function of time; (b) as a function of [Phe]/[L] mole ratio at 24 h. (c) Titration of L with different control molecules: Gly, Ala, 3-PPA, Phe, and Phe-OMe, and the fluorescence is at 24 h in all the cases.

Even the titrations carried out between L and Gly/Ala exhibited only *ca.* (6.0 ± 1.0)-fold change in the fluorescence intensity suggesting that the side chain phenyl moiety is indeed needed for exhibiting large fluorescence enhancement. All this indicates that though Gly or Ala can interact with L, the species formed in this case is much different from that formed between Phe and L. Thus the results obtained from the fluorescence studies seem to suggest the involvement of amine group in conjunction with the phenyl moiety present in Phe in forming the corresponding species responsible for the large fluorescence enhancement as that observed in the case of [L+Phe]. It would be only the amine moiety that is responsible in the case of Gly or Ala, and hence it brings only a marginal fluorescence increase as observed in the case of [L+Gly] or [L+Ala].

The fluorescence data fits well with a 1:1 complex formed through hydrogen-bond interactions involving the amine moiety of the amino acid in the case of Gly, Ala, and Phe. However, the complex formed initially seems to interact and/or aggregate through the phenyl moiety of Phe, which cannot happen in the case of Gly or Ala due to the absence of this moiety. Therefore, the possible presence of both the hydrogen bonding and the hydrophobic or the $\pi \cdots \pi$ interactions in the species formed in the case of [L+Phe] has been further addressed based on other experimental and computational studies as reported in this article.

**MALDI Studies.** The formation of the complex species between L and Phe followed by its growth was monitored by measuring the mass spectra of the solution of [L+Phe] by matrix-assisted laser desorption ionization (MALDI) at various time intervals. With increasing time, higher molecular weight species were formed at the cost of the initially formed 1:1 species. Thus, as a function of time, species were grown with *m/z* values in the range, 2220−2280, 2330−2400, 2420−2640, 2690−2810, and 3350−3500 Da, suggesting the growth of the aggregated species (Figure 3). The aggregations range from pentameric to hexameric to even octameric ones. The species observed at *m/z* values of 2234, 2372, and 2518 are suggestive of the pentameric species, 2729 denotes the hexameric, and that at 3445 denotes the octameric species. The intensity of the peak corresponding to the octamer indeed increased when measured after 24 h. Thus the MALDI titration results in providing evidence for the formation of oligomers of L with Phe, [L+Phe]$_n$, where *n* has been found at least in the range of 4−8.

**Absorption Titration Studies.** The growth of the initially formed 1:1 species has been further monitored by following the changes observed in the absorption spectra of the ∼215 nm band (Experimental Section, Supporting Information, SI 03). No change in the absorbance was observed when L was titrated either with Gly or Ala, but considerable absorbance changes were observed in the titration of L with Phe. The trend observed in this
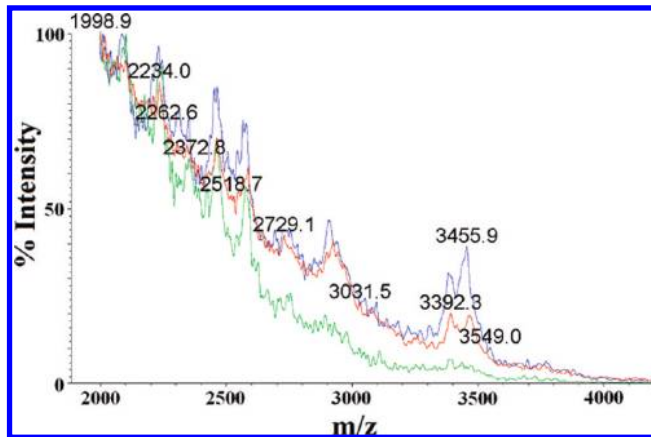
**Figure 3.** MALDI mass spectra measured from the solution of [L+Phe] at different time intervals: 1 h (green); 8 h (red); 24 h (blue).

data is suggestive of the role of the side chain phenyl moiety in exhibiting $\pi \cdots \pi$ interactions in the case of [L+Phe] and not with [L+Ala] or [L+Gly], as the same is not expected in the case of the latter owing to the absence of phenyl side chain moiety. However, the initial complex formed between L and the amino acid can be noticed from the absorbance changes observed with the 350 nm band. Thus the absorption studies not only confirmed the initial formation of the complex between L and the amino acid but also supported the growth of the species through $\pi \cdots \pi$ interactions in case of phenylalanine.

**Prevention of Aggregation in the Presence of Ethidium Bromide (EtBr).** The aggregation of the 1:1 complex units through $\pi \cdots \pi$ interactions developed during a period of time could result in the growth of the species in the solution. This has been further supported by adding EtBr that prevents such aggregation since EtBr is expected to show strong $\pi \cdots \pi$ interactions. Addition of EtBr indeed arrested the fluorescence enhancement that was otherwise observed in the solution without the presence of this. Thus the prevention of aggregation of the complex units in the presence of EtBr has been shown in case of [L+Phe] in comparison with the corresponding control as shown in Figure 4.
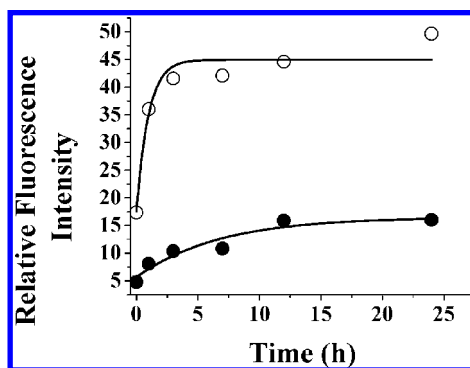
**Figure 4.** Relative fluorescence intensity as a function of time for 1:2 solutions of L and Phe. The filled ones are in the presence of 5 equiv of EtBr and the unfilled ones are the corresponding control without the EtBr.
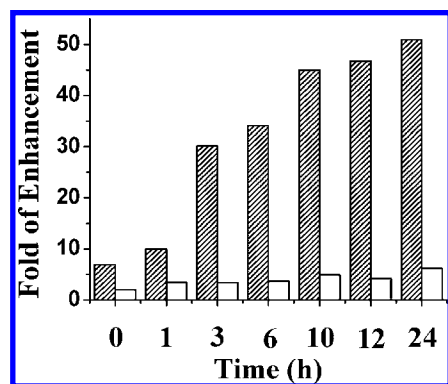
**Figure 5. Histogram showing the fold of fluorescence enhancement for the titration of L *vs* Phe in the absence (dashed) and in the presence (blank) of 9-anthracenaldehyde.**

**Prevention of Aggregation in the Presence of 9-Anthracenealdehyde (9-AA).** The role of aromatic moiety in the disruption of the fiber formation has been further addressed by carrying out two types of fluorescence experiments using 9-anthracenealdehyde (9-AA). In one experiment, the 9-AA was added to a mixture of L and Phe at the beginning, and the fluorescence spectra were measured as a function of time. In the presence of 9-AA, no significant increase was observed in fluorescence intensity, while in the control experiment performed without the addition of 9-AA, it exhibited an increase in the fluorescence by ~50 fold, indicating the fiber formation is prevented in the presence of 9-AA (Figure 5). In another experiment, the fibers were initially allowed to form by mixing L and Phe and leaving the solution for 24 h before 9-AA was added in different mole ratios. A progressive quenching of the fluorescence was observed, suggesting the disruption of the fibers formed (SI 03).

**Microscopy Studies.** Since the initially formed [L+Phe] complex aggregates as a function of time through the π · · · π interactions extended between these complex units, the resulting oligomeric/polymeric and/or fiber species was explored based on atomic force microscopy (AFM), transmission electron microscopy (TEM), and scanning electron microscopy (SEM), as a function of time after the addition of Phe to L. The results have been compared with the data obtained for the control molecular systems.

**AFM Studies.** The AFM studies were carried out to assess the formation of fibers between L and Phe, as well as other aromatic side chain amino acids (Trp and Tyr) and also those not possessing such a side chain (Ala, Pro). The fiber formation has also been studied with different controls for appropriate comparison.

*In the Presence of Phe.* In AFM, the micrographs have been measured for the samples drawn at different time intervals after the addition of Phe to L (Experimental Section). Immediately after the addition of both the components (at time zero), discrete particles of spherical shape were observed with no indication of fiber formation (Figure 6a,b). Within 4 h, these spherical particles started to merge together to form micelles and/or vesicular morphology with a dumbbell shape (Figure 6c,d). Such self-assembled morphology could generate short fibers over a period of time. After 8 h, the formation of the fibers could be clearly seen, and these were well spread all over the mica surface (Figure 6e,f). Though most of the fibers are parallel to each other, some branched chain fibers were also observed. Careful examination of these long fibers formed from the samples prepared at lower concentration revealed that these were actually made up of shorter ones (Figure 6g,h). The shorter ones have lengths of 450−530 nm,
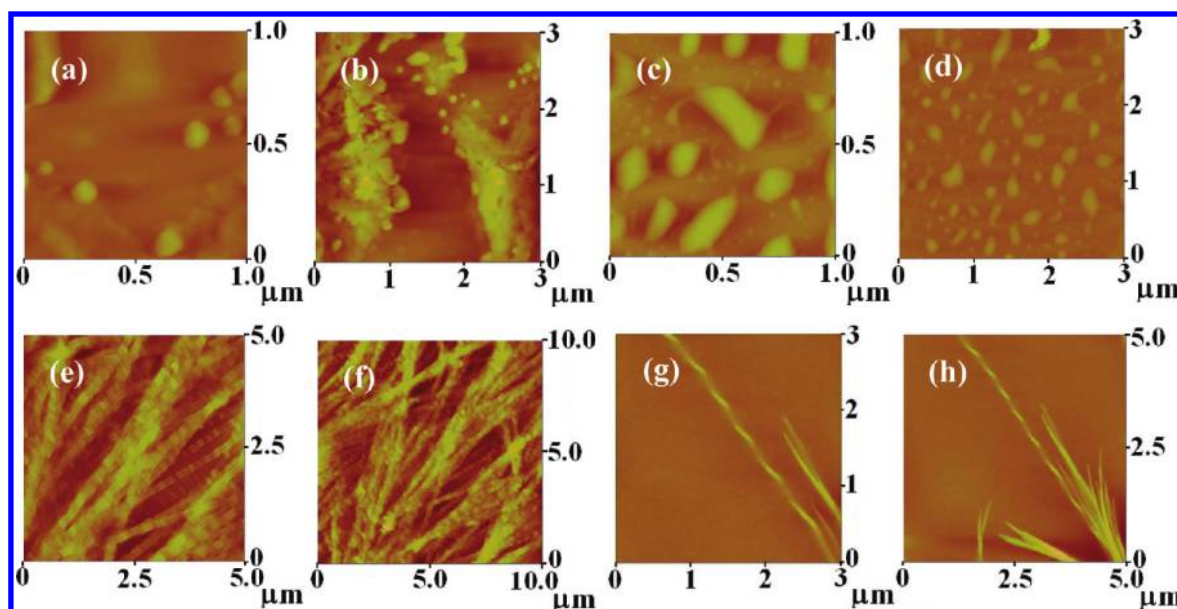


**Figure 6. AFM micrographs of [L+Phe] where the samples were drawn at different time intervals: (a and b) immediately after mixing; (c and d) after 4 h; (e and f) after 8 h, and (g and h) after 8 h but with the samples from an experiment carried out using lower concentration.**
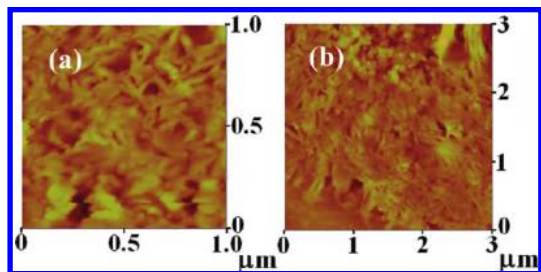
**Figure 7. AFM micrographs of [L+Phe] where the sample was drawn after 24 h. Panels a and b are from different regions of the sample on mica.**

widths of 90−160 nm, and heights of 13−18 nm. It can be noted that the width of the fiber is much higher as compared to their height, imparting a ribbon-like structure to the fiber[36] through the bundling of a number of individual threads in a parallelepiped fashion. These dimensions seem to fit well with the stacking of about 250−300 complex units along the length and stacking of 20−30 such fibers bundled in the width of the ribbon. The undulation morphology of the fibers observed can be the result of the structural defects formed during the process of $\pi \cdots \pi$ stacking.[3]

After 24 h, the long fibers of [L+Phe] were no more observed, instead, a high population of smaller fibers were noticed in the micrographs of AFM as shown in Figure 7, as the shorter ones may have resulted from the breakage of the sufficiently long fibers on the surface of the mica.

*In the Presence of Trp and Tyr.* Since Trp and Tyr possess aromatic side chains, the fibers formed by these were studied by AFM. In the case of [L+Trp], the initially formed spherical particles were joined together to form dumbbell-shaped particles in about 4 h. The fibers formed by Trp after 24 h were short and clustered, and the abundance of fiber formation is rather low when compared to [L+Phe] (Figure 8a,b). On the other hand, the fibers formed from [L+Tyr] were branched but not well spread as that observed in case of [L+Phe] (Figure 8c,d).

*In the Presence of Ala and Pro.* However, in case of [L+Ala], the initially formed spherical particles (sizes of 39−80 nm and heights of 2−4 nm) continue to grow in size but maintain a spherical shape, where the sizes of the particles (sizes of 156−314 nm and heights of 5−11 nm) are about 4−8 times greater than the initial par-

ticles when measured after 8 and 24 h (Figure 9a,b). Even proline does not show any fibers after 24 h (Figure 9c,d). Thus no fibers were found in the case of [L+Ala] and [L+Pro] even after 1 day, suggesting that the presence of the phenyl side chain is essential for the amino acid amphiphile to form fibers with the amphiphile L.

*In the Presence of 3-PPA.* In case of [L+3-PPA], the initially formed spherical particles (sizes of 20−90 nm and heights of 5−14 nm, Figure 10a) continue to grow in size but maintain a spherical shape, where the sizes of the particles (sizes of 180−260 nm and heights of 17−25 nm, Figure 10b) is about 10 to 14 times higher than the initial sizes when measured after 8 h. Over a period of 24 h, these particles tend to aggregate to form bigger ones with no well-defined shape (Figure 10c). Thus no fibers were found in the case of [L+3-PPA] even after 1 day since an initial complex between L and 3-PPA was not formed. Nonformation of the initial complex between L and 3-PPA has already been demonstrated by fluorescence titration studies. All these results further suggest that the presence of phenyl side chain moiety is essential for the amino acid to form fibers with L.

*In the Presence of NaCl and Zn(ClO₄)₂ Salt.* The role of hydrogen bonding and hydrophobic interactions in the formation of the fibers has been further studied by judging the fiber formation or its disruption under the presence of these salts. AFM experiments were carried out using two different salts, NaCl and $Zn(ClO_4)_2$, owing to their diverse interactions in coordination chemistry. From each of the metal salts, two experiments were carried out. (a) One was carried out by adding the salt to the [L+Phe] mixture initially followed by measuring AFM after 12 h, and it was found that none of these salts allow the fiber formation (Figure 11). (b) The other was carried out by adding the salt after the fibers were formed, and disruption of the fibers was found with both the salts. Thus, these salts do not allow fiber formation and were capable of breaking the fibers, if already formed.

*AFM Studies with Galactosyl-salicyl-imino Conjugate ($L_1$) and Phe.* To find out whether the fibers formed are dependent on the glycose part of the glyco-conjugate, AFM studies were carried out between an analogue of L, galactosyl-salicyl-imino conjugate ($L_1$),[34] and Phe. No
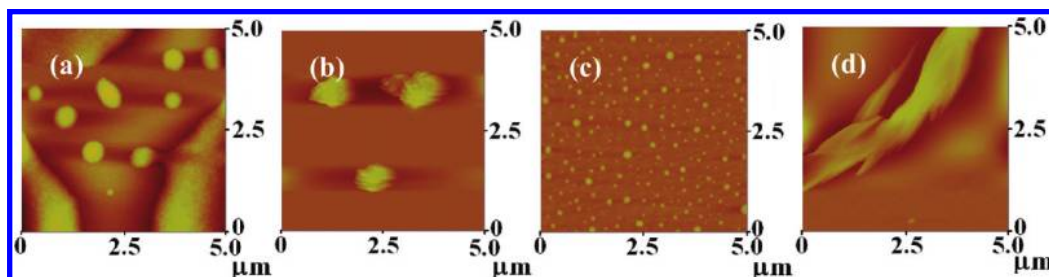


**Figure 8. AFM micrographs of the samples drawn from [L+Trp] in the case of (a and b) and from [L+Tyr] in case of (c and d). Among these the first one is at 0 and the second one is at 24 h.**
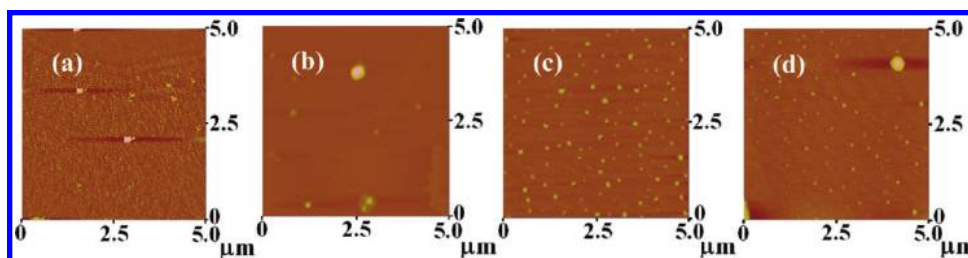
**Figure 9.** AFM micrographs of the samples drawn from (a and b) [L+Ala] and from (c and d) [L+Pro]. Among these the first one is at 0 and the second one is at 24 h.
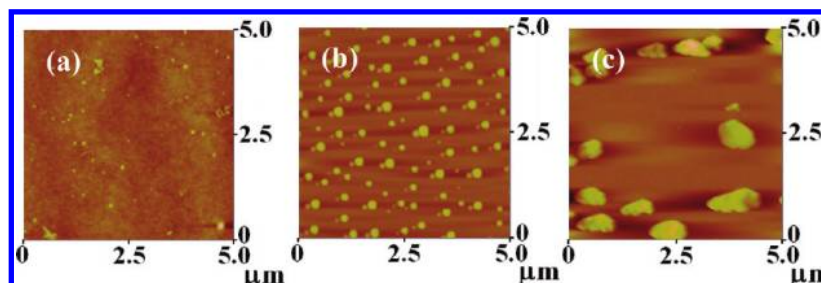


**Figure 10.** AFM micrographs of [L+3-PPA] samples drawn at different time intervals: (a) immediately after mixing; (b) after 8 h, and (c) after 24 h.

formation of fibers was found suggesting that the growth of the fibers is dependent on the nature of the glycose part (Figure 12).

The precursor molecules, L or Phe, alone do not show the formation of fibers of the nature demonstrated for [L+Phe] when left in solution even over a period of 1 day as studied based on AFM (Supporting Information, SI 04). Based on the AFM studies, it is possible to arrange these in the order of their fiber formation ability: Pro and Ala (no fibers) ≪ Trp (short bundles and less abundant) < Tyr (thin, branched, bundled and less abundant) < Phe (best fiber formation and growth and high abundance).

**TEM Studies.** TEM micrographs measured after 8 h of mixing of L with Phe reveal the fibrous nature of the species. The lengths of the fibers were found to be in the range of 100−200 nm, and the widths were 10−20 nm (Figure 13a,b). In both the AFM and TEM studies, the fibers were found to be more aggregated. This may be due to the enhanced interfiber interactions as a result of less efficient packing among the molecules within the individual nanofibers. Even the micrographs measured by high resolution TEM exhibit bunches of fibers as can be seen from Figure 13c,d. Some peptide

amphiphiles conjugated with polydiacetylene also formed such fibers upon photoirradiation as reported in the literature.[3]

**SEM Studies.** Scanning electron micrographs obtained for the powder isolated from the immediately prepared reaction mixture of L and Phe exhibited large crystallites of the size 10−15 μm × 2−3 μm (Figure 14a). The powder isolated after 8 h of reaction, exhibited branched fibers (Figure 14b). The micrograph measured from the powder obtained from the reaction mixture of L and Phe after 24 h exhibited rodlike fibers (Figure 14c). SEM images of the precursor L exhibit very long crystalline rods (Supporting Information, SI 05).

Samples of [L+Ala] and [L+3-PPA] obtained even after 24 h exhibited no fibers unlike that observed in the case of [L+Phe], supporting that the side chain phenyl moiety is absolutely essential for the formation of the fibers (Figure 15).

Though all the three microscopy studies exhibited fiber formation, there seemed to be some basic differences in their size parameters owing to the surfaces used, namely, mica in case of AFM and carbon-coated copper grid in the case of TEM. Further differences may arise from the desolvation technique used, namely, high vacuum for TEM and simple air drying in the case of AFM.

**Powder XRD Studies.** Powder XRD studies were carried out with the solid samples obtained from the reaction mixture of [L+Phe] at different time intervals (Experimental Section). The diffractograms shown in Figure 16 are clearly characteristic of crystalline material and exhibit appreciable variation in the intensity and/or breadth of some peaks when compared to the unaltered ones, where the experiments were carried out on the samples drawn at different time intervals. Compari-
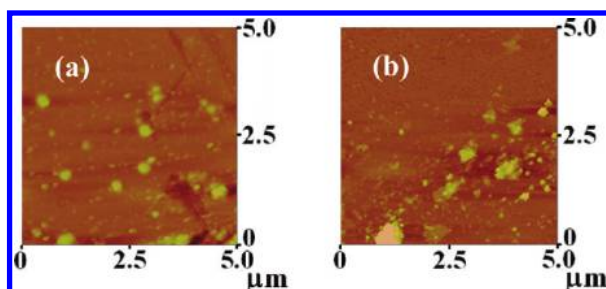


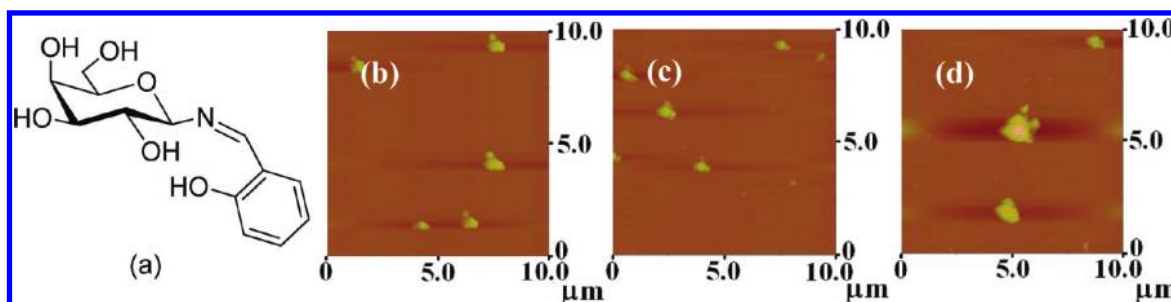**Figure 11.** AFM micrographs of [L+Phe] obtained in the presence of (a) NaCl and (b) $Zn(ClO_4)_2$ after 12 h.

**Figure 12.** (a) Schematic structure of galactosyl-salicyl-imino conjugate ($L_1$). AFM micrographs of the samples drawn from [$L_1$+Phe] at different time intervals: (b) 0 h, (c) 8 h, and (d) 24 h.

son of these diffractograms revealed increased peak intensities with those observed at $2\theta$ values of 13.80, 17.36, 19.23, and 20.73 and a decreased peak intensity at a $2\theta$ value of 40.20. In some cases the peaks were merged or sharpened ($2\theta$ = 26.92, 32.86). These lines could not be indexed in the absence of any reference compound. Thus the powder XRD studies provided qualitative information on the crystallinity of the nanofibers formed in the case of L and Phe, as also noticed from SEM studies.

**DLS studies.** To test the feasibility of the fiber formation as noticed based on microscopy, DLS studies (Supporting Information, SI 06) were carried out as a function of time. It is expected that the solvo-dynamic diameter of the self-assembled species increases over a period of time. Hence the solutions were scanned at different time intervals for DLS, and the results are

shown in Figure 17. Appropriate control studies have also been performed with simple glucosyl-salicyl-imine-conjugate amphiphile (L) as well as with phenylalanine. As can be seen from Figure 17, the peaks of the self-assembled species were shifted to a higher diameter range with increase in time (Supporting Information, SI 06). At zero time, the mean diameter of the species was found to be in the range of ~0.12 μm which gradually increases to ~6.5 μm after 18 h. The progressive increase observed in the solvo-dynamic diameters of the species can be attributed to the formation of different kinds of self-assembled ones. The small diameter species observed at the beginning may result from 1:1 complex by forming a cluster. Observation of peaks with larger diameter (after 4 h) supports the formation of the nanofibers that takes some time to grow as it is a slow kinetic process. L alone or phenylalanine alone ex-
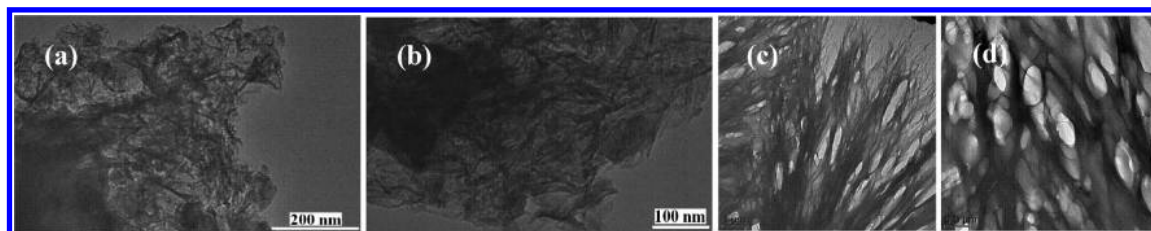


**Figure 13.** TEM micrographs of the sample drawn from [L+Phe] mixture after 8 h: (a and b) normal TEM and (c and d) high-resolution TEM.
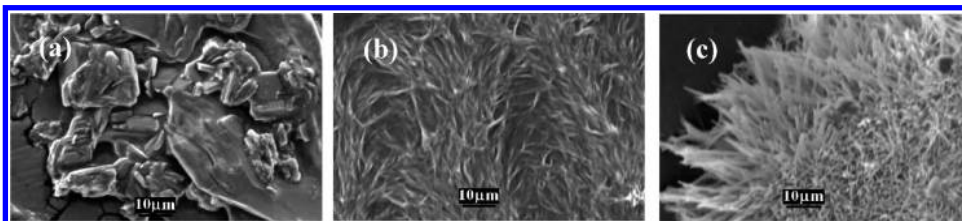


**Figure 14.** SEM micrographs of the sample drawn from [L+Phe] mixture at different time interval: (a) immediately after mixing, (b) after 8 h, and (c) after 24 h.
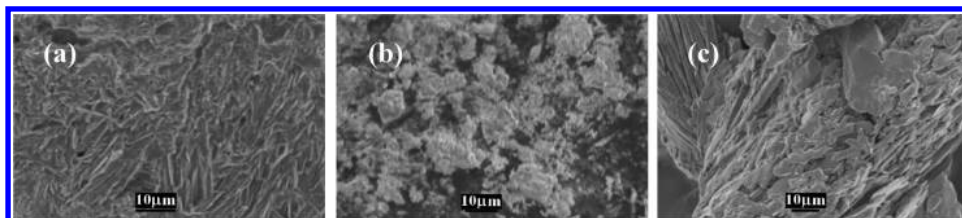


**Figure 15.** SEM micrographs of the sample drawn from the experiments carried out with control molecular systems: (a) [L+Ala] after 8 h, (b) [L+Ala] after 24 h, (c) [L+3-PPA] after 24 h.
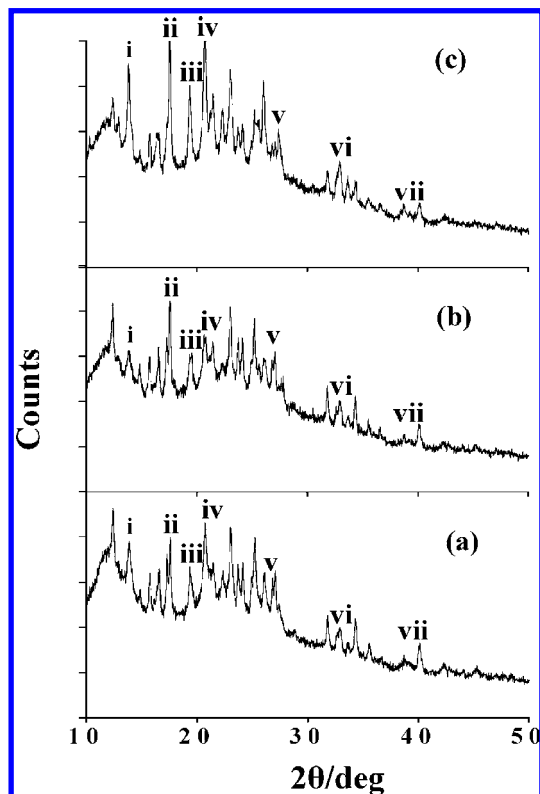
**Figure 16.** Powder XRD diffractograms of [L+Phe] where the samples were drawn at (a) 0 h, (b) 8 h, and (c) 24 h. The peaks of interest are indicated by roman marking.

hibited no considerable aggregation in solution even after one day (Supporting Information, SI 06).

**Computational Modeling of Nanofibers.** From the spectroscopic and microscopy studies, it has been shown that the complex unit formed between L and Phe grows further over a period of time to result in the formation of nanofibers. To model the formation of the fiber, molecular-mechanics-based computational calculations were carried out using HYPERCHEM (Experimental Section).[37] The fiber was modeled by replicating the 1:1 complex unit structure obtained from the DFT computations[38] (Supporting Information, SI 07a) in a cascade manner by forming its oligomers possessing 2, 4,



**Figure 17.** Particle size distribution plot of the species formed at different time interval by dynamic light scattering (DLS).
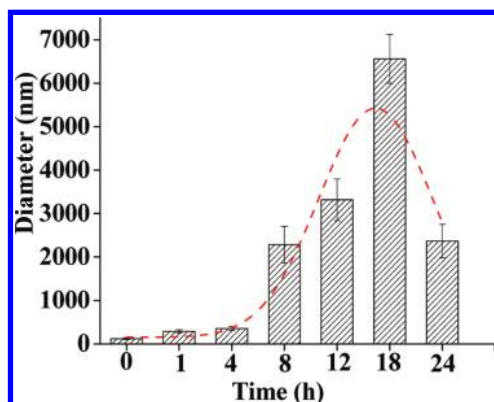
8, 16, and 32 units. The modeled oligomers were then minimized using different force fields, namely, MM+, BIO+(CHARMM), and Amber, and it was found that the MM+ based calculations yielded better results when compared to the others. The dimeric structure was obtained by minimizing the two individual 1:1 complex units placed apart. Similarly, a tetrameric structure was obtained by minimizing two dimers placed at a noninteracting distance. This procedure was continued until a 32-unit thread was formed. Formation of such a thread is unidirectional with dimensions of $(0.60 \pm 0.05) \times (0.90 \pm 0.05) \times (38.0 \pm 0.2)$ nm³ (Figure 18). However, the attempts to form the 1:1 complex of L and the control molecular system 3-PPA were futile, indicating that there is no complex formed between L and 3-PPA (Supporting Information, SI 07b). Indeed we found the same from the fluorescence titration studies. A closer examination of the threads of [L+Phe] exhibited $\pi \cdots \pi$ interactions (phenyl$\cdots$phenyl distance being ~3.9 $\pm$ 0.1 Å) of the type ...ABABABAB....

On the other hand, when the side chain of the amino acid was replaced by methyl moiety to mimic alanine in place of the phenylalanine in the threads, the corresponding thread was broken into smaller pieces with no long-range order, suggesting that the fiber formation is not favored when there is no phenyl side chain (Figure 19).

To see whether L alone forms any polymeric thread through $\pi \cdots \pi$ interactions, MM+ minimizations were performed by taking a 16-unit thread of [L+Phe] followed by removing the Phe units from the same. This resulted in the breakage of the thread to form at least six smaller aggregates of L. Among these, only two aggregates exhibited $\pi \cdots \pi$ interactions and not the others (Supporting Information, SI 07c). Thus the MM+ study suggests that L alone does not form a thread without the presence of Phe and hence supports the experimentally observed results.

Comparison of the cross-sectional dimensions of the thread built on the basis of the computational study with that observed from microscopy suggests that several threads must have been bundled together to form the fibers. The bundling of the individual threads to result in the fibers was achieved by carrying out MM+ minimization on 16 threads. This minimization was carried out by a cascade process by initially making a bundle of 2 followed by 4 followed by 8 and then followed by 16, sequentially at every stage and using the output at each stage for the next higher one. To keep the computational times low, the bundling of the threads to form a fiber was made using threads of 16 unit length rather than that of the 32, as shown in Figure 20. The minimized bundle exhibited dimensions $(2.5 \pm 0.02) \times (4.0 \pm 0.03) \times (16.9 \pm 0.3)$ nm³. Similar computations carried out with Tyr resulted in a polymer that has several nucleating sites for branching (Supporting Information, SI07).
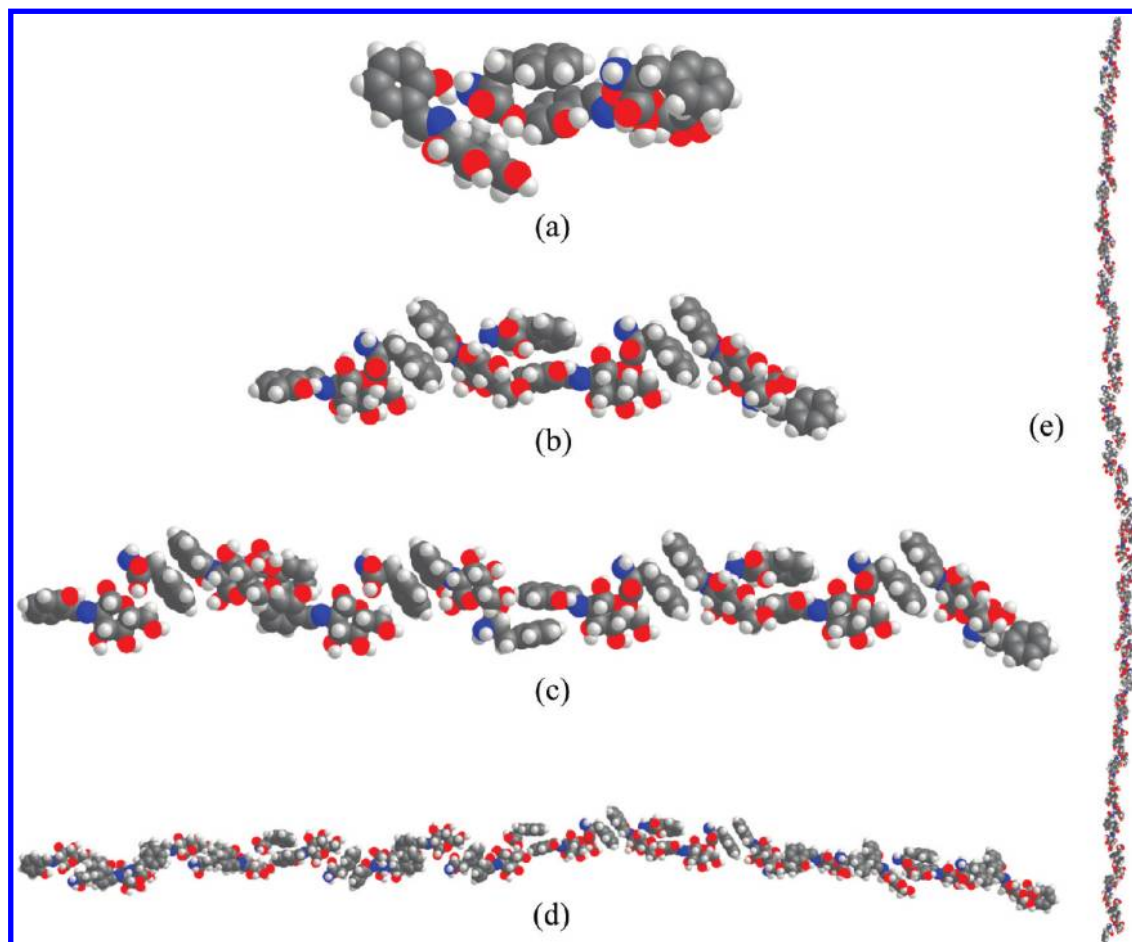
**Figure 18. Minimized structures obtained from the MM+ calculations performed using a 1:1 complex of L and Phe: (a) 2-mer; (b) 4-mer; (c) 8-mer; (d) 16-mer; and (e) 32-mer.**

**Protein−Fiber Interactions.** In view of the importance of the biocompatible nanofibers in medical applications, such as tissue engineering and drug delivery, the nanofibers formed from L and Phe as reported in this paper were studied for their interaction with different serum and legume proteins. While the serum proteins used were highly α-helical in nature, the legume proteins used were highly β-sheet in nature.

The fiber-forming reaction mixture was initially prepared in the presence of the corresponding protein, and the formation of the fiber and the characteristics of the protein were monitored by atomic force microscopy. All the three albumin proteins studied, BSA, HSA, and lactalbumin, allow the formation of fibers, as can be seen from the AFM images (Figure 21, Supporting Information, SI 08). From the micrographs, it is further evident that the branching nature of the fibers is mostly unaltered in the presence of either BSA or lactalbumin, but the branching is almost diminished in the presence of HSA. While these fibers were found to be noninterac-



**Figure 19. MM+ minimization results obtained of a 16-mer fiber of (L+Phe) where the Phe was replaced by simple Ala, leading to smaller fragments.**



**Figure 20. Bundle of fiber obtained from molecular-mechanics-based minimization of 16 threads of a 16-mer [L+Phe]: (a) view along the length and (b) a cross-sectional view.**

**Figure 21.** AFM micrographs of (a, b) {[L+Phe]+BSA}, (c) {[L+Phe]+HSA}, and (d) {[L+Phe]+lactalbumin} samples.
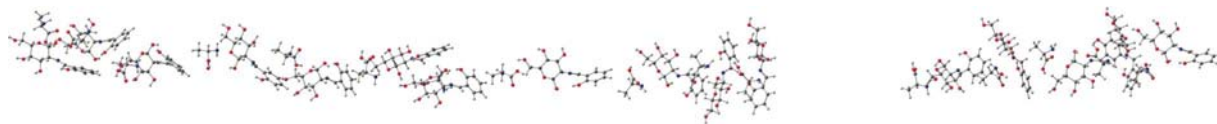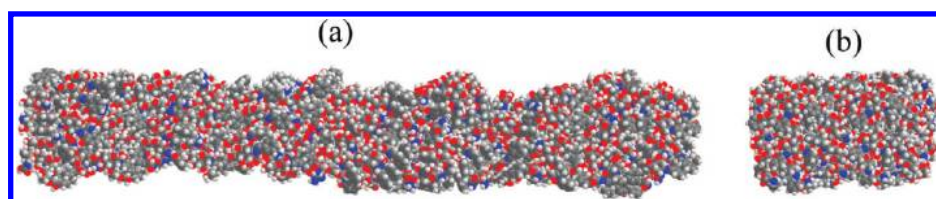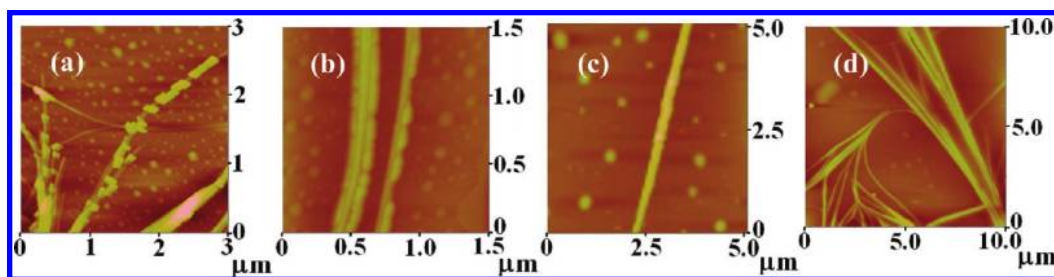
tive in the case of HSA and lactalbumin, the BSA protein molecules were indeed found to adhere to the fibers. A closer examination of the AFM features reveal that while simple BSA protein exhibits spherical particles, the same when bound to the fibers resulted in deformation and hence nonspherical particles, which may be attributed to the conformational and/or shape changes occurring in the BSA. Such deformations have been observed, as reported in the literature, when large proteins and/or other macromolecules were adsorbed/bound to solid materials.[39] In the present case, the deformation of the BSA particles may have allowed the protein to unfold to some extent, which in turn exposes additional sites that would involve in interaction with the fibers. However, for the β-sheet proteins, namely, peanut agglutinin and jacalin, no such fiber formation was observed suggesting that these proteins inhibit the formation of fibers (Figure 22). Thus among the five proteins belonging to the two different classes studied and reported in the paper, only BSA selectively adheres, and hence these fibers would be of interest in a variety of applications.

**Circular Dichroism (CD) Studies.** To understand the changes that may occur in the secondary structures of these proteins when they interact with the fiber, CD titrations were carried out. Appropriate control experiments were performed and subtracted before interpreting the observed results. During the titration, the protein concentration was kept constant by adding varying amounts of fiber forming mixture (Experimental Section). The CD spectra shown in Figure 23a for the titration with BSA shows considerable change in the secondary structural features by strengthening the helicity of the protein owing to the possible interactions present between the fiber and the protein, though one
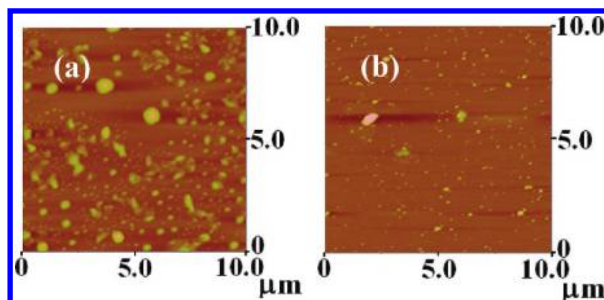
may expect to disrupt the secondary structures upon interaction of protein with the fiber. Increase in the negative ellipticity has also been observed with small peptides, over a period of time, forming nanofibers.[40] On the other hand, the HSA which does not adhere to the fiber but only allows the fiber to form, seems to bring only marginal changes in the ellipticity (Figure 23b) as studied by CD in solution. The slope of ellipticity *versus* concentration is at least one-half in the case of HSA when compared to that of BSA. Similar titrations carried out with β-sheet proteins, such as jacalin, Figure 23c, exhibited no significant changes in the ellipticity, and these result are in line with that observed from the microscopy, namely, no fiber formation (Supporting Information, SI 09).

## CONCLUSIONS AND CORRELATIONS

Molecular self-assembly of biocompatible systems is an interesting target in current research due to its applications in materials as well as in clinical sciences. The self-assembly process among amphiphiles is governed by several noncovalent interactions. Though the individual effect of these interactions are minimal as far as the energetics are concerned, when acting together, they can generate well-ordered supramolecular structures. Among the various noncovalent interactions responsible for such self-assembly, $\pi \cdots \pi$ interactions play an important role. Herein, we report the self-assembly of two different amphiphiles, a glucosyl-salicyl-imino-conjugate (L) and a phenylalanine, forming nanofibers over a period of time through $\pi \cdots \pi$ interactions.

A progressive increase in the fluorescence intensity has been observed as a function of time with phenylalanine. Simple amino acids, such as glycine and alanine, as well as the simple carboxylic equivalent of phenylalanine, 3-phenylpropionic acid (3-PPA), do not show significant changes in the fluorescence intensity, suggesting that both the amino acid portion as well as the side chain phenyl moiety together are needed in the same molecule to show these changes. The fluorescence and absorption spectral changes observed in the titration of L with Phe are consistent with the formation of an initial 1:1 complex followed by aggregation of these. Though the observations in the case of glycine and alanine indicated the initial formation of a 1:1 complex, there is no indication for their further aggregation even
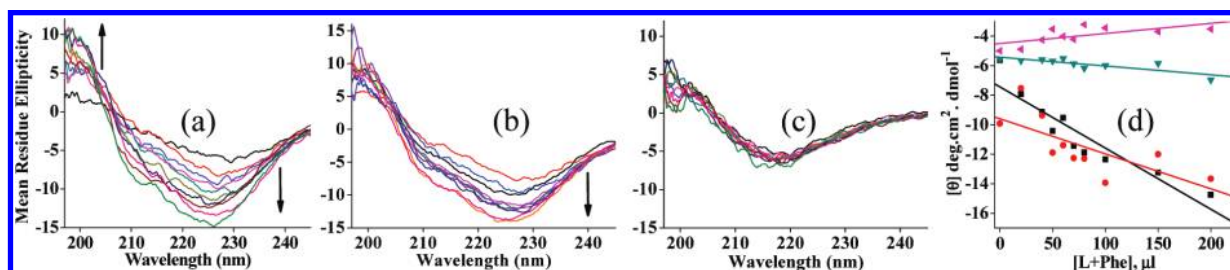


**Figure 22.** AFM micrographs of (a) {[L+Phe]+PNA} and (b) {[L+Phe]+jacalin} samples.

**Figure 23.** Plots of mean residue ellipticity as a function of volume of [L+Phe] addition in the case of: (a) {[L+Phe]+BSA}, (b) {[L+Phe]+HSA}, and (c) {[L+Phe]+Jacalin}. (d) Plots of ellipticity as a function of volume of [L+Phe] addition in case of proteins and lectins: (black) BSA, (red) HSA, (green) Jacalin, and (pink) PNA.

over a period of 1 day. However, under similar experimental conditions, the observations with 3-PPA does not conform either to the formation of 1:1 complex or to its aggregation. The aggregational behavior observed with phenylalanine has been further established by MALDI where the higher aggregate peaks were observed over a period of time. Formation of such aggregates has been indirectly shown by preventing the same using ethidiumbromide.

AFM, TEM, and SEM studies clearly revealed the formation of nanofibers as a function of time after mixing L with phenylalanine. The length and breadth (in nm) of the individual fibers was found in the range of 450−530 and 90−160 and 100−200 and 10−20, respectively, from AFM and TEM. Similar microscopy studies carried out between L and alanine or 3-phenylpropionic acid did not show any fiber formation. Though some fiber formation was observed in case of Trp and Tyr, the nature and abundance of the fibers formed greatly differs from those formed from Phe. Even the change in the carbohydrate moiety, such as changing from glucosyl to galactosyl, does not result in the formation of nanofibers, suggesting the role of glycomoiety in the formation of these fibers. The growth of the fibers as a function of time in the case of [L+Phe] has also been supported by DLS experiments. These fibers were found to be crystalline on the basis of powder XRD studies.

Computational modeling of the nanofiber formation was carried out by taking the DFT optimized 1:1 complex and building the fiber by going through a cascade methodology using molecular mechanics, wherein a dimer is being made from a single complex

unit, and a tetramer from two such dimers, and an octamer from two such tetramers, and so on. The modeling clearly revealed a $\pi \cdots \pi$ interaction of the phenyl moiety of phenylalanine with the phenyl moiety of the L resulting in ...ABABAB...-type of arrangement. A 32-unit thread exhibit dimensions of $(0.60 \pm 0.05) \times (0.90 \pm 0.05) \times (38.0 \pm 0.2)$ nm$^3$. However, when the Phe is being replaced by Ala that lacks side-chain phenyl moiety, the initial thread of [L+Phe] was broken to give smaller fragments. Even L alone does not show the formation of the threads. To model the widths noticed in the microscopy, computational studies were carried out to give bundles of these threads using molecular mechanics calculations. A bundle formed from 16 threads of a 16-mer exhibited dimensions, $(2.5 \pm 0.02) \times (4.0 \pm 0.03) \times (16.9 \pm 0.3)$ nm$^3$.

Because of the biocompatibility of these amphiphiles, their self-assembled nanofibers can probably be used as a new class of molecular transporters or as a protective coating agent over the drugs for delivery. The AFM studies carried out to test the applicability of these fibers resulted in the observation that only BSA selectively adheres among the five proteins belonging to two different classes reported in the paper. The changes occurred in the secondary structural features of these proteins in fiber-forming solutions were studied by CD spectroscopy. Hence these fibers would be of interest in the recovery of BSA from a mixture of proteins and/or transfer of a chemical entity/drug between the fibers and BSA selectively. Suitable biocompatible fibers in the literature have indeed been used for making biodegradable bandages for wounds.[39]

## EXPERIMENTAL SECTION

For all the studies reported in this paper, the D-stereoisomer of glyco-conjugates and the L-stereoisomer of amino acids have been used.

**Characterization of L.** Glucosamine hydrochloride (0.215 g, 1 mmol) salt was neutralized with triethylamine in ethanol before being used in the synthesis. To this, salicylaldehyde (0.15 mL; 1 mmol) was added. The reaction mixture was refluxed for 6 h at 60 °C. The solid product formed, L, (0.25 g) was filtered and washed with cold ethanol several times followed by diethyl ether and was dried under vacuum. Yield −87%. $^1$H NMR (DMSO, δ ppm): δ 2.5 (q, 6H, DMSO), 3.25−3.80 (m, 5H, carbohydrate skeletal C−H), 4.53−4.95 (4d, 4H, C1-OH, C3-OH, C4-OH, C6-OH), 5.16−5.18 (d, H, J-5.5

Hz), 6.19−7.59 (2d, 2t, 4H), 8.6 (s, 1H, CH=N), 13.2 (s, 1H, Ar−OH) ppm. Anal. Calcd for $C_{13}H_{17}NO_6$: C, 55.12; H, 6.05; N, 4.94. Found: C, 54.85; H, 6.61; N. 4.86 ESI-MS *m/z* 284 ([M+H]$^+$, 100%).

**Fluorescence and Absorption Studies.** Fluorescence emission spectra were measured on Perkin-Elmer LS55 fluorescence spectrophotometer by exciting the samples at 320 nm, and the emission spectra were recorded in the 330−550 nm range. Absorption studies were carried out with a JASCO V-570 instrument by measuring the spectra from 800 to 200 nm. The bulk solutions of L and amino acids were prepared in methanol in which 400 μL (4%) of water was added for initially dissolving the amino acid. The bulk solution concentrations were maintained at $1 \times 10^{-3}$ M. All the measurements

were made in 1 cm quartz cell, and the effective concentration of L was maintained as 50 $\mu$M. During the titration different mole ratios of amino acid were added to L, and the emissions of all the samples were measured at different time intervals. In the case of the phenylalanine titration, the background spectra were subtracted.

For the EtBr experiment, the bulk solutions of L, amino acid, and EtBr were prepared in methanol. The bulk solution concentrations were maintained at $1 \times 10^{-3}$ M. During the titration, initially L and EtBr were mixed in 1:2 mol ratio by fixing the effective concentration of L at 50 $\mu$M. Different mole ratios of amino acids were added to these solutions, and all the emission measurements were made at different time intervals.

For the fluorescence experiment with 9-anthracenaldehyde, 150 $\mu$L of L (50 $\mu$M) was added to 300 $\mu$L of 9-anthracenaldehyde (2 equiv) and mixed initially, followed by the addition of increasing amount of Phe (0, 75, 150, 300, 450, 600 $\mu$L).

**MALDI TOF Studies.** Mass spectra were collected using an Axima-CFR MALDI-TOF-MS (Kratos Analytical, Manchester, UK), in the positive ion mode. The concentrations of the samples were kept the same as in the case of the solution studies.

**Microscopy Studies.** AFM studies were performed in multimode Veeco Dimensions 3100 SPM with Nanoscope IV controller instrument. Tapping mode with a phosphorus-doped Si probe having a sharp fine tip at the end was used in all the cases. TEM experiments were performed with a PHILIPS CM200 transmission electron microscope operating at 20–200 kV (resolution, 2.4 Å). High resolution TEM was done on a JEOL JEM 2100F instrument. Carbon-coated copper grids of 400 mesh were used as substrate for the sample. SEM studies were carried out with JEOL JSM-6390 scanning electron microscope. Powder XRD studies were performed with a PHILLIPS PANalytical X-Pert Pro diffractometer. The solvo-dynamic diameter of all the samples were measured in methanol (concentration were kept the same as in the case of fluorescence studies) at 25 °C. The incident laser (Coherent Inc., Santa Clara, CA) radiation used was a 633 nm wavelength of 90°. The scattered light was filtered through a vertical polarization filter. The experiments were carried out using standard cylindrical BI-RC 12 glass cuvettes.

**Sample Preparation.** For AFM, TEM, and DLS studies, L and Phe solutions were made in methanol. Phe solutions were made by dissolving the amino acids in ~400 $\mu$L of deionized water and then adding methanol to the desired volume. The bulk concentration of the solutions was *ca.* $1 \times 10^{-3}$ M for all the cases. For studies at lower concentration, the bulk concentration of L and Phe was *ca.* $1 \times 10^{-4}$ M. For AFM studies with proteins, 100 $\mu$L of protein (1 mg/10 mL) was added to 100 $\mu$L of [L+Phe]. For the AFM studies of [L+Phe] in the presence of salts, the bulk concentration of NaCl and Zn(ClO$_4$)$_2$ was *ca.* $1 \times 10^{-3}$ M.

For AFM and TEM studies, 1.0 mL of L and 1.0 mL of Phe was added to a sample vial, and this mixture was used as stock solution. For DLS studies, 100 $\mu$L of L and 100 $\mu$L of Phe were added to 3.0 mL of methanol solution. Different sample vials were prepared for drawing the samples at different times, and the concentration of these samples was maintained throughout.

For AFM, an aliquot of ~200 $\mu$L was taken from the stock solution at different time intervals and sonicated for ~15 min. Different sample blocks were prepared by spreading ~50 $\mu$L of the mixed solution on a mica sheet and allowing the prepared sheet to dry in air at room temperature. For TEM, the same procedure was followed, and the mixed solution was spread over a carbon-coated copper grid which was then allowed to air-dry.

For powder XRD and SEM studies the solid samples were isolated from the mixture of [L+Phe] at different time intervals and used for experiments.

**Computational Studies.** Coordinates of 1:1 complexes of [L+Phe] was taken from the DFT calculations and were used as templates for the construction of dimers and higher order oligomers. The dimer was constructed initially by taking two 1:1 complex units and placing them farther apart and then minimizing the same. A tetrameric unit was built from two dimers and was minimized. This procedure was adopted to generate higher oligomeric units, namely, 8, 16, and 32. The threads were minimized at each stage before going for the higher aggregate.

Hence all the calculations were performed on the MM+ force field. Such minimized threads were taken to form a bundle and were minimized through molecular mechanics calculations.

**CD Studies.** CD studies were performed with a JASCO J-815 circular dichroism spectrometer. For CD studies with proteins, the protein concentration was kept constant. Hence 40 $\mu$L of protein (1 mg/mL) was added to varying concentrations of [L+Phe], and the spectra were recorded.

*Supporting Information Available:* Characterization and spectral data of L (SI 01); fluorescence data (SI 02); absorption data (SI 03); AFM data (SI 04); SEM data (SI 05); DLS data (SI 06); computational data (SI 07); AFM studies with proteins (SI 08); and CD studies with proteins (SI 09). This material is available free of charge *via* the Internet at http://pubs.acs.org.

## REFERENCES AND NOTES

1. Whitesides, G. M.; Mathias, J. P.; Seto, C. T. Molecular Self-Assembly and Nanochemistry: A Chemical Strategy for the Synthesis of Nanostructures. *Science* **1991**, *254*, 1312–1319.
2. Lehn, J. M. Supramolecular Chemistry. *Science* **1993**, *260*, 1762–1763.
3. Hsu, L.; Cvetanovich, G. L.; Stupp, S. I. Peptide Amphiphile Nanofibers with Conjugated Polydiacetylene Backbones in Their Core. *J. Am. Chem. Soc.* **2008**, *130*, 3892–3899.
4. Pakalns, T.; Haverstick, K. L.; Fields, G. B.; McCarthy, J. B.; Mooradian, D. L.; Tirrell, M. Cellular Recognition of Synthetic Peptide Amphiphiles in Self-Assembled Monolayer Films. *Biomaterials* **1999**, *20*, 2265–2279.
5. Berndt, P.; Fields, G. B.; Tirrell, M. Synthetic Lipidation of Peptides and Amino Acids: Monolayer Structure and Properties. *J. Am. Chem. Soc.* **1995**, *117*, 9515–9522.
6. Yu, Y.-C.; Berndt, P.; Tirrell, M.; Fields, G. B. Self-Assembling Amphiphiles for Construction of Protein Molecular Architecture. *J. Am. Chem. Soc.* **1996**, *118*, 12515–12520.
7. Murakami, Y.; Nakano, A.; Yoshimatsu, A.; Uchitomi, K.; Matsuda, Y. Characterization of Molecular Aggregates of Peptide Amphiphiles and Kinetics of Dynamic Processes Performed by Single-Walled Vesicles. *J. Am. Chem. Soc.* **1984**, *106*, 3613–3623.
8. Shimizu, T.; Masuda, M.; Minamikawa, H. Supramolecular Nanotube Architectures Based on Amphiphilic Molecules. *Chem. Rev.* **2005**, *105*, 1401–1443.
9. Hartgerink, J. D.; Beniash, E.; Stupp, S. I. Self-Assembly and Mineralization of Peptide-Amphiphile Nanofibers. *Science* **2001**, *294*, 1684–1688.
10. Li, L.-S.; Jiang, H.; Messmore, B. W.; Bull, S. R.; Stupp, S. I. A Torsional Strain Mechanism to Tune Pitch in Supramolecular Helices. *Angew. Chem., Int. Ed.* **2007**, *46*, 5873–5876.
11. Ghadiri, M. R.; Granja, J. R.; Buehler, L. K. Artificial Transmembrane Ion Channels from Self-Assembling Peptide Nanotubes. *Nature* **1994**, *369*, 301–304.
12. Rajangam, K.; Behanna, H. A.; Hui, M. J.; Han, X. Q.; Hulvat, J. F.; Lomasney, J. W.; Stupp, S. I. Heparin Binding Nanostructures to Promote Growth of Blood Vessels. *Nano Lett.* **2006**, *6*, 2086–2090.
13. Lim, Y.,-b.; Park, S.; Lee, E.; Jeong, H.; Ryu, J.-H.; Lee, M. S.; Lee, M. Glycoconjugate Nanoribbons from the Self-Assembly of Carbohydrate-Peptide Block Molecules for Controllable Bacterial Cell Cluster Formation. *Biomacromolecules* **2007**, *8*, 1404–1408.
14. Sun, G.; Chu, C.-C. Self-Assembly of Chemically Engineered Hydrophilic Dextran into Microscopic Tubules. *ACS Nano* **2009**, *3*, 1176–1182.

15. Gazit, E. A Possible Role for π-Stacking in the Self-Assembly of Amyloid Fibrils. *FASEB J.* **2002**, *16*, 77–83.
16. Azriel, R.; Gazit, E. Analysis of the Minimal Amyloid-Forming Fragment of the Islet Amyloid Polypeptide: An Experimental Support for the Key Role of the Phenylalanine Residue in Amyloid Formation. *J. Biol. Chem.* **2001**, *276*, 34156–34161.
17. Kayed, R.; Bernhagen, J.; Greenfield, N.; Sweimeh, K.; Brummer, H.; Voelter, W.; Kapurniotu, A. Conformational Transitions of Islet Amyloid Polypeptide (IAPP) in Amyloid Formation *in Vitro*. *J. Mol. Biol.* **1999**, *287*, 781–796.
18. John, G.; Masuda, M.; Okada, Y.; Yase, K.; Shimizu, T. Nanotube Formation from Renewable Resources *via* Coiled Nanofibers. *Adv. Mater.* **2001**, *13*, 715–718.
19. John, G.; Jung, J. H.; Masuda, M.; Shimizu, T. Unsaturation Effect on Gelation Behavior of Aryl Glycolipids. *Langmuir* **2004**, *20*, 2060–2065.
20. Kawasaki, T.; Tokuhiro, M.; Kimizuka, N.; Kunitake, T. Hierarchical Self-Assembly of Chiral Complementary Hydrogen-Bond Networks in Water: Reconstitution of Supramolecular Membranes. *J. Am. Chem. Soc.* **2001**, *123*, 6792–6800.
21. Shiraki, T.; Morikawa, M.; Kimizuka, N. Amplification of Molecular Information Through Self-Assembly: Nanofibers Formed from Amino Acids and Cyanine Dyes by Extended Molecular Pairing. *Angew. Chem., Int. Ed.* **2008**, *47*, 106–108.
22. Aime', C.; Nishiyabu, R.; Gondo, R.; Kanekob, K.; Kimizuka, N. Controlled Self-Assembly of Nucleotide-Lanthanide Complexes: Specific Formation of Nanofibers from Dimeric Guanine Nucleotides. *Chem. Commun.* **2008**, 6534–6536.
23. Iwaura, R.; Yoshida, K.; Masuda, M.; Ohnishi-Kameyama, M.; Yoshida, M.; Shimizu, T. Oligonucleotide-Templated Self-Assembly of Nucleotide Bolaamphiphiles: DNA-Like Nanofibers Edged by a Double-Helical Arrangement of A-T Base Pairs. *Angew. Chem., Int. Ed.* **2003**, *42*, 1009–1012.
24. Kato, T.; Mizoshita, N.; Kishimoto, K. Functional Liquid-Crystalline Assemblies: Self-Organized Soft Materials. *Angew. Chem., Int. Ed.* **2006**, *45*, 38–68.
25. Terech, P.; Weiss, R., G. Low Molecular Mass Gelators of Organic Liquids and the Properties of their Gels. *Chem. Rev.* **1997**, *97*, 3133–3159.
26. Iwaura, R.; Hoeben, F. J. M.; Masuda, M.; Schenning, A. P. H. J.; Meijer, E. W.; Shimizu, T. Molecular-Level Helical Stack of a Nucleotide-Appended Oligo(*p*-phenylenevinylene) Directed by Supramolecular Self-Assembly with a Complementary Oligonucleotide as a Template. *J. Am. Chem. Soc.* **2006**, *128*, 13298–13304.
27. Yagai, S.; Kinoshita, T.; Higashi, M.; Kishikawa, K.; Nakanishi, T.; Karatsu, T.; Kitamura, A. Diversification of Self-Organized Architectures in Supramolecular Dye Assemblies. *J. Am. Chem. Soc.* **2007**, *129*, 13277–13287.
28. Yagai, S.; Monma, Y.; Kawauchi, N.; Karatsu, T.; Kitamura, A. Supramolecular Nanoribbons and Nanoropes Generated from Hydrogen-Bonded Supramolecular Polymers Containing Perylene Bisimide Chromophores. *Org. Lett.* **2007**, *9*, 1137–1140.
29. Dessingou, J.; Joseph, R.; Rao, C. P. A Direct Fluorescence-on Chemosensor for Selective Recognition of Zn(II) by a Lower Rim 1,3-Di-derivative of Calix[4]arene Possessing Bis-{*N*-(2-hydroxynaphthyl-1-methylimine)} Pendants. *Tetrahedron Lett.* **2005**, *46*, 7967–7971.
30. Singhal, N. K.; Ramanujam, B.; Mariappanadar, V.; Rao, C. P. Carbohydrate-Based Switch-on Molecular Sensor for Cu(II) in Buffer: Absorption and Fluorescence Study of the Selective Recognition of Cu(II) Ions by Galactosyl Derivatives in HEPES Buffer. *Org. Lett.* **2006**, *8*, 3525–3528.
31. Ahuja, R.; Singhal, N. K.; Ramanujam, B.; Ravikumar, M.; Rao, C. P. Experimental and Computational Studies of the Recognition of Amino Acids by Galactosyl-imine and -amine Derivatives: An Attempt to Understand the Lectin−Carbohydrate Interactions. *J. Org. Chem.* **2007**, *72*, 3430–3442.
32. Kumar, A.; Singhal, N. K.; Ramanujam, B.; Mitra, A.; Rameshwaram, N. R.; Nadimpalli, S. K.; Rao, C. P. $C_1$-/$C_2$-Aromatic-imino-glyco-conjugates: Experimental and Computational Studies of Binding, Inhibition, and Docking Aspects toward Glycosidases Isolated from Soybean and Jack Bean. *Glycoconjugates J.* **2009**, *26*, 495–510.
33. Pathak, R. K.; Ibrahim, Sk.Md.; Rao, C. P. Selective Recognition of $Zn^{2+}$ in Aqueous Acetonitrile by Salicylaldimine Appended Triazole Linked Di-derivatives of Calix[4]arene by Enhanced Fluorescence Emission: Role of Terminal−$CH_2OH$ Moieties in Conjunction with the Imine in Recognition. *Tetrahedron Lett.* **2009**, *50*, 2730–2734.
34. Singhal, N. K.; Mitra, A.; Rajsekhar, G.; Shaikh, M. M.; Kumar, S.; Guionneau, P.; Rao, C. P. Role of the Orientation of−OH Groups on Sensitivity and Selectivity of the Interaction of $M^{2+}$ with Ribosyl- and Galactosyl-imino-conjugates: Solution Recognition Studies of $M^{2+}$ in MeOH and Selective Recognition of $Cu^{2+}$ in HEPES Buffer, and First Crystal Structure Determination of Dinuclear-Cu(II) Complexes Based on Both the Glyco-imino-conjugates. *Dalton Trans.* **2009**, 8432–8442.
35. Pathak, R. K.; Dikundwar, A. G.; Guru Row, T. N.; Rao, C. P. A Lower Rim Triazole Linked Calix[4]arene Conjugate as a Fluorescence Switch on Sensor for $Zn^{2+}$ in Blood Serum Milieu. Chem. Commun., published online May 12, 2010, http://doi.dx.org/, 10.1039/c0cc00219d.
36. Yang, H.; Pritzker, M.; Fung, S. Y.; Sheng, Y.; Wang, W.; Chen, P. Anion Effect on the Nanostructure of a Metal Ion Binding Self-Assembling Peptide. *Langmuir* **2006**, *22*, 8553–8562.
37. *Hyperchem 8.0.4*; Hypercube, Inc.: Gainesville, FL, 2007.
38. Mitra, A.; Chinta, J. P.; Rao, C. P. 1-(D-Glucopyranosyl-2′-deoxy-2′-iminomethyl)-2-hydroxybenzene as Chemosensor for Aromatic Amino Acids by Switch-on Fluorescence. *Tetrahedron Lett.* **2010**, *51*, 139–142.
39. Edwards, J. V., Buschle-Diller, G., Goheen, S. C. Modified Fibers with Medical and Specialty Applications. Goheen, S. C., Edwards, J. V., Rayburn, A., Gaither, K, Castro, N., Eds.; Springer: The Netherlands, 2006; pp 49−65.
40. Lu, K.; Jacob, J.; Thiyagarajan, P.; Conticello, V. P.; Lynn, D. G. Exploiting Amyloid Fibril Lamination for Nanotube Self-Assembly. *J. Am. Chem. Soc.* **2003**, *125*, 6391–6393.